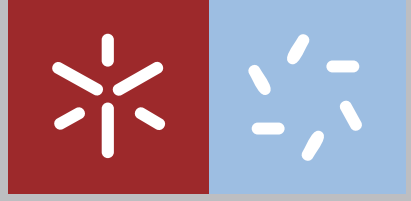

Universidade do Minho
Escola de Ciências

Flora José da Rocha Ferreira

Multi-bump solutions in dynamic neural fields: Analysis and Applications

Março de 2014

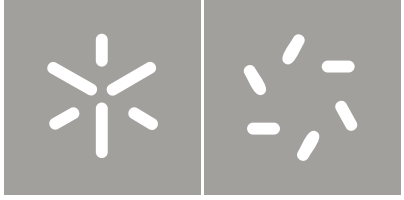

Universidade do Minho
Escola de Ciências

Flora José da Rocha Ferreira

Multi-bump solutions in dynamic neural fields: Analysis and Applications

Tese de Doutoramento
Doutoramento em Ciências / Especialidade em Matemática

Trabalho efectuado sob a orientação do
Professor Doutor Wolfram Erlhagen

Março de 2014

Acknowledgments

First and foremost I would like to thank my scientific adviser, Prof. Dr. Wolfram Erlhagen, and Prof. Dr. Estela Bicho. I appreciate all their help, contributions and ideas which made my PhD experience productive and stimulating. The good advice and support they granted me has been invaluable on both academic and personal levels. For that I am truly grateful to them.

I also would like to thank the group members of the Mobile and Anthropomorphic Robotics Laboratory at University of Minho with who I had the pleasure to work: Carlos Faria, Eliana Costa e Silva, Emanuel Sousa, Gianpaolo Gulletta, Luís Louro, Manuel Pinheiro, Tiago Malheiro, Toni Machado, Rui Silva, and Weronika Wojtak. The group has been a source of friendship as well as good advice and collaboration.

Lastly, I would like to thank my family and friends for all their love and encouragement. In special to my husband for his support and to my son who was born during this PhD and gave me an extra motivation.

Work supported by Portuguese FCT Grant SFRH/BD/42375/2007, financed by POPH-QREN-Type 4.1-Advanced Training, co-funded by the European Social Fund and national funds from MEC.

Abstract

The work described here has the goal of providing new mathematical results about the formation of spatio-temporal patterns in dynamic neural fields (DNFs) that can be applied and tested in the domains of cognitive modelling and cognitive robotics. Specifically, the conditions for the existence and stability of multiple localized excitations in one-dimensional fields with external input were analysed. These multi-bump solutions represent the core of an original dynamic field model of fast sequence learning that was developed and subsequently tested in a real-world robotics experiment.

While the existence and the stability of different types of patterns in DNFs have been addressed in many theoretical studies in the past, little attention has been paid thus far on the initial and input conditions that guarantee the evolution of these patterns. Following Laing et al. (2002), we apply a connectivity function with oscillatory rather than monotonic decay to study analytically and numerically the formation of multiple regions of excitation when several localized inputs are applied simultaneously or sequentially to the field. For the existence and stability proofs, we extend the ideas of Amari's original work on pattern formation in fields with connectivity functions of lateral inhibition type.

Based on the mathematical results, a novel model of multi-item memory of sequential events is proposed that exploits the processing mechanism of self-sustained activity in recurrently connected neural populations modelled by DNFs. A threshold accommodation dynamics is applied to establish a stable multi-bump solution with a gradient of excitation that represents in its relative activation strengths the temporal order and the relative timing of sequence elements. In line with findings in neurophysiological studies with monkeys, this memory representation pre-activates to varying degrees corresponding neural populations in a decision field. The competitive dynam-

ics of this field allows recalling all sequence elements in the correct order and with the correct timing.

The working memory model was extended to integrate also the sequence learning part in the modelling. Neural populations in a perceptual field represent in their self-sustained activation patterns the sensory cue (e.g., colour) that defines the sequence. The challenge for many modelling approaches to represent repeated elements is autonomously solved by the field dynamics since repeated sensory cues automatically activate different neuronal subpopulations. The memory of previous sequence demonstrations also preshapes the perceptual field. This preshaping mechanisms affects the time course of suprathreshold population activity and is thus fundamental to adjust the relative activation strengths of the memory gradient in successive sequence demonstrations. The numerical simulation show that the purely activation based learning principles implemented in the model are able to acquire and represent the order and timing of a sequence in just very few demonstration-executing cycle. To directly test the assumptions about the time course of population activity in the various interconnected field layers and to verify the model predictions, we conducted a robotics experiment. The learning model was integrated in the dynamic field based control architecture of the humanoid robot ARoS. In the experiment, ARoS had to learn a short musical sequence from human demonstrations to subsequently execute the piece of music on a keyboard. The successful results of the real-time robotics implementation are discussed in relation to theoretical ideas and experimental findings about sequencing and timing in humans and other animals.

Resumo

O objetivo deste trabalho é fornecer novos resultados matemáticos sobre a formação de padrões espaço-temporais em campos dinâmicos neuronais (DNFs) que podem ser aplicados e testados nos domínios da modelação cognitiva e robótica cognitiva. Em particular, foram analisadas as condições para a existência e a estabilidade de múltiplas regiões localmente excitadas num campo unidimensional com uma entrada externa. Estas múltiplas regiões representam o base de um modelo de campos dinâmicos que foi desenvolvido para aprendizagem de sequências e posteriormente analisado numa experiência robótica em ambiente real.

Embora haja vários estudos sobre a existência e a estabilidade dos diferentes tipos de padrões em DNFs, pouca atenção tem sido dada sobre as condições iniciais e de entrada que garantem a evolução desses padrões. Tendo por base Laing et al. (2002), aplicou-se uma função de conectividade com decaimento oscilatório em vez de um decaimento monótono permitindo o estudo analítico e numérico da formação de múltiplas regiões de excitação quando várias entradas localizadas são aplicadas num campo dinâmico simultaneamente ou sequencialmente. Nas demonstrações da existência e estabilidade, foram estendidas as ideias do trabalho original de Amari em formação de padrões em campos dinâmicos com funções de conectividade do tipo inibição lateral.

Tendo por base os resultados matemáticos, foi elaborado um novo modelo de memória de sequências de eventos que explora o mecanismo de processamento da atividade auto-sustentada em populações neuronais com ligações recorrentes modeladas por DNFs. Uma solução multi-picos estável com um gradiente de excitação é obtida a partir de uma dinâmica de adaptação do limiar de ativação do campo. Este gradiente representa, na sua força de ativação, a ordem temporal e o tempo relativo entre os elementos de sequência. De acordo com resultados obtidos em estudos neurofisiológicos

com macacos, esta representação de memória pré-ativa, em níveis diferentes, as populações neuronais correspondentes no campo de decisão. A dinâmica competitiva deste campo permite recordar todos os elementos da sequência na ordem correta e com os intervalos de tempo corretos.

O modelo de memória de trabalho foi estendido para integrar também a parte de aprendizagem da sequência na modelagem. Os padrões de ativação auto-sustentadas das populações neuronais no campo percetual representam o estímulo sensorial (por exemplo, cor) que define a sequência. O desafio para muitas abordagens de modelização de representar elementos repetidos é autonomamente resolvido pela dinâmica do campo que, de forma automática, representa elementos repetidos em diferentes subpopulações neuronais. A memória da sequência posteriormente demonstrada também pré-ativa o campo percetual. Este mecanismo de pré ativação afeta o tempo que a população demora a ficar ativa e é, portanto, essencial para ajustar as forças de ativação relativas do gradiente de memória em demonstrações sucessivas da sequência. As simulações numéricas mostram que os princípios de aprendizagem baseados puramente em ativação que foram implementados no modelo são capazes de adquirir e representar a ordem e o tempo de uma sequência ao fim de poucas demonstrações. Para testar diretamente os pressupostos sobre as evoluções temporais de atividade da população nos diferentes campos interligados e verificar as previsões do modelo, foi realizada uma experiência robótica. O modelo de aprendizagem foi integrado numa arquitetura dinâmica no robô humanoide ARoS. Na experiência o ARoS teve de aprender uma curta sequência musical, a partir de demonstrações executadas por um humano e, posteriormente, reproduzi-la num teclado. A experiência de implementação robótica em tempo real foi bem sucedida. Os respetivos resultados são discutidos em comparação com as ideias teóricas e resultados experimentais obtidos em experiências sobre sequências e tempo em seres humanos e outros animais.

Contents

List of Figures

List of Tables

Part I

General introduction

Chapter 1

General introduction

Dynamic neural fields (DNFs) have been introduced in the 1970's by Wilson and Cowan (1973) and Amari (1977) as a mathematical model of the formation of activity patterns in neural tissue that abstract from the fine biophysical details of neural firing. Typically, a continuum description of neural populations is used so that the mean neural firing activities can be described by scalar fields in terms of time and one or two space variables. Dynamic neural field models are very popular for two main reasons. They offer the right level of complexity to explain key aspects of neural population dynamics as observed in numerous neurophysiological studies (e.g., Erlhagen et al., 1999; Jancke et al., 1999), and at the same time, DNF models are simple enough to allow analytical treatment that contributes to a better understanding of neural processing mechanisms. In recent years, the analysis of the existence and stability of coherent structures in neural field such as spatial localized activity bumps, spatially or spatiotemporal oscillation patterns, and travelling waves has been a very active area of research in the emerging field of mathematical neuroscience (for a review see Coombes, 2005).

A directly related line of research that drives the development of a dynamic field theory is the modelling of cognitive processes. The architecture of dynamic field models reflects the hypothesis supported by anatomical and psychological findings that strong recurrent interactions in local populations of neurons form a basic mechanism for cortical information processing. The recurrent excitatory and inhibitory inputs from neighbouring neurons cause non-trivial dynamic behaviour in neural populations. Most importantly, population activity which is initiated by time-dependent external signals

may become self-sustained in the absence of any external input. Such attractor states of the population dynamics may be used by the nervous systems to guide complex behaviour that goes beyond a simple mapping of sensory input onto motor output. Persistent neural activity is observed in many brain regions, but seems to be particular prominent in prefrontal areas. The prefrontal cortex (PFC) is commonly believed to be crucially involved in higher cognitive processes like working memory, decision making or planning of goal-directed behaviour (Miller, 2000). Dynamic field models have applied the attractor paradigm to a large variety of neurocognitive phenomena in the domains of perception, cognition and action (e.g., Erlhagen and Schöner, 2002, for an overview see Schöner, 2008).

More recently, researchers have started to exploit the theoretical concepts and neural processing mechanisms offered by dynamic field models to endow autonomous robots with human-like cognitive functionalities. Implementing and testing dynamic field models in robots that are controlled in closed-loop by sensory information is seen as an excellent opportunity to get feedback about hidden model assumptions and missing links to the sensory and motor surfaces. The humanoid robot ARoS developed at the University of Minho is a good example of the dynamic field approach to cognitive robotics. ARoS is able to coordinate its actions and decisions with human partners in order to achieve common goals in a shared task. The control architecture consisting of a large number of coupled dynamic neural fields is inspired by the neurocognitive mechanisms and neural circuits supporting human joint action (Bicho et al., 2011).

This doctoral thesis presents results that contribute to all three research areas of dynamic field theory described above: mathematical analysis, cognitive modelling, and robotics implementations. The specific research topic of the thesis is the modelling of a multi-item working memory function formalized by self-sustained and stable multi-bump solutions in dynamic fields. Working memory refers to the distinct memory ability of humans to retain information in storage for short time intervals. It is fundamental for cognitive tasks such as remembering the order of a series of sensory cues or the planning and performing of action sequences. In DNF models, the memory state can be represented by a stimulus induced bump attractor of localized field activity. To implement a working memory function the field dynamics must be bistable. The

bump attractor must coexist with a stable resting state of neural population activity (representing the absence of stimulus information), such that the memory state can be switched on and off by transient inputs.

The main goal of the mathematical analysis presented in this thesis is to contribute to a more rigorous understanding of the formation of single- and multi-bump solutions in the presence of external inputs to the dynamic field. While many mathematical studies have addressed in the past the existence and stability of localized activity patterns, surprisingly little attention has been paid to the initial and input conditions that guarantee the evolution of these patterns. For applications of DNF theory that are based on complex architectures of coupled dynamic fields this question is central. In his original paper, Amari (1977) performed a stability analysis for a single bump with stationary input. Since in his field model recurrent inhibition is spatially more widespread than excitation (lateral inhibition type interactions) stable multi-bump solutions do not exist. Strong competition between regions with high activity mediated by lateral inhibition will destroy multi-bump patterns whenever small spatial perturbation to the activation profiles are applied. More recently, Laing et al. (2002) proposed and analysed a connectivity function that supports the stable persistence of multiple regions of high activity, and thus may serve as a basis to implement a multi-item memory function.

In the second part of the thesis, dedicated to applications of DNF theory, the obtained mathematical results are applied in a modelling study. It aims at testing the hypothesis that the memories of order and timing information of sequential events share a common neural substrate. In an analysis by synthesis approach, the sequence model is then tested in a real-world robotics experiment. The robot ARoS learns from observing a human teacher to memorize and execute on a keyboard a short musical sequence.

1.1 Dynamic Neural Fields

1.1.1 Dynamic Neural Field Equation

The neuronal activity of the population (or field) is described by the following non-linear partial integro-differential equation proposed by Amari (1977)

$$\tau \frac{\partial u(x,t)}{\partial t} = -u(x,t) + \int_{-\infty}^{\infty} w(x-y) f\left(u(y,t)\right) dy - h + S(x,t). \tag{1.1}$$

This equation describes neuronal activity on a single layer of interconnected neurons along a one-dimensional infinite domain. The function $u(x,t)$ represents the membrane potential or activity of a neuron at time t and spatial position x. The function $S(x,t)$ represents a time-varying external input with spatial structure. The parameter $h > 0$ determines the resting level to which the field activity converges without external stimuli, and the parameter $\tau > 0$ defines the time scale of the field dynamics. The output function $f(u)$ gives the firing rate or firing probability as a function of u.

For the mathematical analysis of pattern formation, Amari chooses the Heaviside step as output function

$$f(u) = H_0(u) = \begin{cases} 0, & u \leq 0 \\ 1, & u > 0 \end{cases}. \tag{1.2}$$

It represents a simplification of real neural firing which typically shows a more gradual increase of the rate with increasing u. In Amari's model, a neuron can be either active or inactive, but only active neurons contribute to the current interaction with in local neural population. It is important to stress that the choice of the Heaviside function facilitates the mathematical analysis. However, the main results about the existence and stability of localized excitation also hold for a field with a smooth firing rate function of sigmoidal type (Kishimoto and Amari, 1979).

The coupling function $w(x,x') = w(x-x')$ describes the distance dependent connectivity strength from neurons at position x to those at position x'. Amari (1977) studied the dynamics of pattern formation in equation (1.1) when the coupling function is of lateral inhibition type. In general, a lateral inhibition type connectivity $w(x)$ satisfies the following properties:

(H_1) $w(x)$ is symmetric, i.e., $w(-x) = w(x)$ for all $x \in \mathbb{R}$;

(H_2) w is both continuous and integrable on $\mathbb{R}$;

(H_3) $w(x) > 0$ on an interval $(-\overline{x}, \overline{x})$, and $w(-\overline{x}) = w(\overline{x}) = 0$;

(H_4) $w(x) < 0$ on $(-\infty, -\overline{x}) \cup (\overline{x}, \infty)$;

(H_5) $w(x)$ is decreasing on $(0, \infty)$.

Lateral inhibition establishes excitatory connections for nearby neuronal elements and inhibitory connections for neuronal elements separated by a distance greater than a certain position, $\overline{x}$. One example of a coupling function that satisfies conditions $(H_1) - (H_5)$ is a Gaussian function with a constant global inhibition

$$w(x) = w_{exc} e^{\left(-\frac{x^2}{2\sigma_{exc}^2}\right)} - w_{inh}, \tag{1.3}$$

where $w_{exc} > 0$ and $\sigma_{exc} > 0$ define, respectively, the amplitude and standard deviation, and $w_{inh} > 0$ represents the constant inhibition for distant neurons (Erlhagen and Bicho, 2006) (Figure 1.1, left). Another example is a "Mexican-hat" type function given by the difference of two Gaussian functions, that can also be added with a constant global inhibition

$$w(x) = w_{exc} e^{\left(-\frac{x^2}{2\sigma_{exc}^2}\right)} - w_{inh_1} e^{\left(-\frac{x^2}{2\sigma_{inh}^2}\right)} - w_{inh_2}, \tag{1.4}$$

where $w_{exc} > w_{inh_1} > 0$ and $\sigma_{exc} > \sigma_{inh} > 0$ and $w_{inh_2} > 0$ (Figure 1.1, right).

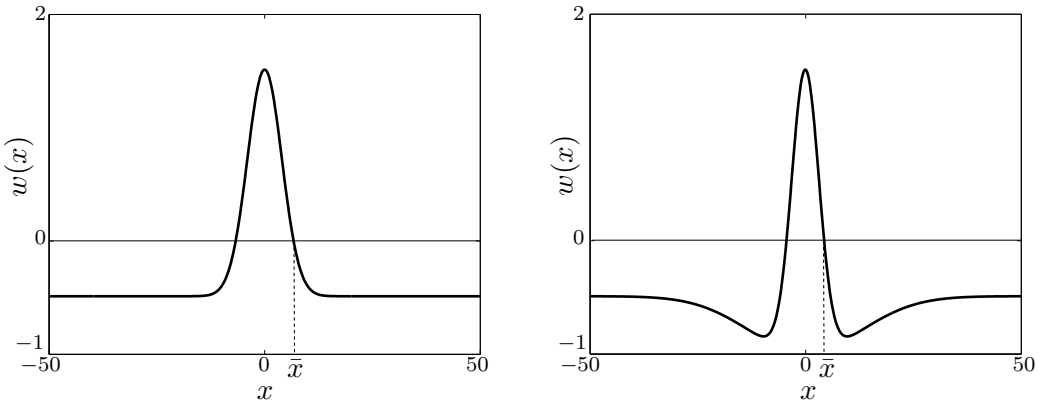

Figure 1.1: The coupling function, $w(x)$, defined in (1.3) for $w_{exc} = 2$, $\sigma_{exc} = 4$ and $w_{inh} = 0.5$ (left). The coupling function, $w(x)$, defined in (1.4) for $w_{exc} = 2.5$, $\sigma_{exc} = 0.05$, $w_{inh_1} = 0.5$, $\sigma_{inh} = 0.003$ and $w_{inh_2} = 0.5$ (right).

Motivated by labelling studies showing that the spatial coupling between groups of neurons in the prefrontal cortex forms approximate periodic stripes (Gutkin et al., 2000), Laing et al. (2002) proposed a coupling function with oscillatory rather than monotonic decay

$$w(x) = e^{-k|x|} \left(k \sin |x| + \cos(x)\right). \tag{1.5}$$

where the parameter $k > 0$ controls the rate at which the oscillations of w decay with distance.

In this thesis, we study the formation of one or more excited regions in dynamics fields using an adapted version of the connection function proposed by Laing et al. (2002):

$$w(x) = Ae^{-k|x|} \left(k \sin |\alpha x| + \cos(\alpha x)\right), \tag{1.6}$$

where the parameters $A > 0$ and $0 < \alpha \leq 1$ are added to control the amplitude and the zero crossings, respectively. The oscillations of w decay more rapidly as k increases (compare Figure 1.2). The larger the value α, the smaller the distance between consecutive zeros of w (compare Figure 1.3).

The coupling functions $w(x)$ in (1.5) and (1.6) satisfy (H_1), (H_2) and the following properties:

(H_6) $w(x)$ is an oscillatory function that tends to zero as $x \to \pm\infty$;

(H_7) $w(0) > 0$, and $w(x)$ changes sign infinitely often on $(0, \infty)$.

1.1.2 Stable states of the field dynamics

Dynamic field theory provides a basis for characterizing the representational states underlying behaviour through the notion of activation fields spanned over a metric dimension such as movement amplitude and direction, position and orientation in space, or frequency and colour (Erlhagen et al., 1999; Johnson et al., 2008). For example, consider the situation in which a neural field is applied over a spatial dimension coding the feature colour (hue), that is, the neurons are tuned to represent different colours. When an object with a specific colour is presented, a subpopulation representing the respective hue value will become highly active whereas surrounding neurons encoding

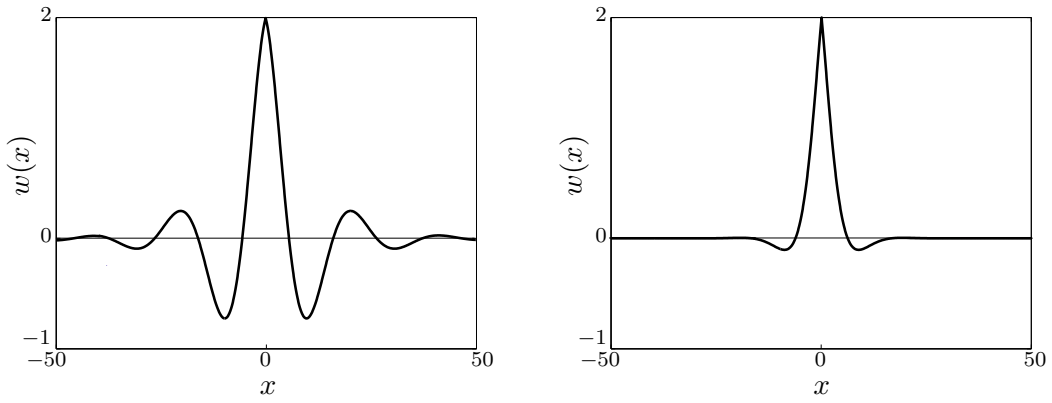

Figure 1.2: The coupling function, $w(x)$, defined in (1.6) for $A = 2$, $\alpha = 0.3$ and $k = 0.1$(left) and $k = 0.3$(right).

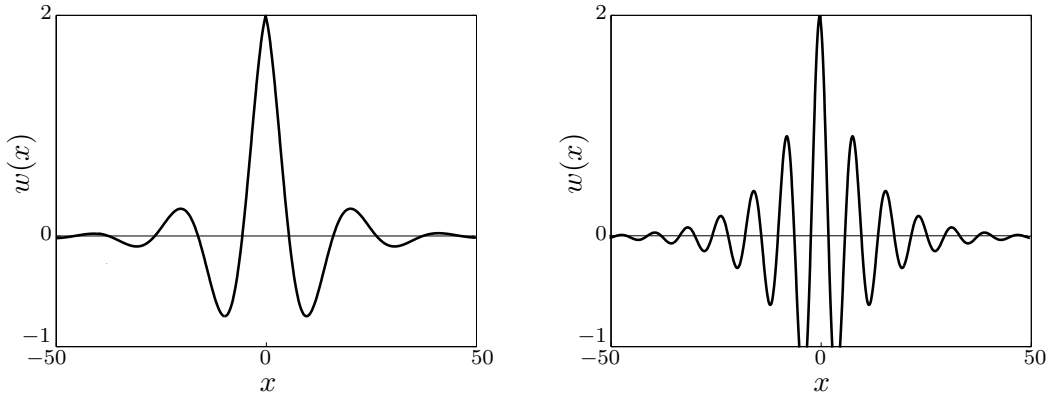

Figure 1.3: The coupling function, $w(x)$, defined in (1.6) for $A = 2$, $k = 0.1$ and $\alpha = 0.3$ (left) and $\alpha = 0.8$ (right).

other hue values remain at a low firing rate. The activity of each neuron is defined by the interplay between inputs from neighbouring neurons and external input from the vision system. To understand the processing of visual information in the neuronal population it is important to characterize the stable states of the field dynamics. To get an overview, it is convenient to follow Amari (1982) and define the average activity of a pool of N interconnected neurons in response to an external input. Its dynamic behaviour is governed by

$$\frac{du}{dt} = -u - h + W f_p(u) + S. \tag{1.7}$$

where W is the average interaction strength, S the average external input that the pool receives, and f_p denotes the output function of the pool. The output function with threshold 0 can be the Heaviside function used by Amari or any other nonlinear transfer function with saturation like, for instance, a smooth sigmoidal function with slope parameter β

$$f_p(u) = \frac{1}{1 + e^{-\beta u}}, \tag{1.8}$$

or a ramp function

$$f_p(u) = \begin{cases} 0, & u < 0 \\ \beta u, & 0 \leq u < \frac{1}{\beta} \\ 1, & u \geq \frac{1}{\beta} \end{cases}, \tag{1.9}$$

where $\beta > 0$ controls the slope. Depending on the strengths of W and S, the neuron pool can have two types of dynamic behaviour. Assuming that f_p is given by (1.9), if $S = 0$ and $W > h$, the dynamics is bistable, having three fixed points at $u_{a_1} = -h$, $u_r = \frac{h}{\beta W - 1}$ and $u_{a_2} = W - h$. Since the slope at u_{a_1} and at u_{a_2} is negative, these fixed points are asymptotically stable states, also called attractor states. On the other hand, as the slope at u_{a_r} is positive, this fixed point is an unstable state, also called repeller (Perko, 1996, for a discussion in the context of DFT see Schöner, 2009). Excitatory input, $S > h$, shifts the rate of change upwards by a constant amount, generating a new attractor at $u_{a_s} = W - h + S$. In this case, the dynamics is monostable with one stable state at a high excitation level (see Figure 1.4). If $S - h < 0$, the dynamics is also monostable with, however, a fixed point at a negative baseline or resting level.

Thus in general, depending on the strengths of the neural connectivity and the external input, patterns of activation can be in different attractor states (Johnson et al., 2008; Schöner, 2009):

- Resting state: in the absence of inputs, the attractor is at the resting level of the activation, a negative activation value ($-h$) by convention.

- Input-driven state: a localized input, $S(x)$, can form bumps in the field. When weak localized input is presented that does not reach the threshold for triggering the recurrent interaction within the neuronal pool, the solution remains sub-threshold, $u(x) = S(x) - h$. For stronger inputs, the recurrent interactions cause an amplification of the field response at stimulated sites, leading to a self-stabilized

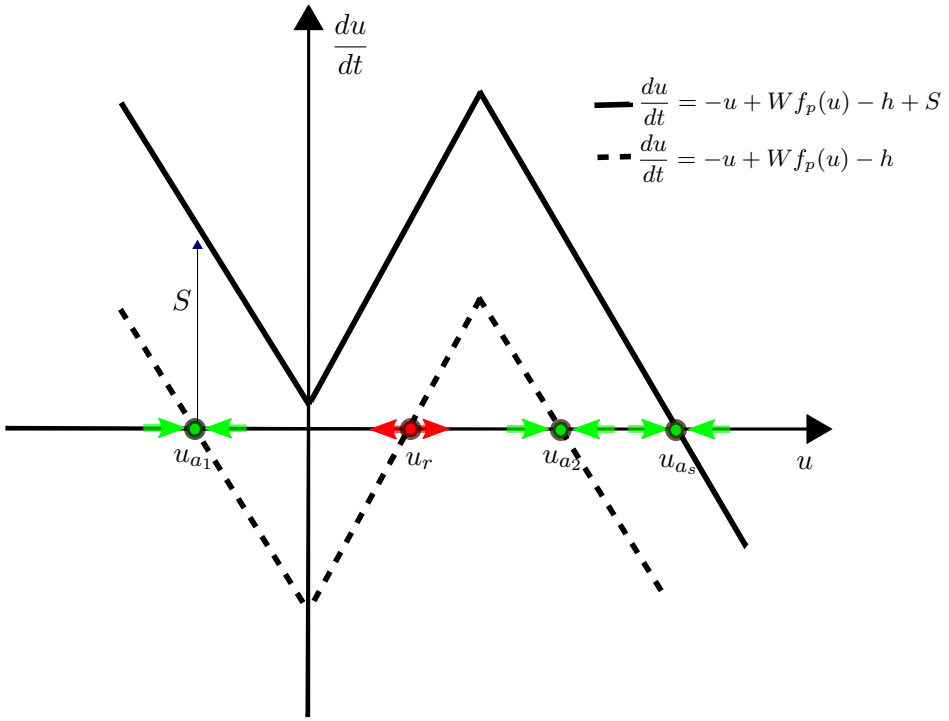

Figure 1.4: The rate of change of activation $\frac{du}{dt}$ is plotted as a function of u for the case of the ramp function (1.9). The fixed points are $u_{a_1} = -h$, $u_r = \frac{h}{\beta W - 1}$ and $u_{a_2} = W - h$, if $S = 0$ (dashed line) and $a_{a_s} = W - h + S$ if $S > h$ (solid line).

activation peak. If the input is removed, the suprathreshold activity will decay back to the stable resting state.

- Self-sustaining state: under appropriate conditions on the connectivity function W, and the parameter h, the field dynamics is bistable with the stable resting state coexisting with a localized activation pattern or bump that is self-sustained without supporting external input. A sufficiently strong transient input destabilises the resting state and a bump evolves. The self-sustained pattern is only marginally stable, that is, external perturbations of the activation profile may change the bump position (Amari, 1977). The bump can be destabilized by increasing the global inhibition, $-h < 0$, in the field. Suprathreshold activity will converge to the stable resting state of the field dynamics.

1.1.3 Single bump versus multiple bumps

In dynamic field models, strong recurrent excitation counterbalanced by lateral inhibition gives rise to stimulus-selective attractor states of neural populations that may serve a working memory function. Higher brain areas such as the PFC that show persistent activity are known to be involve in other cognitive functions as well (Miller, 2000). For instance, decision making defined as the process to choose an option between different alternatives in ambiguous sensorimotor tasks is believed to be mediated by the same neural processing mechanisms that support working memory. Indeed, in dynamic fields of Amari type a strong winner-takes-all competition between sufficiently active neural subpopulations is mediated by lateral inhibition. If two different groups of neurons at resting state receive transient external input, their activities first ramp up together before diverging from each other due to the increasing influence of the feedback inhibition. One population reaches finally a stable bump state which stores the decision in working memory whereas the activity of the other population declines. Normally, the population that gets the strongest overall input will win the competition (Figure 1.5, left). In the unlikely case of exactly equal input strengths, the decision may be forced by a noise term added to the field dynamics (Erlhagen and Schöner, 2002).

It is important to note that for dynamic fields of lateral inhibition type multi-bump solutions may exist. For the coupling function (1.3), each suprathreshold bump contributes an additional inhibitory input proportional to its width to other field sites. If the globally inhibitory input, $-h$, in equation (1.1) is adequately chosen, a limited number of bumps of equal width may exist simultaneously in the field (Erlhagen and Bicho, 2006). They are however not stable to small spatial perturbations (Laing et al., 2002; Laing and Troy, 2003; Murdock et al., 2006). From an application point of view even more important, multi-bumps cannot be generated by a temporal sequence of localized inputs to the field. The first input will trigger a localized activity pattern that occupies the total area of suprathreshold activity that the recurrent interactions permit. The strong additional inhibition at field sites that receive subsequent inputs prevent the evolution of suprathreshold activity that may compete with the existing bump to establish an equal width multi-bump pattern.

Laing et al. (2002) have shown analytically and in simulations that the field

dynamics may stabilize multiple regions of suprathreshold activity when a coupling function with an oscillatory pattern of lateral inhibition and lateral excitation (1.6) is used (Figure 1.5, right). The open question how multiple inputs that are presented simultaneously or sequentially may generate these multi-bump excitations from different initial conditions is addressed in this thesis.

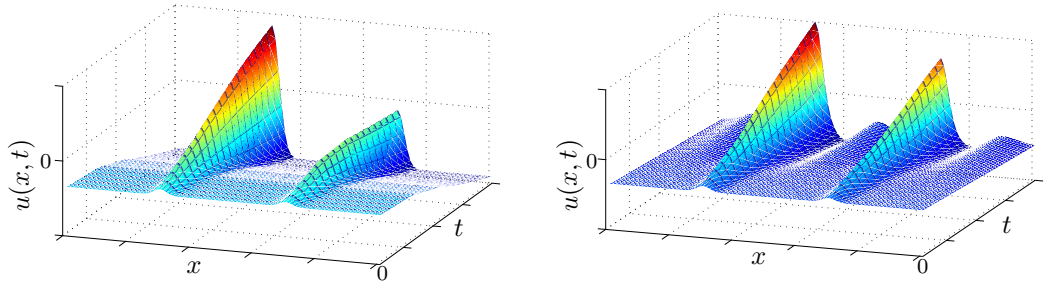

Figure 1.5: The initial temporal evolution of activation is shown when at time $t = 0$ two localized inputs of different strengths are presented. For a coupling function of lateral inhibition type (1.3), only one suprathreshold pattern will be ultimately stabilized (left), whereas for the coupling function of type (1.6) two suprathreshold activation patterns may coexist (right).

1.1.4 The role of subthreshold activation

When weak localized input is applied, the field activation remains below the threshold for triggering the recurrent interactions within the neural population. Consequently, the field activity will decay back to the stable resting state when the external input is removed. While this input-driven state obviously does not represent a working memory function, it may play nevertheless an important functional role in cognitive architectures of interconnected neural fields that model for instance decision processes.

Imagine for example a sensorimotor task in which a decision has to be made to reach towards one of two possible targets located at different positions in space. The neural population activation patterns in the fields represent in this example the parameter movement direction. The decision in which direction to reach is not dependent on the visual input alone but may also be biased for instance by movement history. Input from a neural field reflecting in its activation pattern the memory trace of previous reaching movements may thus preshape the neural populations in the decision field. A subpopulation which gets this additional subthreshold input is more likely to evolve

a suprathreshold excitation and thus to win the competition even if the visual input for the two target directions is equally strong. In models of action preparation, the movement is initiated when a fixed excitation threshold has been reached. Since the level of prior activation affects the rate at which the activation bump rises, all classical effects of task environment on reaction time can be modelled (Erlhagen and Schöner, 2002).

The concept of preshaping as a simple from of learning has been used in various applications. An example on the perceptual level is the fast learning of labels for different objects (Faubel and Schöner, 2008). The dynamic field architecture consists of various interconnected two-dimensional feature label fields that get input from the camera system. Bumps of suprathreshold activation represent objects over a small number of features like colour, shape and size ratio and the associated labels as the second field dimension. The activation of all label feature fields is integrated in a decision field. Learning within the distributed network takes place in a form of laying a memory trace of the existing bump activations of each feature dimension in associated preshaped fields whenever an object has been correctly classified. The preshaped input from previous trials to the feature label fields in turn increases the probability to correctly classify objects when they are presented in different poses.

The preshaping of neural populations by past experience plays also an important role in the dynamic field model of learning the order and timing of demonstrated sequences presented in Chapter 7. Subthreshold input from a sequence memory layer allows the learning system to deal with noisy and potentially ambiguous input signals and to iteratively adjust the precise timing of suprathreshold activation bumps.

1.2 The dynamic neural field approach to robotics

Over the last years, there is an increased interest by part of the robotics community to apply the neuro-plausible processing mechanisms offered by dynamic field theory for the development of brain-inspired control architectures. The main goal is to advance towards a new generation of robots with high-level cognitive capacities by implementing neurophysiological mechanisms supporting human cognition. Real-time cognitive processes are seen as patterns of neuronal activity that continuously change under the

influence of multiple external (e.g., sensory information) and internal (e.g., memory representations) forces. This neurodynamics view on cognition strongly contrasts with the classical artificial intelligence (AI) approach that implements cognitive behaviour as a sequence of logical operations performed on discrete symbols without temporal dimension (Levesque and Lakemeyer, 2008). Although the AI framework still dominates the thinking in the robotics community, it is now widely recognized that the serial planning of complex robot behaviour based on the manipulation of symbols has notoriously problems to cope with real-time interactions in ever changing environments (for discussion see Erlhagen and Bicho, in press).

DNFs have been first introduced into the domain of robotics in navigation tasks to endow the so-called attractor dynamics approach with memory and decision (Schöner et al., 1995, Bicho and Schöner, 1997, Bicho, 2000, for follow up studies Bicho et al., 2008, 2009). In the DNF-based control architectures, the fields are spanned over the heading direction of the robot relative to an arbitrary but fixed frame of reference. The path planning field integrates on-line information about the target location and the location of obstacles coming from on-board sensors. In addition, it receives input from an object memory field that contains self-stabilized activation peaks. They represent the locations of previously detected obstacles that are currently invisible to the sensors due to occlusion. This memorized information is coupled into the movement planning field in the form of inhibitory input, defining undesirable heading directions. Since the field dynamics supports the existence of a single localized activation bump, decision can be made and stabilized even in navigation tasks with several potential targets. The implementations on vehicles equipped with low-level sensors and controlled by non-linear attractor dynamics demonstrate that the navigation behaviour in cluttered environments is quite smooth and robust.

The approach has been later extended to human-robot interaction tasks with the goal to endow the robot with human-like social competences like imitation learning, action understanding and goal inference (Erlhagen and Bicho, 2006). In the robotics community, robot learning by observing an human expert executing a specific task is considered an efficient means to reduce the huge search space in which the robot has to find a solution for a specific problem (Schaal, 1999). DNF architectures that mimic

the neural processing circuits supporting human observational learning and imitation have been applied in simple object manipulation tasks. As a key idea, these architectures implement a direct mapping between neural population representing in their self-stabilized firing patterns a direct mapping between observed motor acts (e.g., a specific grasping behaviour) and corresponding representations in the motor system of the observer (e.g., Andry, 2004; Erlhagen et al., 2006). The capacity to understand the actions of others and infer their goals is fundamental for many joint action task in which two or more agents have to coordinate their decisions to achieve a common goal. The DNF-based control architecture for joint action developed by the group at UM uses action simulation as a core mechanism to achieve this demanding goal (Bicho et al., 2011). The neuronal representation of an observed motor act (e.g., reaching towards a specific object) activates representations of entire motor sequences directed towards a final goal (e.g., reaching, grasping and placing an object at a specific position). The self-sustaining properties of the neuronal population dynamics governed by DNFs allow the system to cope with missing sensory information (e.g., due to occlusion) and to anticipate the action outcomes ahead of their realization. Based on this prediction, the robot then may timely select a complementary behaviour that best serves the team performance (Bicho et al., 2010, 2011).

The thesis work makes two novel contributions to the DNF approach to cognitive robotics. The capacity to organize sequence of behaviours is fundamental for a robot that is supposed to efficiently work in human environments. Many of our daily routine tasks are sequential in nature (e.g., making coffee, preparing the dinner table etc.). The proposed sequence model allows the robot to rapidly learn and memorize short sequences of observed sensorimotor events. Different to other bio-inspired approaches, the learning does not take place as a change in the synaptic connections between different neuronal populations which normally requires a larger number of training experiments (see the neural network approaches by e.g. Elman, 1990; Botvinick and Plaut, 2004; Sousa et al., 2014). In the model, sequential information is reflected by the amplitude of suprathreshold population activity which can be adapted in very few or even only one trial. Moreover, the model does not only learn the order but simultaneously also the timing of sequence elements. Thus far, the important influence of action timing

on fluent and efficient joint action has been to a large extent ignored by the robotics community. We use the fast acquisition of a short musical sequence demonstrated by a human teacher as an example to test the novel predictions of the DNF model in real-world robotics experiments.

1.3 Thesis outline

Part II of the thesis presents analytical and numerical work on the conditions that support the formation of stable multi-bump solutions in response to stationary and transient external input. The analytical studies focus on one-bump and two-bump solutions. All mathematical proofs are only outlined in part II and presented in detail in part V of the thesis. The analytical work is complemented by numerical studies of multi-bump solutions. Part II is organized in four chapters:

- Chapter 2 presents the state of the art of existence and stability studies of local excitations in one-dimensional neural fields.
- Chapter 3 presents a study of the existence and stability of one-bump solutions with and without input.
- Chapter 4 presents a study of the existence and stability of two-bump solutions with and without input.
- Based on the insight from the analysis of two-bumps, Chapter 5 presents analytical and numerical work on the existence and stability of N-bump solutions, for $N \geq 2$.

Part III introduces dynamic neural field models of sequence representation which build on the existence of stable multiple-bumps to implement a working memory function. A real-world robotics experiment of sequence learning is also presented. Part III is organized in four chapters:

- Chapter 6 introduces some basic notations and concepts of sequence representation and learning in the cognitive science that will be used throughout this part of the thesis.

- Chapter 7 presents a dynamic neural field model which exploits the existence of multiple bumps with varying levels of activation to implement a working memory of sequential events.

- Chapter 8 presents an extension of the dynamic neural field model presented in Chapter 7 that is applied to learn and memorize precisely timed sequences of events.

- Chapter 9 validates the theoretical model in a human-robot experiment in which the humanoid robot ARoS learns to execute a musical sequence.

Part IV presents a discussion of results and conclusions for future work.

Part V corresponds to the Appendixes in which all proofs of the Theorems presented in Part III are given. The numerical method used for the simulation studies of the field dynamics is also sketched.

Part II

Mathematical analysis of multi-bump solutions

Chapter 2

Existence and stability of local excitations in one-dimensional neural fields: state of the art

In this chapter, we briefly review the state of the art of studies of local excitation solutions in one-dimensional neural fields, without and with external input (for a recent overview of techniques and results see Coombes, 2005).

2.1 One-bump solution in the absence of external input

In the absence of external input $S(x,t)$ (i.e. $S(x,t) = 0$), Amari (1977) studied the existence and the stability of stationary solutions of (1.1), i.e. solutions given by

$$u(x,t) = \int w(x-y) f\left(u(y,t)\right) dy - h. \tag{2.1}$$

For a given distribution $u(x)$, Amari defines its region of excitation to be the set

$$R[u] = \{x | u(x) > 0\}.$$

A pattern $u(x)$ whose excited region is a finite, open interval,

$$R[u] = (x_1, x_2)$$

is a localized excitation with boundaries at field sites x_1 and x_2. Amari calls a local excitation solution an a-solution, where $a = x_2 - x_1$ is the width of the excited region.

In this case, if $R[u]$ is connected, the pattern is referred as a single-bump, or one-bump solution and has the form $R[u] = (0, a)$. Amari also defines $R[u] = \emptyset$, i.e., $u(x) \leq 0$ for all x so that no region is excited and calls it a $\emptyset$-solution. On the other hand, $R[u] = (-\infty, \infty)$, i.e., $u(x) > 0$ for all x on the whole line is called a ∞-solution.

In order to discuss the existence of one-bump solutions, Amari defines

$$W(x) = \int_0^x w(y)dy \tag{2.2}$$

as the integral of $w(x)$ and the related quantities $W_m = \max_{x>0} W(x)$ and $W_\infty = \lim_{x\to\infty} W(x)$. It follows from the hypothesis (H_1) and (H_2) that $W(x)$ is continuous and odd.

If (2.1) has an one-bump solution, $u(x)$, whose activation is positive over the interval $(0, a)$, then the solution satisfies

$$u(x) = \int_0^a w(x-y)dy - h = W(x) - W(x-a) - h. \tag{2.3}$$

At the point $x = a$, since $W(x)$ is odd and $u(0) = u(a) = 0$, the equation (2.3) reduces to

$$W(a) = h. \tag{2.4}$$

In turn, if $a > 0$ and $h > 0$ satisfy (2.4), then

$$u(x) = W(x) - W(x-a) - h. \tag{2.5}$$

is a single-bump solution of (2.1) for which $R[u] = (0, a)$. For a given $h \geq 0$, (2.4) may have zero, one or two positive solutions, depending on the values of h, W_m and W_∞. In Figure 2.1 we show the integral $W(x)$ corresponding to the coupling function illustrated in Figure 1.1. In this case, $W(x)$ is monotonically increasing for $x > 0$ until it reaches the maximum W_m, and then monotonically decreases. Thus,

$$W_\infty = \lim_{x\to\infty} W(x) = -\infty, \tag{2.6}$$

which implies that the inhibitory connections exist between neurons at any distance in the field. If $0 < h < W_m$, there are two values, a_1 and a_2, which satisfy (2.4), that is, there are two one-bump solutions with different widths for the same value of h. Note that solutions of (1.1) are translationally invariant, that is, if $u(x)$ is a solution, also $u(x-a)$ is a solution for all $a > 0$.

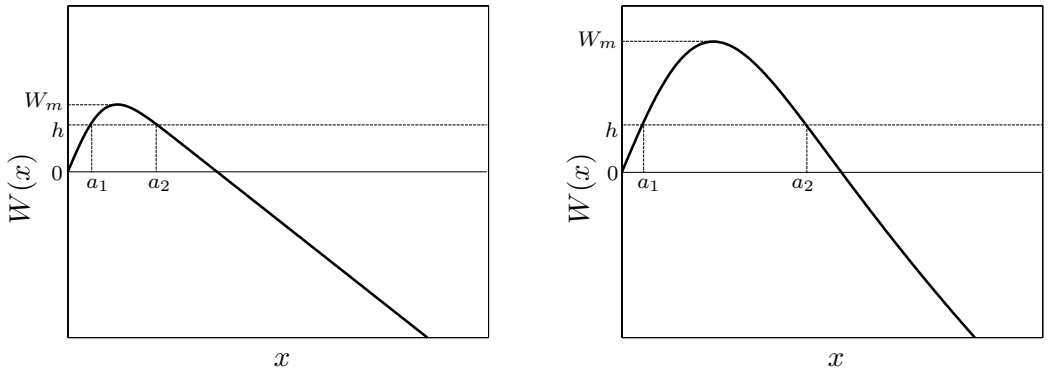

Figure 2.1: The $W(x)$ corresponding to the coupling functions, $w(x)$, illustrated in Figure 1.1.

To analyse the stability of the bumps, Amari reduces the neural field equation to an ordinary differential equation with respect to the boundaries of the excited region. He uses a perturbation approach to show that an one-bump solution of width a is stable if and only if

$$\frac{dW(a)}{da} = w(a) < 0. \tag{2.7}$$

When two solutions of (2.4) exist, as illustrated in Figure 2.1, the solution of smaller width corresponding to a_1 is unstable and the solution of larger width corresponding to a_2 is stable. Note that stability refers here to wave form stability since small external perturbation to the field may change the location of the bumps within the field (for follow up studies of stable bumps based on Amari's ideas see, e.g., Pinto and Ermentrout, 2001; Guo and Chow, 2005a,b).

Depending on the parameter h, a field with a localized initial excitation can show two types of behaviour (Figure 2.2). If $h > W_m$ the dynamics is monostable, all initial excitation converges to the stable resting state $(-h)$. If $0 < h < W_m$, the field dynamics is bistable. An initial localized excitation of a width larger than a_1 converges to the stable bump of width a_2. Initial excitation that is not sufficiently strong or is too narrow will return to resting state over time. This bistable behaviour of the dynamic is crucial for the implementing a memory function in the applications of DNF theory, since a transient localized input of sufficient strength may switch between the two attractors.

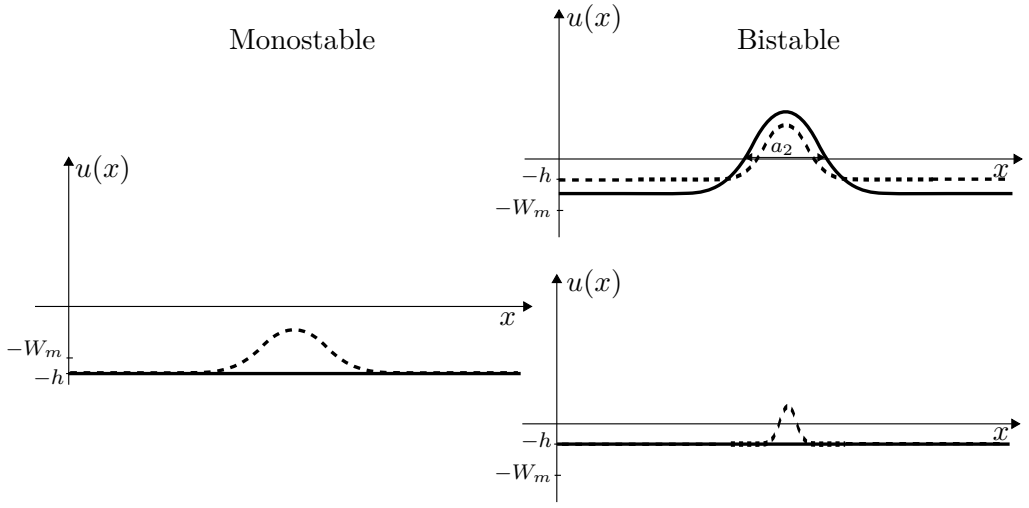

Figure 2.2: Stable resting state h as single attractor (monostable, left panel). Stable bump (top right) and stable resting state (bottom right) coexist as attractors (bistable, rights panels). Dashed lines represent the initial excitation.

2.2 Two-bump solutions in the absence of external input

Laing and Troy (2003) extended the analysis of the Amari model to the case of two-bumps. They defined a two-bump solution as a solution whose region of excitation is the union of two disjoint, finite, open intervals with $R[u] = (0, a) \cup (b, c)$. Thus, a solution $u(x)$ is called a two-bump solution if there are values $0 < a < b < c < \infty$ such that

$$\begin{cases} u > 0 & \text{on}(0, a) \cup (b, c), \\ u(0) = u(a) = u(b) = u(c) = 0, & \\ u < 0 & \text{otherwise.} \end{cases} \tag{2.8}$$

The general form of an equal-width two-bump solution, $c = a + b$, is

$$u(x) = W(x) - W(x - a) + W(x - b) - W(x - a - b) - h. \tag{2.9}$$

Consequently, the necessary conditions for the existence of such solutions are

$$2W(b) - W(a + b) - W(b - a) = 0 \tag{2.10}$$

and

$$W(a) - W(b) + W(a + b) - h = 0. \tag{2.11}$$

It was shown by Laing and Troy (2003) that there is an interval of values for a and corresponding values for $b > a$ such that condition (2.10) is satisfied. Since

it is not easy to determine the sign of h for these values of a and b, Murdock et al. (2006) investigated the existence of two-bump solutions, with the focus on the sign of h. Assuming that $h = |W(p)|$ with $p \in \{a, b, c\}$, they determined parameter values that satisfy the conditions (2.10) and (2.11). They start their proof by introducing the following definition of a quasi-solution.

Definition 1 *Given a triple of positive numbers, $\tau = (a, b, c)$, with $a < b < c$, and $h \geq 0$, the function $u_\tau(x) = W(x) - W(x-a) + W(x-b) - W(x-c) - h$ is defined. If $p \in \{a, b, c\}$, $h = |W(p)|$, and u_τ satisfies $u_\tau(0) = u_\tau(a) = u_\tau(b) = u_\tau(c) = 0$, then u_τ is said to be a p-quasi-solution of (1.1).*

If w is chosen as a "Mexican hat" coupling function with $W_\infty \geq 0$, the authors prove the non-existence of a a-quasi-solutions and the existence of both a b-quasi-solutions and a c-quasi-solutions. However, it is not easy to determine the interval of values of a and b that satisfy the two conditions (2.10) and (2.11). In this thesis, we prove for the coupling function with several zeros-crossing defined in (1.6) that there are specific values of a and b that satisfy the two conditions if $h = |W(a)|$.

2.2.1 Stability of two-bump solutions

The study of the stability of local excitation pattern determines the dynamical properties of the field. For the stability analysis we adopt the approach introduced by Amari (1977) for one-bumps and latter applied by Laing and Troy (2003) for two-bumps. The approach derives equations for the change in width of the two excited regions under small perturbation, and uses linear stability analysis to derive the stability conditions. Let the excited region at time t be

$$R[u(x,t)] = (x_1(t), x_2(t)) \cup (x_3(t), x_4(t)) \tag{2.12}$$

and let

$$c_1 = \frac{\partial u\,(x_1,t)}{\partial x},\ -c_2 = \frac{\partial u\,(x_2,t)}{\partial x},\ c_3 = \frac{\partial u\,(x_3,t)}{\partial x},\ -c_4 = \frac{\partial u\,(x_4,t)}{\partial x}, \tag{2.13}$$

be the spatial slopes of $u(x,t)$ at the boundaries x_1, x_2, x_3 and x_4 of the excited region. After a short time dt, $u(x,t)$ changes to $u(x, t+dt)$ and the intervals of the excited

region become $(x_1(t+dt), x_2(t+dt))$ and $(x_3(t+dt), x_4(t+dt))$ that satisfy

$$u\left(x_i(t+dt), t+dt\right) = 0$$

where $x_i(t+dt) = x_i + dx_i$ $(i = 1, 2, 3, 4)$.
Assuming that dx_i and dt are infinitesimally small, we differentiate $u\left(x_i, t\right)$ for $i = 1, 2, 3, 4$ and obtain

$$\frac{d}{dt}u\left(x_i, t\right) = \frac{\partial u\left(x_i, t\right)}{\partial x}\frac{dx_i}{dt} + \frac{\partial u\left(x_i, t\right)}{\partial t}, \quad i = 1, 2, 3, 4 \tag{2.14}$$

We thus have

$$\frac{dx_i}{dt} = -\frac{1}{\frac{\partial u(x_i,t)}{\partial x}}\frac{\partial u\left(x_i, t\right)}{\partial t}, \quad i = 1, 2, 3, 4 \tag{2.15}$$

Since $u\left(x_i, t\right) = 0$ at time t, we have from (1.1)

$$\begin{array}{rcl} \frac{\partial u(x_i,t)}{\partial t} & = & \int_{x_1}^{x_2} w(x_i - y)dy + \int_{x_3}^{x_4} w(x_i - y)dy - h \\ & = & W(x_i - x_1) - W(x_i - x_2) + W(x_i - x_3) - W(x_i - x_4) - h \end{array} \tag{2.16}$$

Substituing (2.13) into (2.15) and using (2.16), we have

$$\frac{dx_1}{dt} = \frac{1}{c_1}\left[W(x_1 - x_2) - W(x_1 - x_3) + W(x_1 - x_4) + h\right], \tag{2.17}$$

$$\frac{dx_2}{dt} = \frac{1}{c_2}\left[W(x_2 - x_1) + W(x_2 - x_3) - W(x_2 - x_4) - h\right], \tag{2.18}$$

$$\frac{dx_3}{dt} = \frac{1}{c_3}\left[-W(x_3 - x_1) + W(x_3 - x_2) + W(x_3 - x_4) + h\right], \tag{2.19}$$

$$\frac{dx_4}{dt} = \frac{1}{c_4}\left[W(x_4 - x_1) - W(x_4 - x_2) + W(x_4 - x_3) - h\right]. \tag{2.20}$$

Let

$$a(t) = x_2(t) - x_1(t), \quad b(t) = x_3(t) - x_1(t), \quad c(t) = x_4(t) - x_1(t), \tag{2.21}$$

where $a(t)$ is the width of the first bump, $b(t) - a(t)$ is the distance between the bumps, and $c(t) - b(t)$ is the width of the second bump.

Using (2.21) and by subtracting (2.18) from (2.17), (2.19) from (2.17), and (2.20) from (2.17), we have:

$$\frac{da}{dt} = \left(\frac{1}{c_1} + \frac{1}{c_2}\right)[W(a) - h] + \frac{1}{c_1}[W(c) - W(b)] + \frac{1}{c_2}[W(c-a) - W(b-a)], \tag{2.22}$$

$$\frac{db}{dt} = \left(\frac{1}{c_1} + \frac{1}{c_3}\right)[-W(b)] + \frac{1}{c_1}[W(a) + W(c) - h] + \frac{1}{c_3}[W(b-a) - W(c-b) + h], \tag{2.23}$$

$$\frac{dc}{dt} = \left(\frac{1}{c_1} + \frac{1}{c_4}\right)[W(c) - h] + \frac{1}{c_1}[W(a) - W(b)] + \frac{1}{c_4}[W(c-b) - W(c-a)]. \tag{2.24}$$

Considering that the two bumps have equal width, we have

$$c(t) = a(t) + b(t), \forall t > 0. \tag{2.25}$$

Then, $\frac{dc}{dt} = \frac{da}{dt} + \frac{db}{dt}$ implies that $c_3 = c_2$ and $c_4 = c_1$. Thus, the condition (2.25) reduces (2.22)-(2.24) to

$$\frac{da}{dt} = \frac{1}{c_1}[W(a) + W(a+b) - W(b) - h] + \frac{1}{c_2}[W(a) + W(b) - W(b-a) - h], \tag{2.26}$$

$$\frac{db}{dt} = \frac{1}{c_1}[W(a) + W(a+b) - W(b) - h] + \frac{1}{c_2}[W(b-a) - W(a) - W(b) + h], \tag{2.27}$$

Subtracting (2.27) and (2.26) we obtain

$$\frac{db}{dt} - \frac{da}{dt} = \frac{2}{c_2}[W(b-a) - W(a) - W(b) + h], \tag{2.28}$$

The equations (2.26) and (2.28) describe the change of the lengths of the bumps and the distance between the bumps, respectively. The stationary lengths of (2.26) and (2.28) are given by

$$W(a) + W(a+b) - W(b) - h = 0, \tag{2.29}$$

$$W(a) + W(b) - W(b-a) - h = 0, \tag{2.30}$$

in agreement with (2.10) and (2.11).

We define G and H to be the right hand sides of (2.26) and (2.28), respectively. The Jacobian matrix J of (2.26) and (2.28) at $(a, b, a+b)$ is given by

$$J = \begin{pmatrix} G_a & G_b \\ H_a & H_b \end{pmatrix}, \tag{2.31}$$

where G_a, G_b, H_a and H_b are partial derivatives evaluated at $(a, b, a+b)$. They are given by

$$G_a = \frac{1}{c_1}\left[w(a) + w(a+b)\right] + \frac{1}{c_2}\left[w(a) + w(b-a)\right], \tag{2.32}$$

$$G_b = \frac{1}{c_1}\left[w(a+b) - w(b)\right] + \frac{1}{c_2}\left[w(b) - w(b-a)\right], \tag{2.33}$$

$$H_a = -\frac{2}{c_2}\left[w(b-a) + w(a)\right], \tag{2.34}$$

$$H_b = \frac{2}{c_2}\left[w(b-a) - w(b)\right]. \tag{2.35}$$

The eigenvalues, λ, of J satisfy

$$\lambda^2 - (G_a + H_b)\,\lambda + G_a H_b - G_b H_a = 0. \tag{2.36}$$

If the two eigenvalues have negative real part, then $(a, b, a+b)$ is a stable solution with respect to perturbations that preserve the equal-width condition. However, if at least one eigenvalue has positive real part, then $(a, b, a+b)$ is unstable.

Note that if the trace of J is negative and the determinant of J is positive we can conclude that both eigenvalues of the Jacobian matrix have negative real parts, that is, $(a, b, a+b)$ is a stable solution if the following conditions hold

$$G_a + H_b < 0 \tag{2.37}$$

and

$$G_a H_b - G_b H_a > 0. \tag{2.38}$$

We have,

$$G_a + H_b = \frac{1}{c_1}\left[w(a) + w(a+b)\right] + \frac{1}{c_2}\left[w(a) + 3w(b-a) - 2w(b)\right], \tag{2.39}$$

and

$$G_a H_b - G_b H_a = \frac{2}{c_1 c_2}\left[2w(a+b)w(b-a) - 2w(a)w(b) + \left[w(a) - w(b)\right]\left[w(a+b) + w(b-a)\right]\right]. \tag{2.40}$$

For lateral inhibition type of coupling, Laing and Troy (2003) found that families of two-bump solutions exist, but none of the solutions is stable. By using a coupling function with three positive zeros, they found that both stable and unstable two-bump solutions may co-exist.

2.3 Multi-bump solutions in the absence of external input

N-bump solutions refer to a solution with $N > 1$ disjoint, finite connected intervals of excitation (Laing et al., 2002; Laing and Troy, 2003). Thus, a solution $u(x)$ of (2.1) is called N-bump solution if there are values $a_0 < a_1 < a_2 < a_3 < ... < a_{2N-1}$ such that

$$\begin{cases} u > 0 & \text{on} \quad (a_0, a_1) \cup ... \cup (a_{2N-2}, a_{2N-1}) \\ u(a_0) = u(a_1) = ... = u(a_{2N-1}) = 0, & \\ u < 0 & \text{otherwise.} \end{cases} \tag{2.41}$$

In (Laing et al., 2002), the authors investigated for a specific coupling function given by (1.5) the existence and stability of N-bump solutions, for a smooth, sigmoidal transfer function f, using Fourier techniques. For the case of the Heaviside function f, they conjecture that both stable and unstable N-bump stationary solutions might exist for $N \geq 1$. Following this conjecture, we study, in Chapter 5, analytically and numerically the existence and the stability of N-bump solutions for the Amari model with specific coupling function of type (1.6).

2.4 One-bump solution with external input

Kubota et al. (2009) extended the results of the Amari's study of bumps in a lateral inhibition type field with stationary localized input to the case of inputs with arbitrary shape. They examined the conditions for the existence of a localized excitation with $R[u] = (x_1^*, x_2^*)$ when arbitrary time invariant input $S(x)$ is applied. A stationary solution of local excitation with $R[u] = (x_1^*, x_2^*)$ is

$$\begin{aligned} u(x) &= \int_{x_1^*}^{x_2^*} w(x-y)dy - h + S(x) \\ &= W(x - x_1^*) - W(x - x_2^*) - h + S(x). \end{aligned} \tag{2.42}$$

Defining $G(x) \equiv G[x; x_1^*, x_2^*] = -W(x - x_1^*) + W(x - x_2^*) + h$, the three conditions for the existence of steady local excitation solution are:

Steady condition 1: $S(x) = G(x)$, if $x = x_1^*, x_2^*$;

Steady condition 2: $S(x) > G(x)$, if $x_1^* < x < x_2^*$;

Steady condition 3: $S(x) < G(x)$, if $x < x_1^*, x_2^* < x$.

Note that the conditions for the existence of steady local excitations are satisfied for all coupling function $w(x)$ with $w(x) = w(-x)$ and $w(0) > 0$.
According to Kubota et al. (2009), a steady solution of local excitation with $R[u] = (x_1^*, x_2^*)$ is:

- stable if $S^*x_1 > S^*x_2$ and $w(a^*)\,(S^*x_1 - S^*x_2) + S^*x_1 S^*x_2 < 0$;
- unstable if $S^*x_1 < S^*x_2$ and $w(a^*)\,(S^*x_1 - S^*x_2) + S^*x_1 S^*x_2 > 0$;

where $S^*x_i = \frac{d(Sx_i)}{dx}, i = 1, 2$.

2.5 Conclusion

In this chapter, we reviewed the existence and stability studies of one-bump and two-bump solutions of the Amari model in the absence of external input. We also presented the definition of N-bump solution that we is used in the following chapters. For a field with external input, we summarized the results of a recent study that generalize Amari's original analysis to the case of an arbitrary stationary input pattern.

Chapter 3

Analysis of one-bump solutions

In this chapter, we analyse and compare the conditions for the existence and stability of one-bump solutions of (1.1) with coupling function of class (1.6) in the absence of external input, $S(x,t) = 0, \forall t > 0$, and in the presence of an unimodal symmetric input. For the following analysis, we assume that f is the Heaviside firing rate function (1.2) and h is a fixed positive constant. We discuss the field response to a stationary or a transient unimodal symmetric input in terms of its width.

For the particular coupling function defined by (1.6) we add the following condition:

(H_8) w has infinite positive zeros at values $z_n = -\frac{\arctan\left(\frac{1}{k}\right)}{\alpha} + \frac{n\pi}{\alpha}$ for all $n \in \mathbb{N}$.

The integral of $w(x)$ defined in (1.6), for $x \geq 0$ is

$$W(x) = -p_1 \left(e^{-kx} \left(p_3 \sin(\alpha x) + p_2 \cos(\alpha x) \right) - p_2 \right) \tag{3.1}$$

where $p_1 = \frac{A}{k^2+\alpha^2}$, $p_2 = \alpha k + k$ and $p_3 = k^2 - \alpha$.

3.1 One-bump in the absence of external input

Following Amari (1977), the conditions for the existence of an one-bump solution are given by the following theorem:

Theorem 1 *Suppose that hypotheses (H_1) and (H_2) hold. The equation $u(x) = W(x) - W(x-a) - h$ defines a one-bump solution with $R[u] = (0, a)$ if and only if the following*

three conditions are satisfied

(i) $W(x) - W(x-a) - h = 0$, *if* $x = a$,

(ii) $W(x) - W(x-a) - h > 0$, *if* $x \in \left(\frac{a}{2}, a\right)$,

(iii) $W(x) - W(x-a) - h < 0$, *if* $x > a$.

The proof of this Theorem is given in Appendix A.

For a coupling function of lateral inhibition type, one can conclude that $u(x) = W(x) - W(x-a) - h$ defines an one-bump solution if the condition (2.4) (that is equivalent to condition *(i)* of Theorem 1) is satisfied. However, for a coupling function $w(x)$ given by (1.6) this is not true. For example, consider $A = 2$, $\alpha = 0.3$, $k = 0.08$ with $h = W(11.5)$ (Figure 3.1, left) and $A = 2$, $\alpha = 0.3$, $k = 0.05$ with $h = W(9)$ (Figure 3.1, right) we have that the solutions of $W(a) = h$ are $a = 11.5$ and $a = 9$, respectively. These solutions satisfy the condition (2.4) but $u(x)$ is not negative for all $x > a$ as we can confirm in Figure 3.2.

For a given $h > 0$, if (H_1), (H_2), (H_6), (H_7) and (H_8) hold the equation defined in condition *(i)* of Theorem 1 may have zero, one, two or more solutions. Figure 3.1 (left) illustrates that there is no solution if $h > W(z_1)$, there is one solution if $h = W(z_1)$ or $h < W(z_2)$, there are exactly two positive solutions if $W(z_3) < h < W(z_1)$ and there are at least three solutions if $W(z_2) \leq h \leq W(z_3)$.

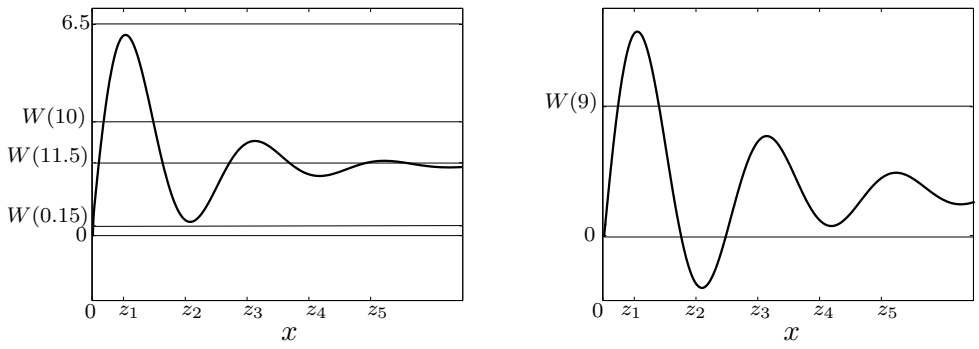

Figure 3.1: Plot of $W(x)$ given by (3.1) with $A = 2$, $\alpha = 0.3$, $k = 0.08$ (*left*) and $k = 0.05$ (*right*). The lines are defined by $h = W(0.15)$, $h = W(10)$, $h = W(11.5)$ and $h = 6.5$ (*left*) and $h = W(9)$ (*right*).

Let a be a value that satisfies condition *(i)*. From the two examples of Figure 3.2 we conjecture that when $h < W(z_3)$ or $W(z_2) < 0$, $u(x) = W(x) - W(x-a) - h$

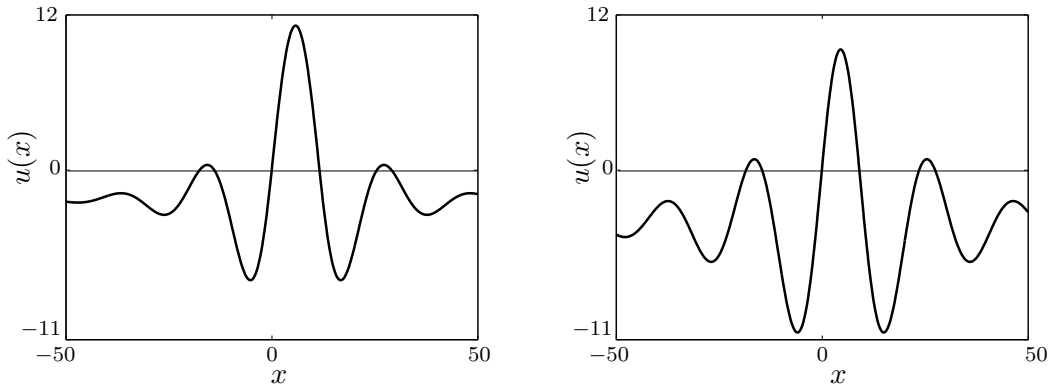

Figure 3.2: Plot of solution (2.3) when W is given by (3.1) with $A = 2$, $\alpha = 0.3$, $k = 0.08$ (*left*) and $k = 0.05$ (*right*). The value of h is $W(11.5)$ (*left*) and $W(9)$ (*right*).

may not define an one-bump solution. In order to derive a necessary condition for the existence of one-bump solutions, we add the following hypothesis:

(H_9) $W(z_2) > 0$.

Note that $W(z_2)$ is negative if the value of k is sufficiently small, i.e., when the oscillations of w are more pronounced.

Theorem 2 *Assume that hypotheses* (H_1), (H_2), $(H_6) - (H_9)$ *hold. Let* $a \in (z_1, z_2)$ *be a solution of* $W(a) = h$. *If* $h > W(z_3)$ *then*

$$u(x) = W(x) + W(x - a) - h \tag{3.2}$$

defines a stable one-bump solution.

The proof of this Theorem is given in Appendix A.

For an one-bump solution of width a if we choose $\alpha = \frac{\pi}{a}$ and $h = W\left(\frac{\pi}{\alpha}\right)$, then $\frac{\pi}{\alpha} \in (z_1, z_2)$ holds and the stability condition (2.7) is satisfied. Suppose $W(z_2) > 0$, to conclude that $u(x) = W(x) + W(x - a) - h$ defines an one-bump solution, by Theorem 2, $h > W(z_3)$ must hold. Consider the following two important properties of (3.1).

Lemma 1 *Let* n *be a natural number,* x *be any non-negative real number, and* W *is defined by (3.1). Then*

$$W\left(x + \frac{n\pi}{\alpha}\right) = \begin{cases} -e^{-\frac{kn\pi}{\alpha}} W(x) + p_1 p_2 \left(1 + e^{-\frac{kn\pi}{\alpha}}\right), \textit{if } n \textit{ is odd} \\ e^{-\frac{kn\pi}{\alpha}} W(x) + p_1 p_2 \left(1 - e^{-\frac{kn\pi}{\alpha}}\right), \textit{if } n \textit{ is even} \end{cases}, \tag{3.3}$$

and

$$W\left(x-\frac{n\pi}{\alpha}\right)=\begin{cases} -e^{\frac{kn\pi}{\alpha}}W(x)+p_1p_2\left(1+e^{\frac{kn\pi}{\alpha}}\right), \textit{if } n \textit{ is odd} \\ e^{\frac{kn\pi}{\alpha}}W(x)+p_1p_2\left(1-e^{\frac{kn\pi}{\alpha}}\right), \textit{if } n \textit{ is even} \end{cases}, \tag{3.4}$$

hold, if $x-\frac{n\pi}{\alpha}>0$.

The proof of this Lemma is given in Appendix A.

Lemma 2 *Assume that* W *is defined by (3.1) and that* (H_1) *holds. Then* $W\left(\frac{\pi}{\alpha}\right) > W(z_3)$.

The proof of this Lemma is given in Appendix A.

In conclusion, if we choose k such that $W(z_2)>0$, $\alpha=\frac{\pi}{a}$ and $h=W\left(\frac{\pi}{\alpha}\right)$, the conditions (2.4) and (2.7) are satisfied and by Lemma 2 $h>W(z_3)$. Consequently, by Theorem 2, $u(x)=W(x)+W(x-a)-h$ defines a stable one-bump solution.

3.2 One-bump with external input

Assume that the external input $S(x)$ has an unimodal and symmetric shape centered at $x=0$ and thus satisfies the following characteristics:

(SH_1) $S(x)$ is continuous on $\mathbb{R}$ and symmetric, i.e., $S(-x)=S(x)$ for all $x\in\mathbb{R}$.

(SH_2) $S(x)>0$ on an interval $(-\overline{x},\overline{x})$, $S(x)<0$ on $(-\infty,-\overline{x})\cup(\overline{x},\infty)$, and $S(-\overline{x})=S(\overline{x})=0$

(SH_3) $S(x)$ is increasing on $(-\infty,0]$ and is decreasing on $[0,\infty)$.

An example of external input with unimodal and symmetric shape localized around $x=0$ is given by

$$S(x)=S_s e^{\left(-\frac{x^2}{2\sigma^2}\right)}-S_i, \tag{3.5}$$

where $S_s>0$ and $\sigma>0$ describe the amplitude and the standard deviation, respectively, and $S_i>0$ is a constant. Note that the constant negative part, $-S_i$, could be also integrated in the globally inhibitory parameter h of the field dynamics. We use it in the definition of the Gaussian input to define a finite input width.

Considering, without loss of generality, $a^* = x_2^* - x_1^*$ the length of a localized excitation in the field, a stationary solution of local excitation with $R[u] = (0, a^*)$ is thus given by

$$\begin{aligned} u(x) &= \int_0^{a^*} w(x-x')dx' + h + S\left(x - \tfrac{a^*}{2}\right) \\ &= W(x) - W(x-a^*) + h + S\left(x - \tfrac{a^*}{2}\right). \end{aligned} \tag{3.6}$$

Defining $G(x) \equiv G[x; a^*] = -W(x) + W(x-a^*) - h$, the three conditions for the existence of steady local excitation solution described in Section 2.4 become:

Steady condition 1: $S\left(x - \frac{a^*}{2}\right) = G(x)$, if $x = a^*$;

Steady condition 2: $S\left(x - \frac{a^*}{2}\right) > G(x)$, if $0 < x < a^*$;

Steady condition 3: $S\left(x - \frac{a^*}{2}\right) < G(x)$, if $x > a^*$.

The steady condition 1 corresponds to the following condition given by Amari (1980). The width $a^* = x_2^* - x_1^*$ of the equilibrium local excitation has to satisfy

$$h - S\left(\frac{a^*}{2}\right) = W(a^*). \tag{3.7}$$

3.2.1 Stability of one-bump solutions with input

Now we analyze the stability of a local excitation which is not necessarily an equilibrium solution with $R[u] = (x_1^*(t), x_2^*(t))$. Following the approach taken by Amari (1977), the motion of the boundaries of the excited region is given by

$$\frac{dx_i^*}{dt} = -\frac{1}{\tau c_i}\left[W\left(x_2^* - x_1^*\right) - h + S\left(x_i\right)\right], i = 1, 2, \tag{3.8}$$

where $c_i = \frac{\partial u(x_i,t)}{\partial x}$.

Let $a^* = x_2^* - x_1^*$, and $S(x)$ a function that satisfies (SH_1), (SH_2) and (SH_3). Subtracting $\frac{dx_2^*}{dt}$ from $\frac{dx_1^*}{dt}$, we have

$$\frac{da^*}{dt} = \frac{1}{\tau}\left(\frac{1}{c_1} + \frac{1}{c_2}\right)\left[W\left(a^*\right) - h + S\left(\frac{a^*}{2}\right)\right]. \tag{3.9}$$

The equilibrium length of (3.9) is given by

$$W\left(a^*\right) - h + S\left(\frac{a^*}{2}\right) = 0. \tag{3.10}$$

in agreement with (3.7). Moreover, an equilibrium a^* is stable if

$$w\left(a^*\right) + \frac{1}{2}S'\left(\frac{a^*}{2}\right) < 0 \tag{3.11}$$

and unstable if

$$w\left(a^*\right) + \frac{1}{2}S'\left(\frac{a^*}{2}\right) > 0, \tag{3.12}$$

where $S'\left(\frac{a^*}{2}\right)$ denotes the derivative of the external input at $x = \frac{a^*}{2}$. From (SH_3) we have $S'\left(\frac{a^*}{2}\right) < 0$. Thus, the condition $w(a^*) < 0$ is sufficient to conclude that a^* is the width of a stable one-bump solution.

3.3 Field response to an unimodal and symmetric external input

When the initial state of the field is $u(x) = -h < 0$ ($\emptyset$-solution), depending on the strength of the stationary input, two situations may occur:

- the field remains in the off-state if $S(0) \leq h$;
- the field develops one or more localized bumps if $S(0) > h$.

Using the coupling function defined in (1.6), the excited region created by an external input with $S(0) > h$ depends on the input shape. Figure 3.3 (top) shows snapshots of local excitation pattern in the presence of a stationary input given by (3.5) with equal amplitude but three different widths is applied. Depending of the input width, the localized patterns converge to different stable states when the input is removed (Figure 3.3, bottom). They converge to the stable resting state (left), an one-bump solution (middle) and a two-bump solution (right). Figure 3.4 shows the plot of the solutions of equation (3.7) for the three cases.

Theorem 3 gives the necessary conditions on the input shape that guarantees that there is an unique $a^* \in (z_1, z_2)$ of (3.7) for $h = W\left(\frac{\pi}{\alpha}\right)$.

Theorem 3 *Assume that hypotheses* (H_1), (H_2), $(H_6) - (H_9)$, *and* $(SH_1) - (SH_3)$ *hold. If* $S(0) > W\left(\frac{\pi}{\alpha}\right)$, $S\left(\frac{z_1}{2}\right) > 0$ *and* $S\left(\frac{z_2}{2}\right) < 0$ *then the equation*

$$W\left(\frac{\pi}{\alpha}\right) - S\left(\frac{x}{2}\right) = W(x) \tag{3.13}$$

has an unique positive solution a^* *that belongs to* (z_1, z_2).

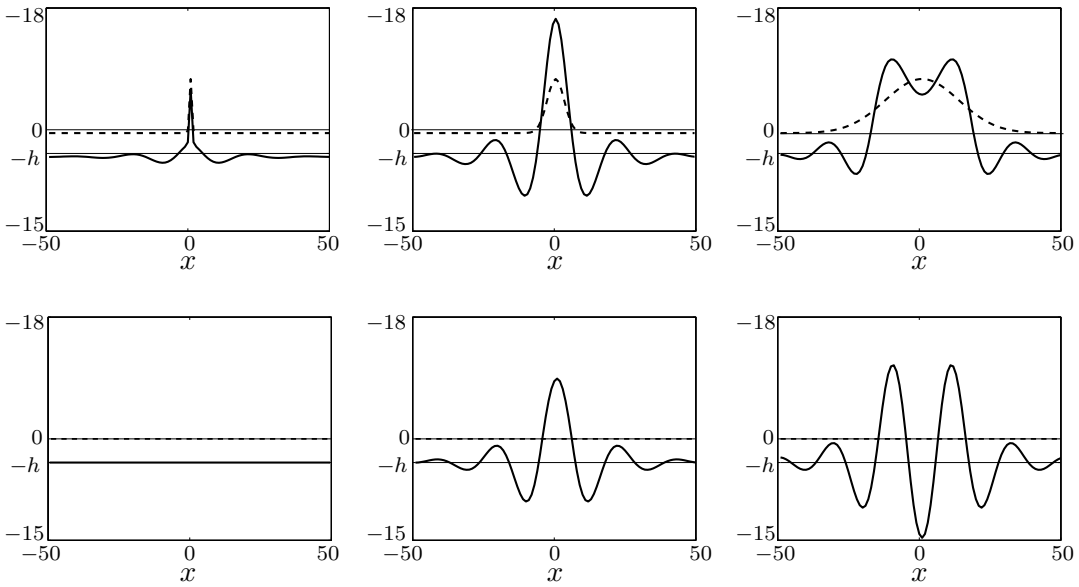

Figure 3.3: Activity u (solid lines) with $h = W(10)$, w defined in (1.6) with $A = 2$, $k = 0.08$ and $\alpha = \frac{\pi}{10}$ and invariant external input S(dashed lines) with $S_s = 8$ and $S_i = 0.5$ and different widths, $\sigma = 0.4$ (left), $\sigma = 3$ (middle), $\sigma = 13$ (right). $S(x) \neq 0$ (top) and $S(x) = 0$ (bottom).

The proof of this Theorem is given in Appendix A.

Note that since $w(x) < 0$ for $z_1 < x < z_2$ the equilibrium local excitation of width a^* is stable.

The following numerical example shows the range of input widths that lead to a stable one-bump. Consider the coupling function w given by (1.6) with $A = 2$, $k = 0.08$, and $\alpha = \frac{\pi}{10}$, $h = W(10)$, and $S(x)$ given by (3.5) with $S_s = 8$, $S_i = 0.5$ and $\sigma > 0$. In this example, $S(0) = 7.5 > W(10)$, thus by Theorem 3 if $S\left(\frac{z_1}{2}\right) > 0$ and $S\left(\frac{z_2}{2}\right) < 0$ there exists a value $a^* \in (z_1, z_2)$ such that $W(10) - S\left(\frac{a^*}{2}\right) = W(a^*)$. Figure 3.5 shows the values of $S\left(\frac{z_1}{2}\right)$ and $S\left(\frac{z_2}{2}\right)$ as a function of $\sigma \in [0, 6]$. Since $S\left(\frac{z_1}{2}\right) > 0$ at $\sigma > 1.1156$ and $S\left(\frac{z_2}{2}\right) < 0$ at $\sigma < 3.2389$,we can conclude that for $1.1156 < \sigma < 3.2389$ there exists $a^* \in (z_1, z_2)$ such that $W(10) - S\left(\frac{a^*}{2}\right) = W(a^*)$.

It is easy to see that the excitation pattern generated by the input is in the basis of attractor of the equilibrium width solution $a = \frac{\pi}{\alpha}$ when the input is removed. Let $a^*(t)$ be the width of the excited region at time t, the equation with $S(x,t) = 0$ that describes the change of width is given by

$$\frac{da^*}{dt} = \frac{1}{\tau c}\left[W(a^*) - h\right] \tag{3.14}$$

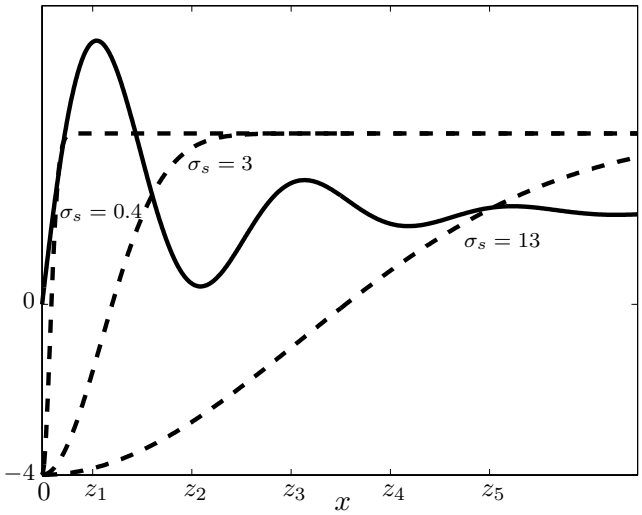

Figure 3.4: An example of the intersection of $h - S\left(\frac{x}{2}\right)$ (dashed lines) with $W(x)$ (solid line) defined in (3.1) with $A = 2$, $\alpha = \frac{\pi}{10}$ and $k = 0.08$, and $h = W(10)$. The input parameters are $S_s = 8$, $S_i = 0.5$, and $\sigma_s \in \{0.4, 3, 13\}$.

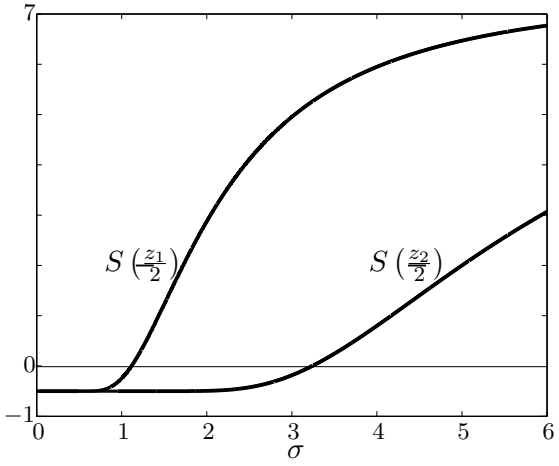

Figure 3.5: Representation of the values of $S\left(\frac{z_1}{2}\right)$ and $S\left(\frac{z_2}{2}\right)$ for each $\sigma \in [0, 6]$.

with $c = \frac{\partial u\left(-\frac{a^*}{2}\right)}{\partial x} = -\frac{\partial u\left(\frac{a^*}{2}\right)}{\partial x} > 0$.

The width increases if $\frac{da^*}{dt} > 0$, decreases if $\frac{da^*}{dt} < 0$ and does not change if $\frac{da^*}{dt} = 0$. Let $h = W\left(\frac{\pi}{\alpha}\right)$ and $W(z_2) > 0$, the width increases if $a^* < \frac{\pi}{\alpha}$, decreases if $a^* > \frac{\pi}{\alpha}$ and does not change if $a^* = \frac{\pi}{\alpha}$. In all cases, the width will tend to the equilibrium width $a = \frac{\pi}{\alpha}$.

3.4 Conclusion

In this chapter, we studied the formation of a stable one-bump in response to an unimodal symmetric input. Choosing $\alpha = \frac{\pi}{a}$, k such that $W(z_2) > 0$ and $h = (\frac{\pi}{\alpha})$, by Lemma 2 and Theorem 2 there exists a stable one-bump solution with width a. To create this solution with a transient unimodal symmetric input, we can conclude from the analysis presented in Sections 3.2 and 3.3 that the shape of S must satisfy $S(0) > W(\frac{\pi}{\alpha})$, $S(\frac{z_1}{2}) > 0$ and $S(\frac{z_2}{2}) < 0$. This means that the amplitude of S must be larger than h and the width of S should neither be too small nor too large.

Chapter 4

Analysis of two-bump solutions

In this chapter, we extend the study of one-bump solutions to two-bump solutions for a specific value of h, $h = W\left(\frac{\pi}{\alpha}\right)$. We start with a proof of the existence of specific values for the bump widths and the distance between bumps that satisfy the necessary conditions for the existence of two-bump solutions in the absence of external input. We then analyse the stability of such solutions. This is followed by the study of the existence and stability of two-bump solutions in the presence of a bimodal symmetric input. In the last section of this chapter, we qualitatively discuss the field dynamics when the field has already one excited region and a second localized input is applied.

4.1 Two-bumps in the absence of external input

The following Theorem proves that there exist specific values of the width a and the distance b that satisfy the two conditions, (2.10) and (2.11) if $h = W\left(\frac{\pi}{\alpha}\right)$ and the coupling function is defined by (1.6).

Theorem 4 *Assume that the coupling function w is given by (1.6). If $h = W\left(\frac{\pi}{\alpha}\right)$ and τ a triple of the form $(a, b, a+b)$, then there exists an a-quasi-solution u_τ of (1.1).*

The proof of this Theorem is given in Appendix A.

4.1.1 Stability of an a-quasi-solution

As described in Subsection 2.2.1, two-bump solutions are stable if conditions (2.37) and (2.38) are satisfied.

	$a \in I_1$	$a \in I_2$	
$b \in I_1$	$w(a+b) > 0$, $w(b-a) > 0$	$w(a+b) < 0$, $w(b-a) < 0$	$w(b) < 0$
$b \in I_2$	$w(a+b) < 0$, $w(b-a) < 0$	$w(a+b) > 0$, $w(b-a) > 0$	$w(b) > 0$
	$w(a) < 0$	$w(a) > 0$	

Table 4.1: Study of the sign of $w(a)$, $w(b)$, $w(a+b)$ and $w(b-a)$.

For w defined in (1.6) and considering its zeros we have:

$$\text{if } x \in (z_{2n-1}, z_{2n}) \text{ for some } \ n \in \mathbb{N}, \text{then } w(x) < 0, \tag{4.1}$$

$$\text{if } x \in (z_{2n}, z_{2n+1}) \text{ for some } \ n \in \mathbb{N}, \text{then } w(x) > 0. \tag{4.2}$$

In order to proceed with the analysis of the signs of the trace and the determinant of the Jacobian J, we chose I_1 of the form (4.1) and I_2 of the form (4.2).

Using the inequalities in the Table 4.1, we conclude that:

- the trace is positive and the determinant is positive when $a \in I_1$ and $b \in I_1$. In this case, the solution is not stable;

- the trace is negative and the determinant is positive when $a \in I_1$ and $b \in I_2$. In this case, the solution is stable.

In the all other cases, the determinant can be either positive or negative. It is thus impossible to conclude about the stability.

Consider $h = W\left(\frac{\pi}{\alpha}\right)$, by Theorem 4 there exists a triple (a, b, c), with $a = \frac{\pi}{\alpha}$, $b > a$ ($W(b) = p_1 p_2$) and $c = b + \frac{\pi}{\alpha}$, that satisfies the conditions (2.10) and (2.11). This solution is stable if $b \in (z_2, z_3)$. Under this conditions, depending of the value of p_3 we have $b = -\frac{\arctan\left(\frac{p_2}{p_3}\right)}{\alpha} + \frac{2\pi}{\alpha}$ if $p_3 < 0$, or $b = -\frac{\arctan\left(\frac{p_2}{p_3}\right)}{\alpha} + \frac{3\pi}{\alpha}$ if $p_3 > 0$, or $\frac{\pi}{2\alpha} + \frac{2\pi}{\alpha}$ if $p_3 = 0$.

Now consider $A = 2$, $\alpha = \frac{\pi}{10}$, $k = 0.08$. For these values (H_1) is satisfied. Assuming $h = W(10)$ by Lemma 2 and as a consequence of Theorem 2 we can conclude that $u(x) = W(x) + W(x-10) - h$ defines an one-bump solution. On the other hand, by Theorem 4 if $a = 10$ and $b = -\frac{\arctan\left(\frac{10\pi+100}{8-125\pi}\right)}{\alpha} + 20$ we have that $u(0) = u(a) = u(b) = u(a+b) = 0$. However, Figure 4.1 shows that (2.9) is not a two-bump solution.

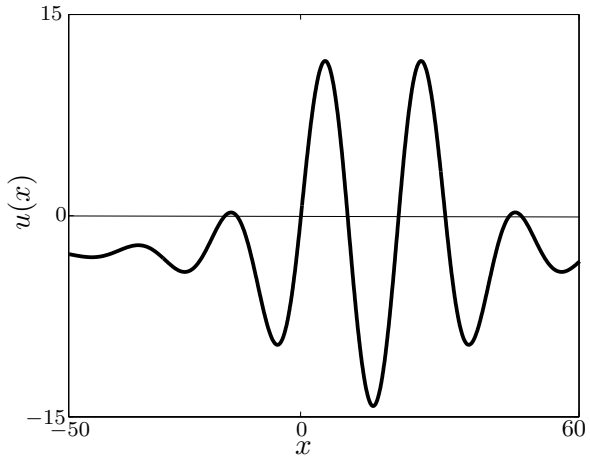

Figure 4.1: Plot of (2.9) when W is given by (3.1) with $A = 2$, $\alpha = \frac{\pi}{\alpha}$, $k = 0.08$. The value of h is $W(10)$ and $a = 10$, $b = -\frac{\arctan\left(\frac{10\pi+100}{8-125\pi}\right)}{\alpha} + 20$.

In order to ensure the existence and the stability of two-bump solution we replace (H_9) by the following hypothesis:

(H_{10}) $W(z_2) > \frac{p_1 p_2}{\left(1+e^{\frac{2k\pi}{\alpha}}\right)}$, with $p_1 = \frac{A}{k^2+\alpha^2}$, $p_2 = \alpha k + k$.

Theorem 5 *Assume that the coupling function w is given by (1.6), and that hypothesis (H_{10}) holds. If $a = \frac{\pi}{\alpha}$ and $b \in (z_2, z_3)$ such that $W(b) = p_1 p_2$, then*

$$u(x) = W(x) - W(x-a) + W(x-b) - W(x-a-b) - W\left(\frac{\pi}{\alpha}\right) \tag{4.3}$$

defines a stable two-bump solution.

The proof of this Theorem is in Appendix A.

4.2 Two-bumps with external input

Now consider that the external input $S(x)$ has a bimodal and symmetric shape. It thus satisfies (SH_1) and the following characteristics:

(SH_4) $S(x) > 0$ on $(-\overline{x_2}, -\overline{x_1}) \cup (\overline{x_1}, \overline{x_2})$, $S(-\overline{x_2}) = S(-\overline{x_1}) = S(\overline{x_1}) = S(\overline{x_2}) = 0$, and $S(x) < 0$ on $(-\infty, -\overline{x_2}) \cup (-\overline{x_1}, \overline{x_1}) \cup (\overline{x_2}, \infty)$;

(SH_5) $S(x)$ is increasing on $\left(-\infty, -\frac{\overline{x_2}-\overline{x_1}}{2}\right)$ and on $\left(0, \frac{\overline{x_2}-\overline{x_1}}{2}\right)$, and is decreasing on $\left(-\frac{\overline{x_2}-\overline{x_1}}{2}, 0\right)$ and on $\left(\frac{\overline{x_2}-\overline{x_1}}{2}, \infty\right)$.

Without restriction, consider a bimodal input localized around $x = 0$ given by

$$S_2(x) = S(x - x_c) + S(x + x_c) \tag{4.4}$$

where S is given by (3.5) and x_c is a positive constant.

The stationary solution of local excitation with equal width $a^* = x_2^* - x_1^* = x_4^* - x_3^*$ and distance between bumps $b^* - a^* = x_3^* - x_2^*$ is defined by

$$\begin{aligned} u(x) &= \int_{x_1^*}^{x_2^*} w(x - x')dx' + \int_{x_3^*}^{x_4^*} w(x - x')dx' - h + S(x) \\ &= W(x - x_1^*) - W(x - x_2^*) + W(x - x_3^*) - W(x - x_4^*) - h + S(x). \end{aligned} \tag{4.5}$$

Since $u(x_1^*) = u(x_2^*) = u(x_3^*) = u(x_4^*) = 0$, it follows that

$$W(x-x_1^*)-W(x-x_2^*)+W(x-x_3^*)-W(x-x_4^*)-h+S(x) = 0, \text{ if } x = x_1^*, x_2^*, x_3^*, x_4^*. \tag{4.6}$$

Since $S(x)$ is symmetric with respect to $x = 0$, the excited region of $u(x)$ is $\left(-\frac{a+b}{2}, -\frac{b-a}{2}\right) \cup \left(\frac{a+b}{2}, \frac{b-a}{2}\right)$ and the four equations (4.5) can be reduced to

$$W(a^*) + W(b^*) - W(b^* - a^*) - h + S\left(\frac{b^* - a^*}{2}\right) = 0, \tag{4.7}$$

and

$$W(a^*) - W(b^*) + W(a^* + b^*) - h + S\left(\frac{b^* - a^*}{2}\right) = 0. \tag{4.8}$$

4.2.1 Stability of two-bump solutions with input

In the following we examine the stability of a steady local excitation solution with $R[u] = (x_1^*, x_2^*) \cup (x_3^*, x_4^*)$. By the approach similar to Subsection 4.1.1, the motion of the boundaries of the excited region are given by

$$\frac{dx_i^*}{dt} = -\frac{1}{\tau c_i}\left[W(x_i^* - x_1^*) - W(x_i^* - x_2^*) + W(x_i^* - x_3^*) - W(x_i^* - x_4^*) - h + S(x_i)\right] \tag{4.9}$$

where $c_i = \frac{\partial u(x_i,t)}{\partial x}$.

Let $a^* = x_2^* - x_1^*$, $b^* = x_3^* - x_1^*$, $c^* = x_4^* - x_1^*$, and assuming that the two excited regions and S are symmetrical with respect to the x axis and with equal width, i.e., $c^* = a^* + b^*$, $x_4 = -x_1$, $x_3 = -x_2$, $S(x_1^*) = S(x_4^*)$ and $S(x_2^*) = S(x_3^*)$, we have

$$\begin{aligned} \frac{da^*}{dt} = &\frac{1}{\tau c_1}\left[W(a^*) - W(b^*) + W(a^* + b^*) - h + S\left(\frac{a^* + b^*}{2}\right)\right] + \\ &\frac{1}{\tau c_2}\left[W(a^*) + W(b^*) - W(b^* - a^*) - h + S\left(\frac{b^* - a^*}{2}\right)\right], \end{aligned} \tag{4.10}$$

$$\begin{aligned}\frac{db^*}{dt} = &\frac{1}{\tau c_1}\left[W(a^*) - W(b^*) + W(a^*+b^*) - h + S\left(\frac{a^*+b^*}{2}\right)\right] + \\ &\frac{1}{\tau c_2}\left[W(a^*) - W(b^*) + W(b^*-a^*) - h - S\left(\frac{b^*-a^*}{2}\right)\right],\end{aligned} \tag{4.11}$$

Subtracting (4.11) from (4.10) we obtain

$$\frac{db^*}{dt} - \frac{da^*}{dt} = -\frac{2}{\tau c_2}\left[W(a^*) + W(b^*) - W(b^*-a^*) - h + S\left(\frac{b^*-a^*}{2}\right)\right], \tag{4.12}$$

The stationary lenghts of (4.10) and (4.12) are given by

$$\begin{aligned}W(a^*) + W(b^*) - W(b^*-a^*) - h + S\left(\tfrac{b^*-a^*}{2}\right) = 0 \\ W(a^*) - W(b^*) + W(a^*+b^*) - h + S\left(\tfrac{a^*+b^*}{2}\right) = 0\end{aligned} \tag{4.13}$$

We define G^* and H^* to be the right sides of (4.10) and (4.12), respectively. The Jacobian matrix J of (4.10) and (4.12) at (a^*, b^*, a^*+b^*) is defined as

$$J = \begin{pmatrix} G^*_{a^*} & G^*_{b^*} \\ H^*_{a^*} & H^*_{b^*} \end{pmatrix}, \tag{4.14}$$

where $G^*_{a^*}$, $G^*_{b^*}$, $H^*_{a^*}$ and $H^*_{b^*}$ are partial derivatives evaluated at $(a, b, a+b)$, and are given by

$$G^*_{a^*} = \frac{1}{\tau c_1}\left[w(a^*) + g_1(a^*, b^*)\right] + \frac{1}{\tau c_2}\left[w(a^*) + g_2(a^*, b^*)\right], \tag{4.15}$$

$$G^*_{b^*} = \frac{1}{\tau c_1}\left[-w(b^*) + g_1(a^*, b^*)\right] + \frac{1}{\tau c_2}\left[w(b^*) - g_2(a^*, b^*)\right], \tag{4.16}$$

$$H^*_{a^*} = -\frac{2}{\tau c_2}\left[w(a^*) + g_2(a^*, b^*)\right], \tag{4.17}$$

$$H^*_{b^*} = -\frac{2}{\tau c_2}\left[w(b^*) - g_2(a^*, b^*)\right]. \tag{4.18}$$

where $g_1(a^*, b^*) = w(a^*+b^*) + \frac{1}{2}S'\left(\frac{a^*+b^*}{2}\right)$, and $g_2(a^*, b^*) = w(b^*-a^*) - \frac{1}{2}S'\left(\frac{b^*-a^*}{2}\right)$. The eigenvalues, λ, of J satisfy

$$\lambda^2 - \left(G^*_{a^*} + H^*_{b^*}\right)\lambda + G^*_{a^*}H^*_{b^*} - G^*_{b^*}H^*_{a^*} = 0. \tag{4.19}$$

If the two eigenvalues have negative real parts, then (a^*, b^*, a^*+b^*) is a stable solution with respect to symmetric perturbations of an equal width two-bump solution. Thus, (a^*, b^*, a^*+b^*) is a stable solution if the trace

$$G^*_{a^*} + H^*_{b^*} < 0 \tag{4.20}$$

and the determinant

$$G^*_{a^*}H^*_{b^*} - G^*_{b^*}H^*_{a^*} > 0. \tag{4.21}$$

We have,

$$G^*_{a^*} + H^*_{b^*} = \frac{1}{\tau c_1}\left[w(a^*) + g_1\left(a^*, b^*\right)\right] + \frac{1}{\tau c_2}\left[w(a^*) - 2w(b^*) + 3g_2\left(a^*, b^*\right)\right], \tag{4.22}$$

and

$$\begin{aligned} G^*_{a^*}H^*_{b^*} - G^*_{b^*}H^*_{a^*} = \frac{4}{\tau^2 c_1 c_2}\left[w(a^*) - w(b^*)\right]\left[g_1\left(a^*, b^*\right) + g_1\left(a^*, b^*\right)\right] \\ + \frac{8}{\tau^2 c_1 c_2} w(a^* + b^*) g\left(a^*, b^*\right) \\ - \frac{2}{\tau^2 c_1 c_2}\left[4w(a^*)w(b^*) + S'\left(\frac{b^* - a^*}{2}\right) S'\left(\frac{a^* + b^*}{2}\right)\right]. \end{aligned} \tag{4.23}$$

If

$$w(a^*) < 0, w(b^*) > 0 \text{ and } w(a^* + b^*) < 0, \tag{4.24}$$

and

$$S'\left(\frac{b^* - a^*}{2}\right) > 0 \text{ and } S'\left(\frac{a^* + b^*}{2}\right) < 0, \tag{4.25}$$

the conditions (4.20) and (4.21) are satisfied.

4.3 Field response to a bimodal symmetric external input

When the field is initially at resting state $u(x) = -h < 0$, depending on the input strength, two situations may occur:

- the field remains in the off-state if $S\left(\frac{\overline{x_2} - \overline{x_1}}{2}\right) \leq h$;
- the field develops one or more localized bumps in the field if $S\left(\frac{\overline{x_2} - \overline{x_1}}{2}\right) > h$.

Using the coupling function defined in (1.6), the excited region created by a external input with $S\left(\frac{\overline{x_2} - \overline{x_1}}{2}\right) > h$ depends on the relative location of the input bumps. As a concrete example, Figure 4.2 (top panels) shows that two identical inputs given by (4.4) produce different patterns depending on the value of x_c, that is, the relative locations of the two inputs to the field. As show in Figure 4.2 (bottom panels), the excitation pattern converges to an one-bump (left), a two-bump (middle) and a three-bump solution (right).

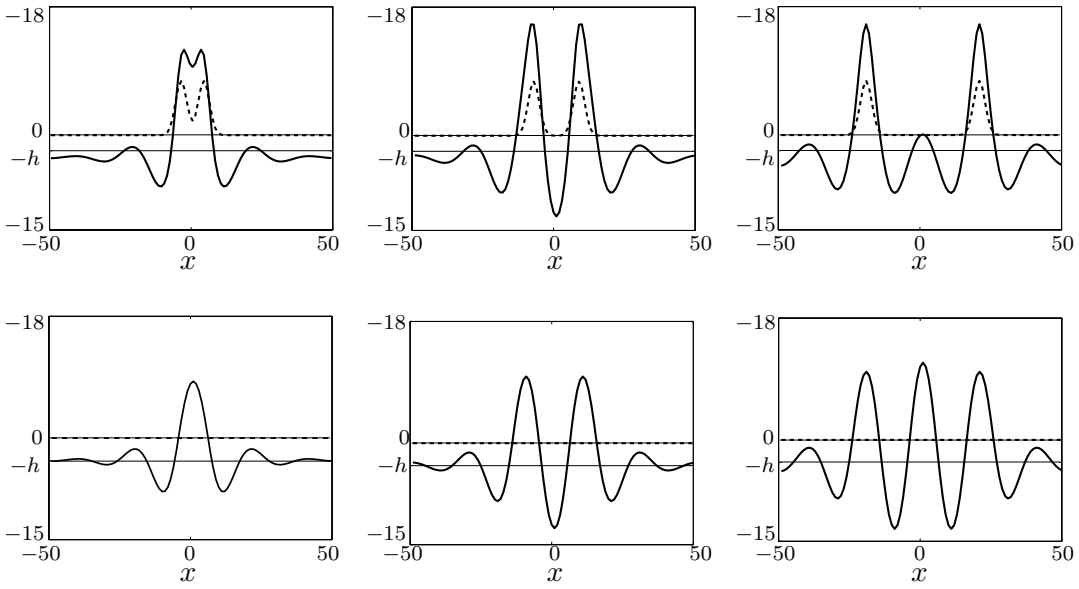

Figure 4.2: Activity u (solid lines) with $h = W(10)$, w defined in (1.6) with $A = 2$, $k = 0.1$ and $\alpha = \frac{\pi}{10}$ and invariant external stimulus S_2 (dashed lines) with $S_s = 8$, $S_i = 0.5$, $\sigma = 2$ and different value of x_c, $x_c = 5$ (left), $x_c = 8$ (middle), $x_c = 20$ (right). $S_2(x) \neq 0$ (top) and $S_2(x) = 0$ (down).

Suppose $h = W\left(\frac{\pi}{\alpha}\right)$ and that hypothesis (H_{10}) holds. By Theorem 5, $u(x) = W(x) - W(x-a) + W(x-b) - W(x-a-b) - h$ with $a = \frac{\pi}{\alpha}$ and $b \in (z_2, z_3)$ such that $W(b) = p_1 p_2$, defines a stable two-bump solution. Given the results of Figure 4.2, a crucial question is what conditions on the input guarantee that a stable two-bump evolve when the input is removed. We know that if $a^* \in (z_1, z_2)$, $b^* \in (z_2, z_3)$ and $a^* + b^* \in (z_2, z_3)$ the conditions (4.24) are satisfied. Thus, we introduce the subset Ω of $\mathbb{R}^2$ (see Figure 4.3) as

$$\Omega = \left\{(x, y) \in \mathbb{R}^2 | x > z_1 \wedge x + z_1 < y < x + z_2 \wedge -x + z_3 < y < -x + z_4\right\}. \quad (4.26)$$

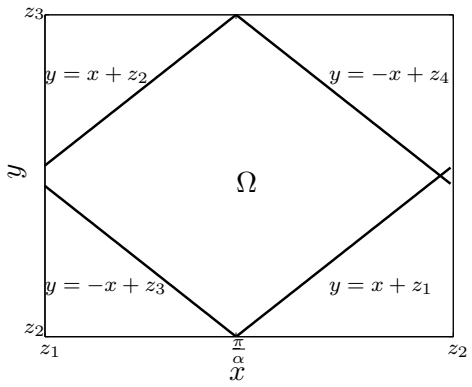

Figure 4.3: Region $\Omega \subset \mathbb{R}^2$.

The following Theorem 6 gives the necessary conditions for the existence of values $(a^*, b^*) \in \Omega$ that satisfy the conditions (4.7) and (4.8) if $h = W\left(\frac{\pi}{\alpha}\right)$.

Theorem 6 *Assume that the coupling function w given by (1.6), and that hypotheses (H_{10}), (SH_1), (SH_4) and (SH_5) hold. If $S\left(\frac{\overline{x_2}-\overline{x_1}}{2}\right) > W\left(\frac{\pi}{\alpha}\right)$, $S\left(\frac{z_1}{2}\right) < 0$, $S\left(\frac{z_2}{2}\right) > 0$, $S\left(\frac{z_3}{2}\right) > 0$ and $S\left(\frac{z_4}{2}\right) < 0$, then there exists a point (a^*, b^*) belonging to the region $\Omega \subset \mathbb{R}^2$ (4.26) such that*

$$W(a^*) + W(b^*) - W(b^* - a^*) - W\left(\frac{\pi}{\alpha}\right) + S\left(\frac{b^* - a^*}{2}\right) = 0, \tag{4.27}$$

and

$$W(a^*) - W(b^*) + W(a^* + b^*) - W\left(\frac{\pi}{\alpha}\right) + S\left(\frac{b^* + a^*}{2}\right) = 0. \tag{4.28}$$

The proof of this Theorem is given in Appendix A.

We illustrate Theorem 6 with an example. Consider the coupling function w given by (1.6) with $A = 2$, $k = 0.1$, and $\alpha = \frac{\pi}{10}$, $h = W(10)$, and $S(x)$ given by (4.4) with $S_s = 8$, $S_i = 0.5$, $\sigma > 0$, $x_c > 0$. We seek a solution (a^*, b^*) such that $\frac{z_1}{2} < \frac{b^*-a^*}{2} < \frac{z_2}{2}$ and $\frac{z_3}{2} < \frac{b^*+a^*}{2} < \frac{z_4}{2}$. Thus, to satisfy the conditions (4.25) we choose $x_c \in \left(\frac{z_2}{2}, \frac{z_3}{2}\right)$. In this example we have $S(x_c) = 7.5 > W(10)$. By Theorem 6, if $S\left(\frac{z_1}{2}\right) < 0$, $S\left(\frac{z_2}{2}\right) > 0$, $S\left(\frac{z_3}{2}\right) > 0$ and $S\left(\frac{z_4}{2}\right) < 0$, then there exists a point (a^*, b^*) belonging to Ω (4.26) such that (4.27) and (4.28) are satisfied. Figure 4.4 shows the region as a function of σ and x_c where the four conditions on S are satisfied.

Using $\sigma = 2$ and $x_c = 10$ by Newton's method (for a description of the method see Appendix B.2) with initial approximations $a_0^* = 10$ and $b_0^* = 20$, one solution of the nonlinear system of equations (4.27) and (4.28) is $(a^*, b^*) \approx (10.2669; 21.0692)$.

When the input disappears, i.e., $S(x, t) = 0$, the motion of the width a^* and the distance between the two bumps $b^* - a^*$ are given by

$$\begin{aligned} \frac{da^*}{dt} = &\frac{1}{\tau c_1}\left[W(a^*) - W(b^*) + W(a^* + b^*) - h\right] + \\ &\frac{1}{\tau c_2}\left[W(a^*) + W(b^*) - W(b^* - a^*) - h)\right], \end{aligned} \tag{4.29}$$

$$\frac{db^*}{dt} - \frac{da^*}{dt} = -\frac{2}{\tau c_2}\left[W(a^*) + W(b^*) - W(b^* - a^*) - h\right]. \tag{4.30}$$

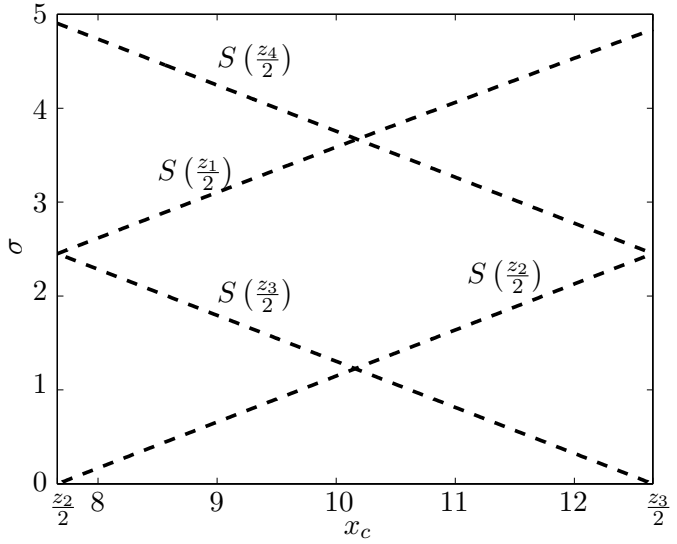

Figure 4.4: The curves of $S\left(\frac{z_1}{2}\right)$, $S\left(\frac{z_2}{2}\right)$, $S\left(\frac{z_3}{2}\right)$ and $S\left(\frac{z_4}{2}\right)$, as function of x_c and σ.

In this case, it is not trivial to study the signs of $\frac{da^*}{dt}$ and $\frac{db^*}{dt} - \frac{da^*}{dt}$ as function of a^* and b^* compared to the values a and b that belong to (z_1, z_2) and (z_2, z_3), respectively, and that satisfy the conditions (4.7) and (4.8). However, it is expected that the solution (a^*, b^*) will converge to the unique equilibrium solution (a, b) that belongs to Ω.

As $h = W\left(\frac{\pi}{\alpha}\right)$, by Theorem 4 there exists a triple (a, b, c), with $a = \frac{\pi}{\alpha}$ and $b = -\frac{\arctan\left(\frac{p_2}{p_3}\right)}{\alpha} + \frac{2\pi}{\alpha}$, and $c = a + b$ that satisfy the conditions (2.10) and (2.11). As $a^* \approx 10.2669$ and $b^* \approx 21.0692$ it is expected that a^* converges to $a = 10$ and b^* converges to $b = -\frac{10\arctan\left(\frac{\pi+10}{1-10*\pi}\right)}{\pi} + 20$. Using Newton's method with initial approximation $a^* = 10.2669$ and $b^* = 21.0692$, one solution of the nonlinear system of the equations (2.10) and (2.11) is $(a, b) = (10; 21.2981877)$ as expected.

4.4 Field response to a localized input when the field already has one excited region

Consider the connection function (1.6) and that the initial state of the field is a stable localized excitation with width $a = \frac{\pi}{\alpha}$ centered at x_{0_1}, i.e.,

$$u(x, 0) = \int_{x_{0_1} - \frac{a}{2}}^{x_{0_1} + \frac{a}{2}} w(x - x')dx' - h. \tag{4.31}$$

Consider without restriction $x_{0_1} = 0$, $u(x, 0)$ is then given by

$$u_0(x,0) = \begin{cases} -2p_1 e^{kx} \cosh\left(\frac{ka}{2}\right)(p_3\cos(\alpha x) + p_2\sin(\alpha x)) - h, & x < -\frac{a}{2} \\ 2p_1 e^{-\frac{ka}{2}}\left(-p_3\cos(\alpha x)\cosh(kx) + p_2\left(e^{\frac{ka}{2}} - \sin(\alpha x)\sinh(kx)\right)\right) - h, & -\frac{a}{2} \le x \le \frac{a}{2} \\ 2p_1 e^{-kx}\cosh\left(\frac{ka}{2}\right)(-p_3\cos(\alpha x) + p_2\sin(\alpha x)) - h, & x > \frac{a}{2} \end{cases} \tag{4.32}$$

If $x_{0_1} \neq 0$ the $u(x,0) = u_0(x - x_{0_1}, 0)$.

Figure 4.5 shows an example of $u_0(x,0)$ with width $a = 10$.

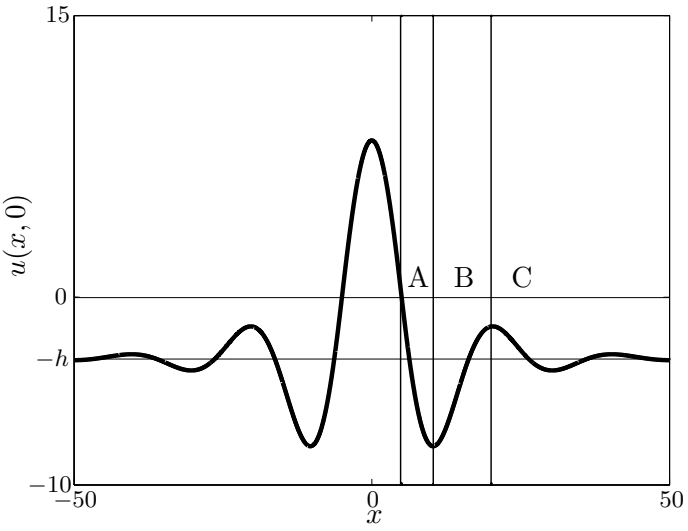

Figure 4.5: An example of $u_0(x,0)$ with $a = 10$, $A = 2$, $\alpha = \frac{\pi}{10}$ and $k = 0.1$.

When the initial state is an one-bump solution the analysis of a new excitation pattern is more complex compared to the case of the constant initial state,$-h$, described before. An important new feature is that the input strength necessary to generate suprathreshold activity depends on the distance of the second input to the existing bump. As can be seen in Figure 4.5, the minimum input strength necessary to create a second input is lower in region with $u(x,0) > -h$ and higher in region with $u(x,0) < -h$ compared to the case of a constant initial condition.

Two phenomena may occurs when a second excitation is triggered: repulsion or attraction. Consider the regions A, B and C as shown in Figure 4.5. The intensity of

inhibition increase in region A, decrease in region B and tends to $-h$ in region C as the distance becomes larger. When the second input creates a local excitation in region A, the two local excitations mutually attract and tend to fuse in one local pattern. This occurs because the inhibition is larger in the far sites of the local excitations than in the near sites. When the second input creates a local excitation in region B, they repulse each other forming two separate local excitations. When the second input creates a local excitation in region C, the interactions between the two patterns are weak so that the new bump persist at the input location.

Consider that the initial state of the field is $u(x,0)$ (4.32), and a second input with width $a = \frac{\pi}{\alpha}$ is presented to the right side of the initial bump (Figure 4.6). Let the excited region at time t be $R[u] = (x_1^*(t), x_2^*(t)) \cup (x_1^*(t), x_2^*(t))$ and the motion of the boundaries is given by (4.9). Assuming that $x_2^* - x_1^* \approx a = \frac{\pi}{\alpha}$, $S(x_1^*) \approx S(x_2^*) \approx 0$ and $h = W(\frac{\pi}{\alpha})$, and using Lemma 1 we have

$$\begin{aligned}
\frac{dx_1^*}{dt} &= \frac{e^{-\frac{k\pi}{\alpha}}}{\tau|c_1|}\left[W(x_4^* - x_2^*) - W(x_3^* - x_2^*)\right] \\
\frac{dx_2^*}{dt} &= \frac{1}{\tau|c_2|}\left[W(x_4^* - x_2^*) - W(x_3^* - x_2^*)\right] \\
\frac{dx_3^*}{dt} &= \frac{1}{\tau|c_3|}\left[\left(e^{-\frac{k\pi}{\alpha}} + 1\right)W(x_3^* - x_2^*) - W(x_4^* - x_3^*) - S(x_3)\right] \\
\frac{dx_4^*}{dt} &= \frac{1}{\tau|c_4|}\left[-\left(e^{-\frac{k\pi}{\alpha}} + 1\right)W(x_4^* - x_2^*) + W(x_4^* - x_3^*) + S(x_4)\right]
\end{aligned} \tag{4.33}$$

When $W(x_4^* - x_2^*) < W(x_3^* - x_2^*)$ we have $\frac{dx_1^*}{dt} < 0$ and $\frac{dx_2^*}{dt} < 0$, i.e., the initial bump moves to the left side (repulsion) and when $W(x_4^* - x_2^*) > W(x_3^* - x_2^*)$ we have $\frac{dx_1^*}{dt} > 0$ and $\frac{dx_2^*}{dt} > 0$, i.e., the initial bump moves to the right side (attraction). If the second input is sufficiently distant from the initial bump, the movement of the initial bump is negligible since $W(x_4^* - x_2^*) \approx W(x_3^* - x_2^*) \approx p_1 p_2$ while attraction or repulsion gradually increase with smaller distances.

For applications of dynamic field theory a quite interesting phenomenon is that the identical input can produce different responses depending on the current state of the field. Consider the example illustrated in Figure 3.3 (left) in which the input width is not sufficient to create an one-bump. Figure 4.7 illustrates that the identical input applied to a field in which one bump already exists (left panel) may create a second bump that persists when the input is removed (right panel).

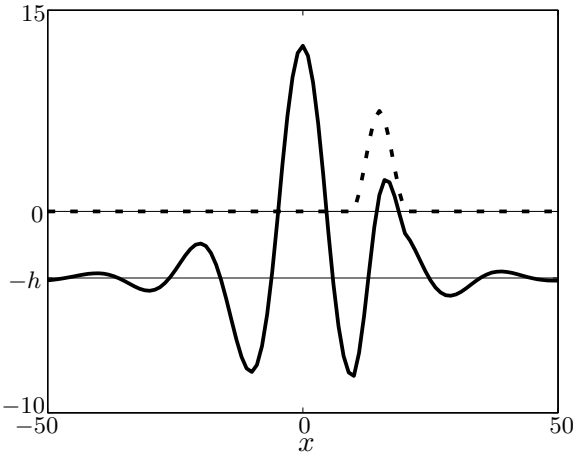

Figure 4.6: An example of the excited region $R[u]$ at time t (solid line). The external input (dashed line) is given by $I(x) = max[S(x), 0]$ where $S(x-15)$ is defined by (3.5) with $S_s = 6$, $S_i = 1$ and $\sigma = \frac{5}{\sqrt{2\ln(6)}}$.

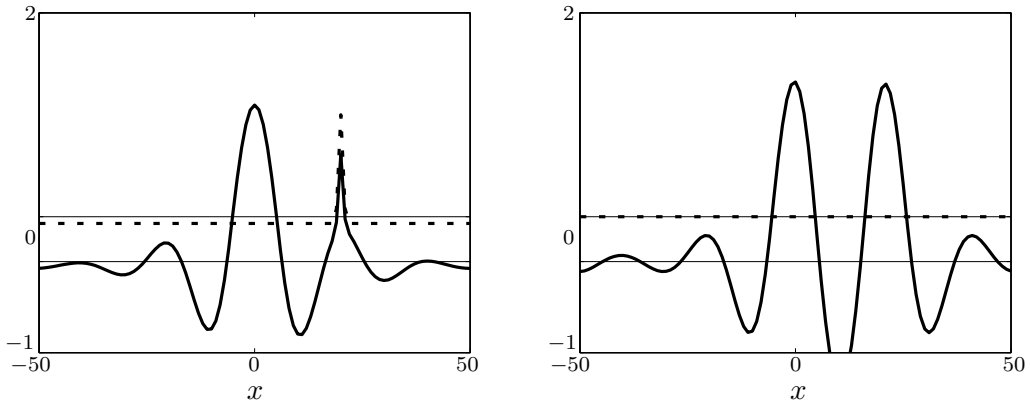

Figure 4.7: Snapshot of field activity (solid line) with initial state $u(x, 0)$ (4.32) when an external input $S(x-20)$ (dashed line) given by (3.5) with $S_s = 8$, $S_i = 0.5$ and $\sigma = 0.4$, is applied (left). Stable two-bump solution after the input has been removed (right).

4.5 Conclusion

In this chapter, we studied the formation of a stable two-bump solution in response to: (1) a bimodal symmetric input, when the initial state is a negative constant, and (2) an unimodal symmetric input, when the initial state is an one-bump solution. For fixed $h = W\left(\frac{\pi}{\alpha}\right)$ and $\alpha = \frac{\pi}{a}$, k such that $W(z_2) > \frac{p_1 p_2}{\left(1+e^{\frac{2k\pi}{\alpha}}\right)}$, with $p_1 = \frac{A}{k^2+\alpha^2}$, $p_2 = \alpha k + k$, by Theorem 4 and Theorem 5 there exists a stable two-bump solution with equal

width a. To create this solution with a transient, bimodal symmetric input we can conclude from the analysis in Sections 4.2 and 4.3 that S must satisfy the conditions $S\left(\frac{\overline{x_2}-\overline{x_1}}{2}\right) > W\left(\frac{\pi}{\alpha}\right)$, $S\left(\frac{z_1}{2}\right) < 0$, $S\left(\frac{z_2}{2}\right) > 0$, $S\left(\frac{z_3}{2}\right) > 0$ and $S\left(\frac{z_4}{2}\right) < 0$.

Chapter 5

Analysis of multi-bump solutions

In this chapter, the mathematical analysis of two-bump solutions in one-dimensional dynamic fields is extended to the numerical study of N-bump solutions. The existence and stability of N-bump solutions with and without external input is discussed for specific examples of the connectivity function. Recall that a N-bump solution is one whose region of excitation is the union of N disjoint, finite, open intervals, that is, $R(u) = (a_0, a_1) \cup (a_2, a_3) \cup ... \cup (a_{2N-2}, a_{2N-1})$. From (1.2), (2.1), and (2.41) it follows that $u(x)$ can be written as

$$u(x) = \sum_{i=0}^{N-1} \left(\int_{a_{2i}}^{a_{2i+1}} w(x - x')dx' \right) - h. \tag{5.1}$$

Then, using (2.2) the N-bump solution of equation (1.1) is of the form

$$u(x) = \sum_{i=0}^{N-1} \left(W\left(x - a_{2i}\right) - W\left(x - a_{2i+1}\right) \right) - h. \tag{5.2}$$

For simplicity we assume that the N-bump solution is symmetric. In this sense, consider the following proposition.

Proposition 1 *Suppose that hypotheses (H_1), (H_2), (H_6) and (H_7) hold. If u is symmetric with respect to the point $\frac{a_0+a_{2N-1}}{2}$, the system of equations*

$$\begin{cases} u(a_0) = 0 \\ u(a_1) = 0 \\ \quad ... \\ u(a_{2N-1}) = 0 \end{cases} \tag{5.3}$$

can be reduced to

$$\begin{cases} u(a_0) = 0 \\ \dots \\ u(a_{N-1}) = 0 \end{cases}. \tag{5.4}$$

The proof of this Proposition is given in Appendix A.

In the example studies, we assume, without loss of generality, that $a_0 = 0$ and apply Newton's method (see Appendix B) to approximate a solution of system (5.4). To discuss the stability of N-bump solutions we follow the approach used to study the linear stability of two-bump solutions in Subsection 2.2.1 and compute the eigenvalues of the Jacobian matrix

$$J = \begin{pmatrix} J_{11} & \cdots & J_{1N} \\ \vdots & \ddots & \vdots \\ J_{N1} & \cdots & J_{NN} \end{pmatrix}, \tag{5.5}$$

where $J_{ij} = \frac{\partial}{\partial a_j}\left(\frac{da_i}{dt} - \frac{da_0}{dt}\right)$, with $\frac{da_i}{dt} = -\frac{1}{c_i}\frac{\partial u(a_i,t)}{\partial t}$, $c_i = (-1)^i \frac{\partial u(a_i,t)}{\partial x}$ and $\frac{\partial u(a_i)}{\partial t} = \sum_{k=0}^{N-1} W(a_i - a_{2k}) - W(a_i - a_{2k+1})$, for all $i, j \in \{0, 1, ..., N\}$. If all eigenvalues have negative real part then the solution is stable. Otherwise, if at least one eigenvalue has positive real part then the solution is unstable.

5.1 An example of stable multi-bump solutions

We consider a connectivity function (1.6) with $A = 2$, $\alpha = \frac{\pi}{10}$ and $k = 0.1$. Table 5.1 shows the approximate solutions of (5.4) for each $N \in \{2, 3, 4, 5, 6\}$, when the initial values are $a_i = 10i$ for $i = \{1, 2, 3, 4, 5, 6\}$. Table 5.2 displays the eigenvalues of (5.5) for the solutions described in Table 5.1. All eigenvalues have negative real part and thus all solutions are stable. Figure 5.1 shows the plot of solution (5.2) where $a_0 = 0$, the values of a_j for $j \in \{1, ..., N\}$ correspond to the values shown in Table 5.1 and $a_j = a_N + a_{N-1} - a_{2N-1-j}$ for $j \in \{N+1, ..., 2N-1\}$ representing two-bump, three-bump, four-bump, five-bump and six-bump solutions, respectively.

For the case of a two-bump solution, we can directly compare the analytical results for the width a and distance $b - a$ of bumps with the numerical approximation.

We know from Theorem 4 and Theorem 5 that for $h = W\left(\frac{\pi}{\alpha}\right)$ and $k^2 < \alpha$ there exists a two-bump solution of (1.1) with $a = \frac{\pi}{\alpha}$ and $b = \frac{-\arctan\left(\frac{p_2}{p_3}\right)}{\alpha} + \frac{2\pi}{\alpha}$. With $A = 2$, $\alpha = \frac{\pi}{10}$ and $k = 0.1$, we have $k^2 < \alpha$. Consequently, there exists a two-bump solution of (1.1) with $a = 10$ and $b \approx 21.2982$, which is in perfect agreement with the approximate values in Table 5.1 for the case $N = 2$.

N	Solutions
2	$a_1 = 10$; $a_2 = 21.2982$
3	$a_1 = 10$; $a_2 = 21.1910$; $a_3 = 31.1361$
4	$a_1 = 10$; $a_2 = 21.1786$; $a_3 = 31.1190$; $a_4 = 42.2083$
5	$a_1 = 10$; $a_2 = 21.1770$; $a_3 = 31.1168$; $a_4 = 42.1943$; $a_5 = 52.1296$
6	$a_1 = 10$; $a_2 = 21.1768$; $a_3 = 31.1165$; $a_4 = 42.1926$; $a_5 = 52.1272$; $a_6 = 63.1930$

Table 5.1: Solutions of (5.4) for $N \in \{2, 3, 4, 5, 6\}$ when $A = 2$, $\alpha = \frac{\pi}{10}$ and $k = 0.1$.

N	Eigenvalues
2	$\lambda_{1,2} = -0.4928 \pm 0.0888i$
3	$\lambda_1 = -0.5169$; $\lambda_{2,3} = -0.2031 \pm 0.1972i$
4	$\lambda_{1,2} = -0.1964 \pm 0.0787i$; $\lambda_{3,4} = -0.6383 \pm 0.0347i$
5	$\lambda_1 = -0.0737$; $\lambda_2 = -0.3808$; $\lambda_3 = -0.6025$; $\lambda_4 = -0.6922$; $\lambda_5 = -0.8029$
6	$\lambda_1 = -0.0526$; $\lambda_2 = -0.3057$; $\lambda_3 = -0.5338$; $\lambda_4 = -0.6344$; $\lambda_5 = -0.7123$; $\lambda_6 = -0.8055$

Table 5.2: Eigenvalues of (5.5) for the solutions described in Table 5.1.

5.2 Approximate values for bump width and bump distance

For the applications of N-bump solutions in cognitive neuroscience and robotics we are particularly interested in the width and relative distance of the localized patterns in the field. The parameter k governs the rate at which the oscillations of the connection function w decay with distance and therefore controls the strength of interaction between

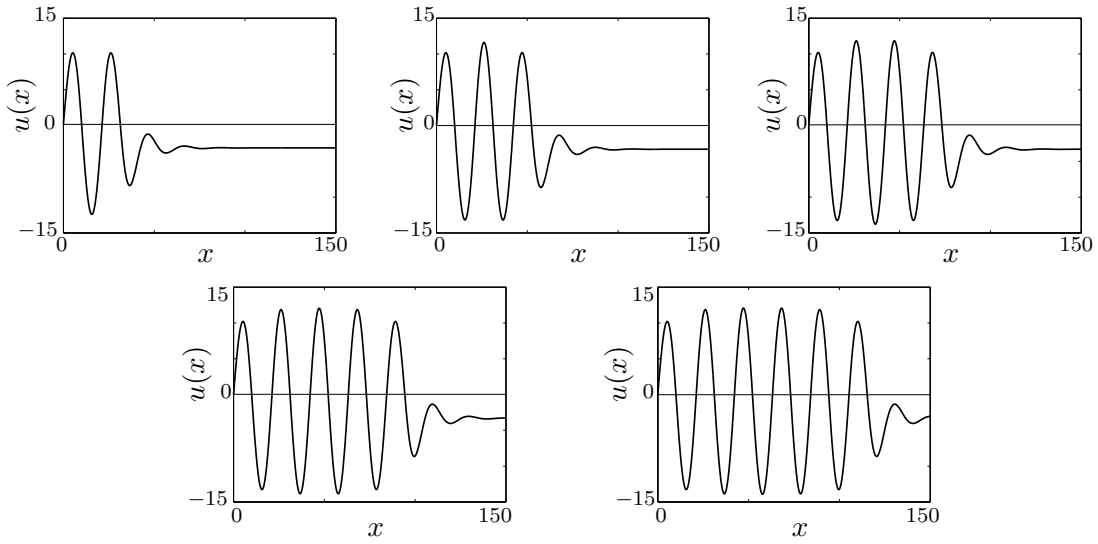

Figure 5.1: Field activity u given by (5.2) with $h = W(10)$, w is defined in (1.6) with $A = 2$, $k = 0.1$ and $\alpha = \frac{\pi}{10}$.

the bumps. Table 5.3 compares the bump widths for different k values and distances between successive bumps for a six-bump solution. Since we assume that the solution is symmetric, it is sufficient to compute the width of the first three bumps and the relative distance between the first four suprathreshold patterns. For the three tested values of k, the width of the first bump is always 10 and the width of the two other bumps is slightly smaller. The relative distance between the first two bumps is largest in all cases and increases with increasing bump numbers. In general, the dependence on k manifests in a decreased range of the obtained values with increasing k, that is, the variability in the parameters describing the spatial pattern appears to be reduced. This behaviour of the field dynamics can be understood by taking into account that the parameter k controls the damping of the periodic connectivity function. With larger k, the interactions between spatially distant bumps are less pronounced and the shape of each individual bump is mainly determined by the excitatory-inhibitory interactions of neighbouring field sites. The predicted approximation in the shape of individual bumps can be clearly seen in Figure 5.2 (right panel) where the field dynamics with $k = 0.2$ supports a six-bump solution with approximately equal bump amplitudes (compare with the case $k = 0.1$, left panel).

k	Bumps width	Distance between bumps
0.1	$a_1 - a_0 = 10$	$a_2 - a_1 = 11.1768$
	$a_3 - a_2 = 9.9398$	$a_4 - a_3 = 11.0760$
	$a_5 - a_4 = 9.9346$	$a_6 - a_5 = 11.0658$
	Range: 0.0654	Range: 0.1110
0.15	$a_1 - a_0 = 10$	$a_2 - a_1 = 11.8322$
	$a_3 - a_2 = 9.9673$	$a_4 - a_3 = 11.7756$
	$a_5 - a_4 = 9.9661$	$a_6 - a_5 = 11.7734$
	Range: 0.0339	Range: 0.0588
0.2	$a_1 - a_0 = 10$	$a_2 - a_1 = 12.4094$
	$a_3 - a_2 = 9.9887$	$a_4 - a_3 = 12.3836$
	$a_5 - a_4 = 9.9886$	$a_6 - a_5 = 12.3806$
	Range: 0.0114	Range: 0.0234

Table 5.3: Bump widths and distances between bumps for a six-bump solution with $k = 0.1$, $k = 0.15$ and $k = 0.2$.

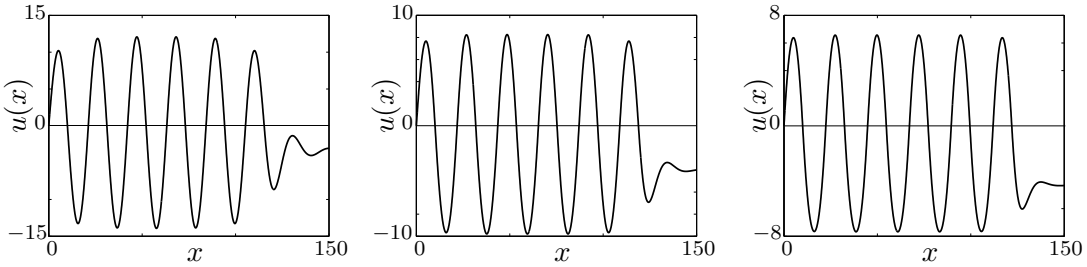

Figure 5.2: Field activity u given by (5.2) with $h = W(10)$, w is defined in (1.6) with $A = 2$, $\alpha = \frac{\pi}{10}$ and $k = 0.1$ (left), $k = 0.15$ (center) and $k = 0.2$ (right).

5.3 Dependence of a N-bump solution on initial conditions

In the previous section we have discussed N-bump solutions with approximately equal distances between individual bumps. These solutions are obtained when the field dynamics starts from a periodic pattern of initial activation that approximately matches the periodicity of the N-bump solution. Stable N-bump solutions with significant dif-

ferences in the relative distance of individual bumps can be also found by adapting the initial conditions accordingly. Table 5.4 presents an example for the connectivity function w with parameters $A = 2$, $\alpha = \frac{\pi}{10}$ and $k = 0.2$ and initial activation values of different field sites that are not equally spaced. The solution of (5.4) describes a six-bump. The eigenvalues of the Jacobian (5.5) are all real and negative, that is, the six-bump pattern shown in Figure 5.3 is stable.

Initial values	Solutions	Eigenvalues
$a_1 = 10$	$a_1 = 10$	$\lambda_1 = -0.3111$
$a_2 = 20$	$a_2 = 22.4324$	$\lambda_2 = -0.2501$
$a_3 = 30$	$a_3 = 32.4322$	$\lambda_3 = -0.2310$
$a_4 = 60$	$a_4 = 64.8401$	$\lambda_4 = -0.0648$
$a_5 = 70$	$a_5 = 74.8401$	$\lambda_5 = -0.0002$
$a_6 = 100$	$a_6 = 107.2720$	$\lambda_6 = -0.0023$

Table 5.4: Initial conditions (left column), numerical solutions of the system (5.4) (middle column) and the respective eigenvalues of the Jacobian (5.5) for the case $N = 6$ with $A = 2$, $\alpha = \frac{\pi}{10}$ and $k = 0.2$.

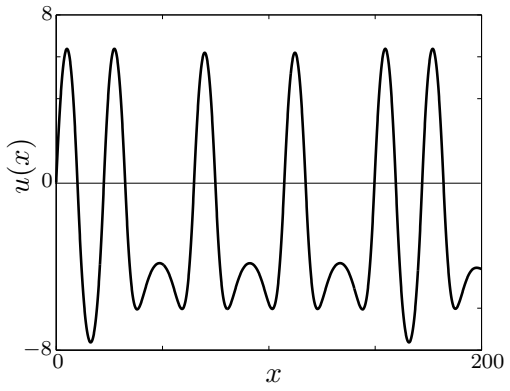

Figure 5.3: Field activity u with $h = W(10)$, w is defined in (1.6) with $A = 2$, $\alpha = \frac{\pi}{10}$ and $k = 0.2$ and initial activation at field sites 10, 20, 30, 60, 70 and 100.

5.4 Formation of multi-bump solutions with external input

5.4.1 Field response to stationary multi-modal and mono-modal external inputs

For the first numerical study, we consider a multi-modal input given by the sum of Gaussian centred at equally spaced field locations

$$I(x) = \sum_{j=1}^{n} S_s e^{\left(-\frac{(x-x_{c_j})^2}{2\sigma^2}\right)} - S_i. \tag{5.6}$$

with $S_s = 6$, $S_i = 1.5$, $\sigma = 3$, $x_{c_j} = 20j + 5$ for $j \in \{1, ..., 6\}$. The spatial domain was discretized by a 150 grid with circular boundaries conditions (for details of the numerical integration see Appendix B.1). Applying this stationary input, multi-bump solutions can be generated as shown in Figure 5.4. Note that the numerically obtained six-bump solution corresponds to the six-bump solution of (5.4) in Figure 5.1 when the pattern is centred in the interval $[0, 150]$.

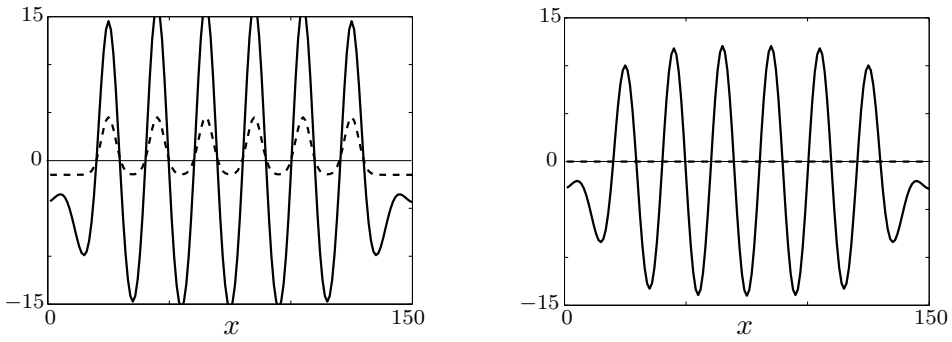

Figure 5.4: Snapshots of field activity u (solid lines) with $h = W(10)$, w is defined in (1.6) with $A = 2$, $k = 0.1$ and $\alpha = \frac{\pi}{10}$, the stationary external input (dashed lines) is given by (5.6) with $S_s = 6$, $S_i = 1.5$, $\sigma = 3$, $x_{c_j} = 20j + 5$ for $j \in \{1, ..., 6\}$. $S_2(x) \neq 0$ (left) and $S_2(x) = 0$ (right).

For the second simulation study, we consider a single, localized input at $x = x_c$ given by (3.5)

$$S(x - x_c) = S_s e^{\left(-\frac{(x-x_c)^2}{2\sigma^2}\right)} - S_i. \tag{5.7}$$

with fixed parameters $S_s = 6$, $S_i = 0.5$, $x_c = 75$ and vary the width of the Gaussian, $\sigma \in \{20, 30, 40\}$. The number of bumps generated by this stationary input

pattern depends on its width as shown in Figure 5.5 (top panels). As more field sites become activated above threshold with increasing stimulus width, more bumps will evolve. Note that the larger bump located at the centre of the external stimulation is actually a two-bump solution of the homogeneous field dynamics. It emerges when the external stimulus is removed (compare the top and the corresponding bottom panels of Figure 5.5).

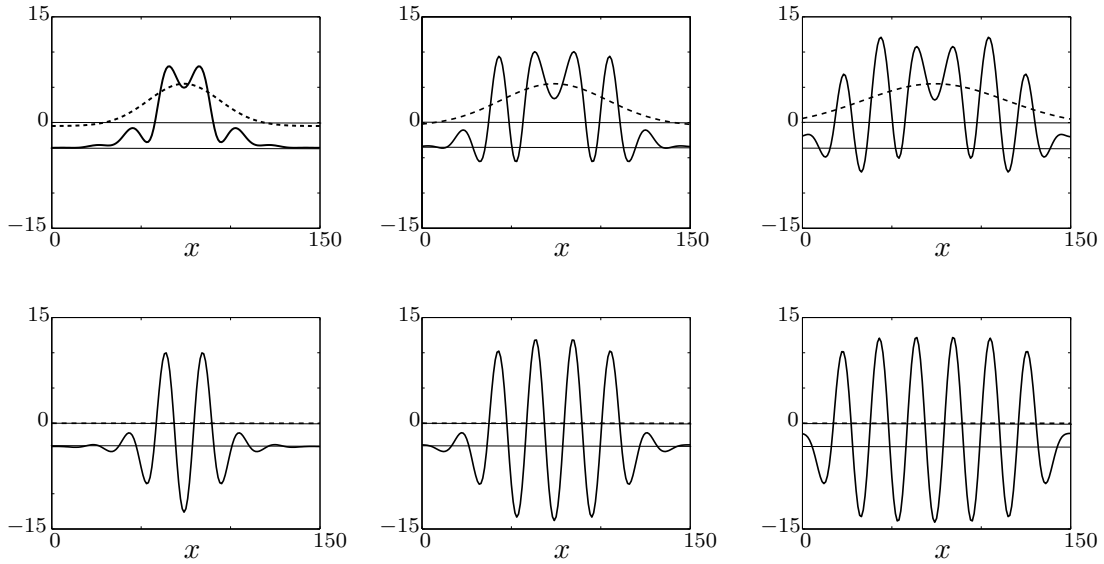

Figure 5.5: Snapshots of field activity u (solid lines) with parameters used in Figure 5.4 except the input width. The stationary external input is given by $S(x-75)$(dashed lines) with $S_s = 6$ and $S_i = 0.5$ and three different widths, $\sigma = 20$ (left), $\sigma = 30$ (middle), $\sigma = 40$ (right). $S(x) \neq 0$ (top panels) and $S(x) = 0$ (bottom panels).

5.4.2 Field response to transient external inputs

The numerical results of Figure 5.5 suggest that stable multi-bump solutions may be generated by external input that exists only for a finite time. This means that the initial condition given by the state of the field at the time of input removal is in the basin of attraction of the multi-bump solutions discussed before.

For a concrete example, consider the external input $S(x - x_c)$ given by (5.7) and parameters of the connection function like in Figure 5.1. Choosing $\sigma = 3$ we have $S\left(\frac{z_1}{2}\right) \approx 3.1580$ and $S\left(\frac{z_2}{2}\right) \approx -0.3262$. Since $S(0) > W(10)$, $S\left(\frac{z_1}{2}\right) > 0$ and $S\left(\frac{z_2}{2}\right) < 0$. By Theorem 3 we know that there exists a solution $a^* \in (z_1, z_2)$ such that the equation

$W(10) - S\left(\frac{x}{2}\right) = W(x)$ is satisfied. This means that for a stationary input with $\sigma = 3$ the field dynamics evolves an excited region of width a^* which converges to an one-bump solution of width $a = 10 < a^*$ when the input disappears (compare left column of Figure 5.6, input at $x_c = 40$). The existing bump together with a second transient input centred at $x_c = 80$ generates a three-bump solution. The lateral excitation caused by the two suprathershold activity patterns is strong enough to trigger the evolution of a bump between the two stimulated regions $x_c = 80$ and $x_c = 40$ (Figure 5.6, right column). The situation is different when the same sequence of inputs is applied to a field with weaker lateral interactions. Figure 5.7 shows snapshots of the field dynamics with $k = 0.2$ instead of $k = 0.1$ used in Figure 5.6. As can be seen in the left column, the field develops a two-bump solution with field activity between the two stimulated locations below threshold. Additional bumps may be created by sequentially applying localized input at the respective field sites (compare the middle and right columns of Figure 5.7). The total number of bumps that can be created depends on the length of the finite domain Ω of the field and the parameters of the connectivity function that control the width and relative distance of bumps. The formation of stable multi-bump solutions by a temporal sequence of inputs is central for the applications in the sequence learning model.

5.5 Conclusion

In this chapter, we have investigated the existence and stability of N-bump solutions. We described in Section 5.1 for a specific connection function of type (1.6) stable N-bumps for $N \in \{2, 3, 4, 5, 6\}$. If we wish to generate these N-bump solutions by applying N transient inputs in which each individual input generates just one bump, the parameters of S and w must be carefully chosen. As can be seen in numerical studies of multi-bump solutions, for different values of σ the number of bumps generated differs. Moreover, the results in Section 5.2 and Subsection 5.4.2 illustrate that if the interaction between bumps, which is modulated by the parameter k, is strong, localized inputs may generate additional suprathreshold activation at field sites without external stimulation. On the other hand, if the goal is to generate N-bumps with approximately equal shape of individual local excitations, the amplitude of the recurrent excitatory

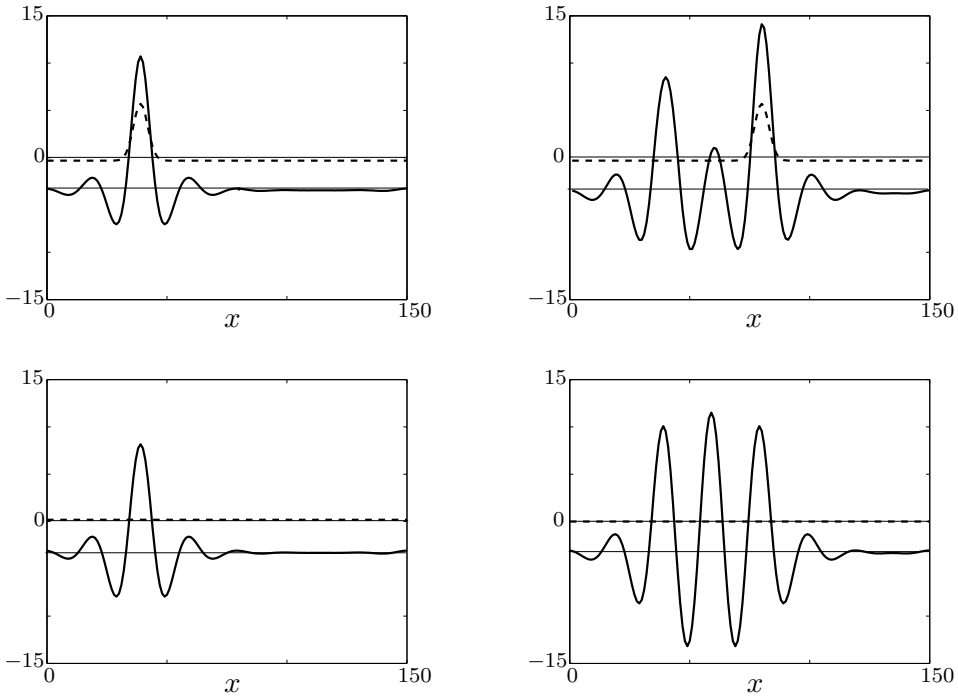

Figure 5.6: Snapshots of activity u (solid lines) with parameters used in Figure 5.5 except the stimulus width. An input of width $\sigma = 3$ is sequentially applied first at location $x_c = 40$ (left) and subsequently at location $x_c = 80$ (right). $S(x) \neq 0$ (top panels) and $S(x) = 0$ (bottom panels).

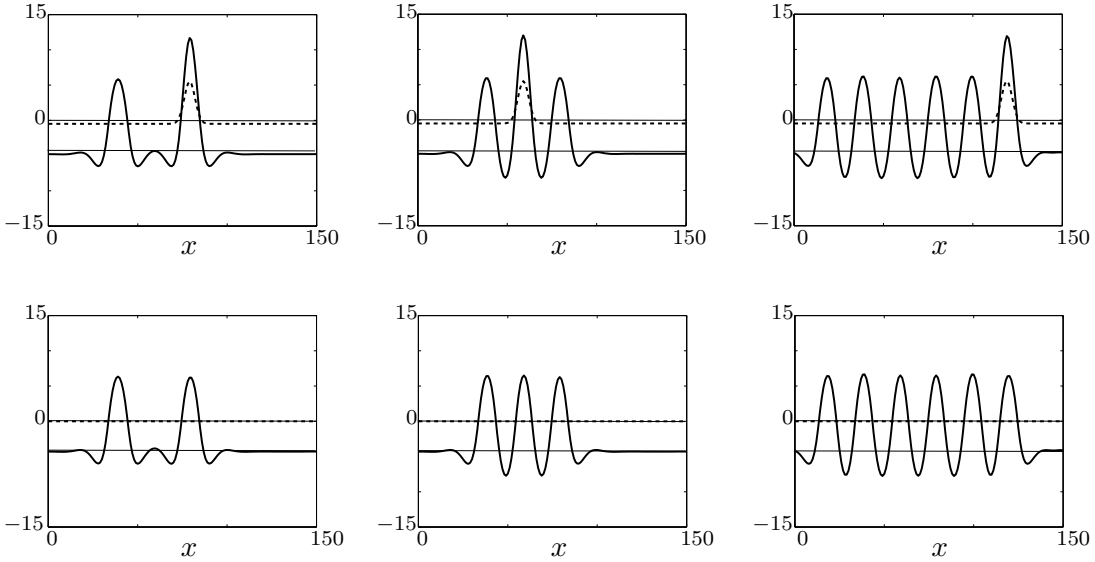

Figure 5.7: Snapshots of activity u (solid lines) with field parameters used in Figure 5.6 except $k = 0.2$ instead of $k = 0.1$. A two-bump (left), three-bump (middle) and six-bump solution (right) is generated by sequentially applying localized input of width $\sigma = 3$ (dashed lines). $S(x) \neq 0$ (top panels) and $S(x) = 0$ (bottom panels).

interactions controlled by k should be sufficiently small. If the parameters of S and w are adequately chosen, N localized inputs applied simultaneously or sequentially define the location of N bumps in the field, as shown in the example of Section 5.4.

Part III

A dynamic neural field model of sequential events and its validation in a real-world robotics experiment

Chapter 6

Sequence Learning

In this chapter we introduce basic notations and concepts of sequence learning and representation from the cognitive science literature that will be used in the dynamic neural field models.

6.1 Memory: STM, LTM and WM

Intelligent behaviour crucially depends upon the ability to encode, store and recall sequences of events. Virtually every aspect of our everyday routine tasks is embedded in a sequential context. We see this in tasks like speaking, getting dressed, cooking a meal or playing a musical instrument for which different events in a specific order must be encoded and stored in memory. The stored information can be later recalled from short term memory (STM) or long term memory (LTM). The two main differences between STM and LTM are the time period for which information is remembered and the storage capacity. While in STM the information persists only for a brief period of time and the capacity is small, information in LTM may be hold for a lifetime and the storage capacity is huge (Cowan, 2008). From the concept of STM emerged the notion of working memory (WM). WM involves the temporary storage and manipulation of information, in contrast to STM, which refers just to the information storage (Baddeley, 1992). In this sense, working memory of serial order can be described as the cognitive system which temporarily stores a sequence of events for recalling it in a behavioural context.

6.2 Behavioural paradigms for serial order: ISR and SRT

Two main behavioural paradigms have been used in the past to study sequence learning: the immediate serial recall (ISR) task and the serial reaction time (SRT) task (for a recent review see Rhodes et al., 2004). An immediate serial recall paradigm can be divided into two phases. A list of items or events (e.g. letters, numbers, spatial targets, musical notes) is first presented in a specific order. Subsequently, the subject has to recall the items in the order in which they were presented. The types and rate of errors that occur during recall are used as a measure for sequence learning. In a typical SRT task, participants are asked to react as quick as possible with specific button presses to a series of stimuli presented on a screen. Sequence learning is demonstrated by a reduced reaction time to movement initiation for stimuli that are repeated in a fixed temporal order compared to a random order. Since subjects are typically unaware of the temporal structure embedded in the presentation, the performance in SRT paradigms is often considered a measure for implicit sequence learning (Nissen and Bullemer, 1987; Dominey, 1998).

In this work, we used the ISR paradigm for the robotics experiments. However, as discussed in Section 9.2, predictions of the DNF model of sequential events are also in line with basic results of SRT experiments with humans.

6.3 Three theories of memory for serial order

In the vast cognitive science literature about sequence representation there are three main theories of serial order: chaining, positional and ordinal theories (for an overview see Henson, 1998). There exists still no general agreement about the neuro-cognitive mechanisms supporting the organization of sequential events in humans and other primates since the specific predictions of all three theories are to some extent supported by experimental findings. The coexistence of different theoretical approaches based on distinct processing mechanisms is perhaps not surprising given that the nervous system has to organize a broad range of sequential events on very different levels of abstraction ranging from simple motor sequences (e.g., finger movements) to complex behavioural sequences (e.g., making coffee) .

Chaining theory assumes that temporal order is stored by the formation of associations between successive items in a list. The order is retrieved by a chain of associations where each item cues the recall of its successor. The simplest chaining models assume only associations between pairs of items in successive positions (Henson, 1998). In compound models, however, the cue consists of a number of preceding items (e.g., Murdock, 1995). Chaining is perhaps the most intuitive way to represent serial order and is the backbone of recurrent neural network models of serial behaviour (e.g., Botvinick and Plaut, 2006).

Positional theory assumes that order is stored by associating each item with its position in the sequence. For example, in one of the first conceptual models proposed by Conrad (1965), it is assumed that numbered boxes are hold in in memory into which elements of a sequence can be placed. The order of elements can be retrieved by stepping through the boxes in a predetermined routine. Whereas chaining models use item-item associations, positional models use position-item associations to represent serial order (e.g., Burgess and Hitch, 1999; Brown et al., 2000).

Ordinal theories assume that order is stored by a relative value along a single dimension. For example, Grossberg (1978) postulates that order is stored in a primacy gradient of activation over the items such that each item has a higher level of activation than its successor. Serial recall is based on an interactive process of selecting the most active item and subsequently suppressing its activation. If some random noise is added to the selection process, a correct item may be recalled but in wrong order (see for instance the behaviour of the "Primacy Model" (Page and Norris, 1998)). Importantly, when an item is recalled in the incorrect ordinal position there is a tendency for a transposition with items that are close in the target sequence. Moreover, ordinal models are simpler than associative models because order information is implicit in the representations, rather than encoded explicitly by forming associations between items or items and positional codes. Ordinal models do not require feedback from preforming individual steps to execute the whole sequence. This might be an advantage over associative models when sequence execution has to be very fast (e.g., a pianist's finger tapping) and there is not enough time to cue the next response. On the other hand, the lack of associations between sequence elements makes it difficult to encode longer term

dependencies that are for instance important to represent causality in goal-directed sequential behaviour ([e.g., a certain behaviour can only be executed if a specific set of behaviours has been already performed (Sousa et al., 2014)).

6.4 Ordinal models: Competitive Queuing (CQ)

In his seminal article about the problem of serial order in behaviour, Lashley (1951) argued that sequences are represented by a parallel activation of neural representations of all sequence elements. In other words, all elements of a planned sequence are simultaneously active prior to sequence production. Based in this hypothesis, Grossberg (1982, 1978) introduced a model of WM for serial evens in which temporal order is represented by the strength of activation of successive list items that decreases across list positions to form a primacy gradient. To reproduce the sequence, the item with the currently highest activation is selected for output and subsequently suppressed. This inhibition enables the next item from the activation gradient. The reproduction of the sequence is finished when there are no active nodes in the WM representation left. This model class was first called Item-and-order WM and later termed competitive queuing to stress the competitive selection process (for a discussion of CQ models see Houghton, 1990). Electrophysiological recordings from prefrontal cortex (PFC) (e.g., Averbeck et al., 2002, 2003) support three key predictions of CQ models: (1) neural ensembles represent list items, (2) their relative activation strengths encode temporal order, and (3) neural population representations are reset by inhibitory mechanisms (e.g., self-inhibition).

The DNF model presented in this thesis belongs to the class of ordinal theories that represent serial order as an activation gradient of neural populations encoding individual events. Lateral inhibition implements a completion between neural ensembles that leads to a decision of which item to execute next. The DNF model differs from conceptually similar CQ models (e.g., connectionist implementations (Houghton, 1990)) in two main aspects. First, the dynamic field based implementation allows us to rigorously analyse multi-item WM and its formation, and second, the model introduces the idea that the activation gradient can be also used to memorize and reproduce the relative timing of events.

6.5 Recurrent neural network models

Recurrent neural networks (RNN) have been very popular in the past to model the learning and processing of sequences (e.g., Cleeremans and McClelland, 1991; Dominey, 1998). RNN models are connectionist models that use distributed patterns of activation in networks of neuron-like elements to represent information. Importantly, the recurrent connections between state units and context units allow information from previous time steps to influence the current state of the network. The recurrent connections can thus be used to represent sequence context. Indeed, RNN models have been frequently applied for tasks that require the prediction of items in a sequence based on their predecessors (e.g., Cleeremans, 1993). Learning in RNNs takes place as a modification of the synaptic weights of the recurrent connections. It is well known, however, that learning over multiple time steps introduces significant technical challenges. Perhaps more importantly for the robotics applications addressed in this thesis, there are normally a large number of processing cycles of network activity and weight modifications required to learn and represent a sequential task. RNNs thus do not provide an adequate theoretical framework to rapidly memorize sequences of events. In contrast, the activity based learning in the dynamic field model demonstrates the acquisition of order and timing information in very few sequence demonstrations.

6.6 Benchmark properties of serial order recall

Traditionally, benchmarks for modelling serial behaviour are different types of errors that typically occur when humans and non-human primates learn motor or behavioural sequences (Smyth and Scholey, 1996; Henson, 1998; Botvinick and Plaut, 2006; Botvinick et al., 2009). Although the proposed dynamic field model primarily focuses on different aspects of sequence events than the majority of previous sequence models (e.g., a shared memory representation for order and timing, fast learning etc.) it is worth to mention the types of errors that have been used to distinguish theories. Some of these errors will be discussed in more detail in Chapter 8.

(i) Omission errors

An omission occurs when a sequence item is omitted during serial recall. This

error may be caused by a failure of the encoding (memory) or the recall (selection) of the event. In the dynamic field model, the rise and decay of suprathreshold activity may be initially not quick enough to represent and memorize all sensory events during (fast) sequence demonstrations. The mechanism of preshaping of neural populations from past experiences plays a crucial role in speeding up the processing.

(ii) Transposition errors

A common phenomenon in serial recall studies is the transposition of items, that is, an item is recalled in wrong order but near to its position in the target sequence. Additive noise in the decision field with the activation gradient as input can produce such errors in the DNF model.

(iii) Repetition errors

Crucial for a correct recall is that already produced items cannot become activated again. Feedback inhibition from a working memory field representing past events guarantees normally the long-lasting suppression of already executed items. If the inhibition is not strong enough, repletion errors may occur. Importantly, the model dynamics allows repetitions if the sequence contains repeated elements.

Chapter 7

DNF model of ordinal and timing properties of sequential events

In this chapter, we start with a review of relevant findings in the fields of psychology and neuroscience that have inspired the model. Next, we describe the architecture and the mathematical details of the model. A report of a series of model simulations is given, followed by a short discussion of the results.[1]

7.1 Neuroscientific and psychological grounding of the model

7.1.1 The parallel sequence code and iterative choice cycle

The central idea implemented in the DNF model is that in goal-directed sequence planning all sequence elements appear to be activated in parallel at the beginning of sequence execution. There is compelling neurophysiological support for a parallel activation of neuronal populations encoding different sequence elements (Averbeck et al., 2002, 2003). The researchers trained two monkeys to control a cursor for drawing simple geometric figures (triangle, square, trapezoid, inverted triangle) on a screen. Recordings from the prefrontal cortex (PFC) showed that at the beginning of the sequence of cursor movements, there exists a parallel activation of different neuronal populations

[1] The content of this chapter is based on the paper by Ferreira et al. (2011)

representing all individual segments of the shape that has to be drawn. It is worth noting that the activation patterns in PFC most likely do not directly control the hand movements of the monkey, but represent more abstract sequential information of the goal-directed cursor movements that could be executed for instance with different effectors (Tanji et al., 2007). Serial order is encoded by a pre-activation gradient, that is, the population representing the first segment is highest and the activation of the population encoding the last element is lowest. The parallel representation continues to unfold during the execution of the sequence. After a specific segment has been executed, its activation decreases, and the population representing the subsequent shape segment becomes the most strongly activated (see Figure 7.1).

The observed pattern of neuronal population dynamics is conceptually consistent with a competitive choice process in which i) the segment with the highest activation is selected for performance, ii) once the segment has been executed it is deleted from the set of competitors, and iii) the process is repeated until the sequence reaches completion. This iterative performance of serial behaviour without any reliance to associative links between items is the hallmark of competitive queuing models reviewed in the previous chapter (Rhodes et al., 2004).

7.1.2 Relationship between the time course of population activity and elapsed time

A second important assumption of the DNF model is that elapsed (interval) time since sequence onset or between sequence elements is represented by a continuous increase or decrease of population activity until a threshold is reached which is associated with the expected occurrence of the next event (either perceptual or motor). Studies with monkeys that directly investigated the neural basis of timing report ensemble activity showing a monotonic relationship between neuronal population activity and elapsed time (e.g., Janssen and Shadlen, 2005, Genovesio et al., 2006b, for a review see Durstewitz, 2004). Janssen and Shadlen (2005) recorded the neuronal activity in posterior parietal cortex, while monkeys had a saccadic eye movement to peripheral targets after a variable delay period. The timing of the "Go" signal (dimming of the fixation point) was a random value. Many neurons systematically modulated their spike rates as a

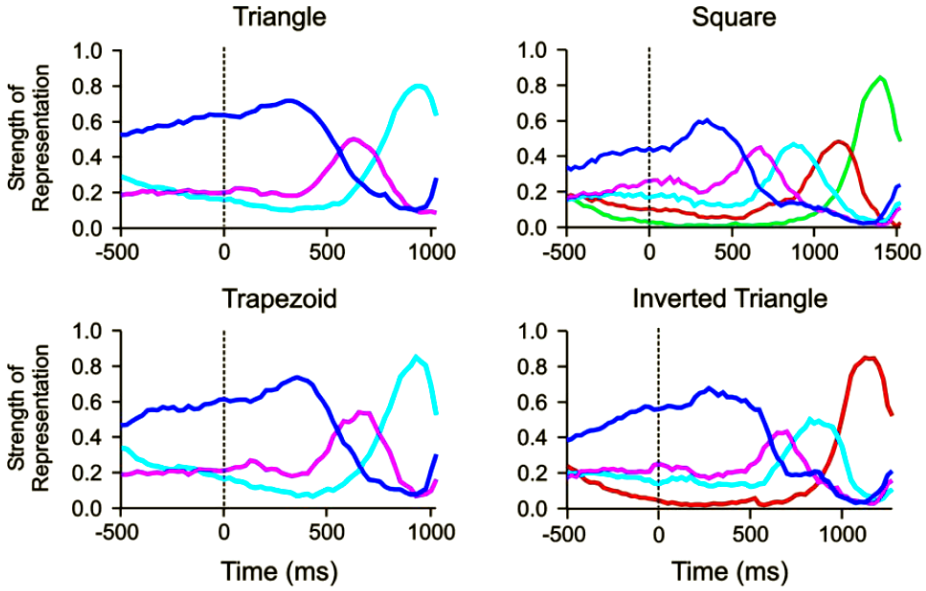

Figure 7.1: The time course of neural activity of different subpopulations in PFC during the drawing tasks are shown. Note the activation gradient at the beginning of the cursor movement at time t=0. The relative strength of activation of the individual shape elements represents the serial order of task execution (from Averbeck et al. (2002), Figure 2).

function of elapsed time. Their firing patterns reflect the probability that the "Go" signal will occur. Genovesio et al. (2006b) also examined the representation of elapsed time in PFC using a similar task in which the monkey had to move the eyes after one of three possible delay periods between the onset and the offset of a visual stimulus. Many neurons showed ramp-like increases in firing rate that depended on the preceding delay period.

7.1.3 Separate subpopulations in PFC for past and future events

The architecture of the model implements the idea that memories of already achieved events and memories of upcoming events are stored in the activity patterns of separate but connected neuronal ensembles. To avoid repetition errors it is important to keep track of past events when planning the immediate and more distal future. On the other hand, mistaking a pending event as already accomplished causes the error of omission. Genovesio et al. (2006a) examined neuronal activity in the prefrontal cortex while monkeys performed a spatial task. The monkeys had to select one of three spatial

goals (future goal) depended on their memory of previous spatial goal. During each trial, the decision of the future spatial goal was made based on the combination of a symbolic visual cue that had appeared in the previous trial and the previous goal that the monkey selected. When a symbolic visual cue presented at the fixation target was the same as in the previous trial, the monkey stayed with its previous goal as future goal. When the visual cue changed, the monkey was required to select one of the two remaining positions as its future goal. The authors report that populations of prefrontal neurons had activity that reflected either previous goals or future goals, but only rarely did individual cells reflect both.

7.2 Model description

In the experiments designed to test the neural processing of serial order in goal-directed behaviour, typically simple reaching or saccadic eye movements towards objects are used. The temporal order may be defined by the spatial object position (that is, movement direction and amplitude) or object features like colour, weight or size. The central idea of dynamic field models is that suprathreshold population activity of neurons tuned to these continuous dimensions represents specific parameter values. Figure 7.2 presents an overview of the model architecture which is inspired by the experimental findings summarized in Section 7.1. The self-sustained activation pattern in the sequence memory field u_{mem} stores all items of a sequence with a strength of activation that decreases from item to item as a function of elapsed time since sequence onset. This activation gradient is achieved by combining a field dynamics that guarantees the evolution of a single, self-stabilized bump in response to a localized transient input representing a perceived event with a state-dependent threshold accommodation dynamics for the firing rate function. Through excitatory connections, neurons in u_{mem} project their activation to corresponding neurons in decision field u_{de}. This input leads to a subthreshold pre-activation of neural populations that mirrors the primacy gradient of strengths in u_{mem}. Sequence recall starts with a continuous increase of the baseline activity which brings neural populations closer to the threshold for the evolution of a self-stabilized bump. The order and timing of sequence elements can be retrieved by using the baseline dynamics to first trigger a suprathreshold response of the population

with the highest pre-activation which then becomes suppressed due to inhibitory feedback from the working memory field u_{wm}. Self-stabilized population activity in this field is initially driven by the activation dynamics of the corresponding population in u_{de} and may thus be described as a memory for already achieved events or goals.

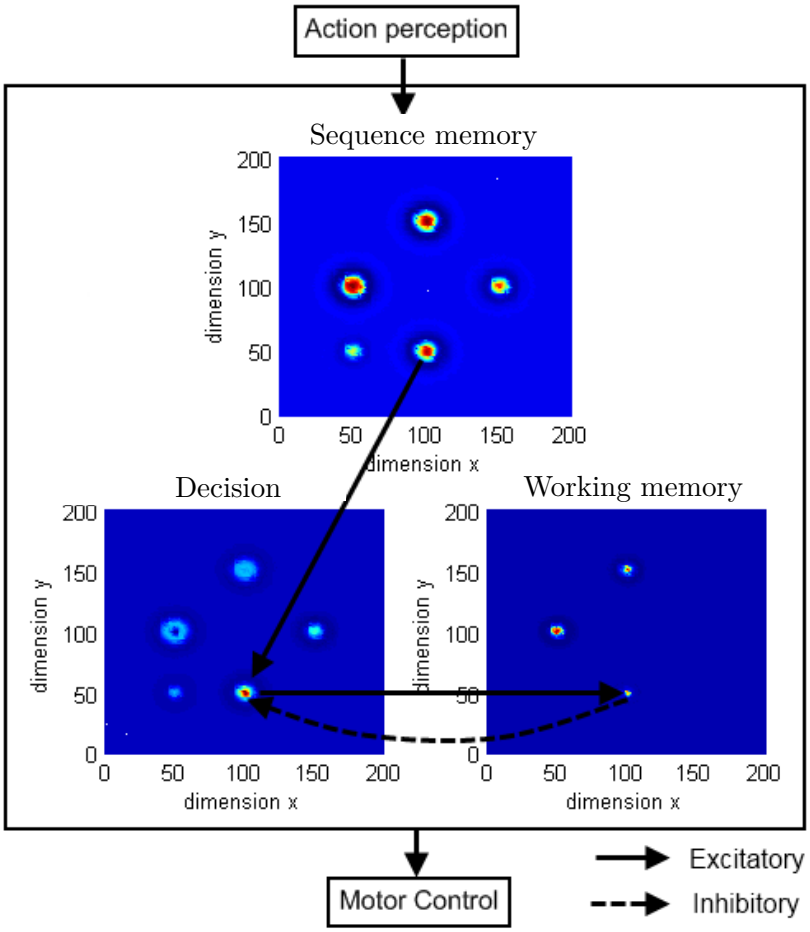

Figure 7.2: Sketch of the model architecture. For illustration purpose, localized activity patterns in two-dimensional fields are shown. The strength of neuronal population activation is colour coded.

7.3 Model equations

The dynamics in the sequence memory field is governed by the following equation:

$$\tau_{u_{mem}} \dot{u}_{mem}(x,t) = -u_{mem}(x,t) + h_{mem}(x,t) + \int w_{osc}(x-x') f\left(u_{mem}(x',t)\right) dx' + S(x,t) \tag{7.1}$$

where $u_{mem}(x,t)$ represents the activity at time t of a neuron encoding dimension x. The parameter $\tau_{u_{mem}} > 0$ defines the time scale of the field. The firing rate function f is taken as the Heaviside step function with threshold 0. $S(x,t)$ represents the time-dependent, localized input to the field, and is given by (3.5). To model working memory for several events separated in time we used the connection function w_{osc} given by (1.6). The variable $h_{mem}(x,t)$ defines the baseline level of activation which we chose to vary with time. Note that by including $h_{mem}(x,t)$ in the definition of the firing rate function $f = f\,(u - h_{mem})$ it becomes clear that changing the baseline level is equivalent to changing the threshold of f. Following the idea of the phenomenological model for threshold accommodation in dynamic fields discussed by Coombes and Owen (2007), we apply the following state-dependent dynamics for the baseline activity:

$$\dot{h}_{mem}(x,t) = (1 - g(u_{mem}(x,t)))\,(-h_{mem}(x,t) + h_{mem_0}) + \lambda_h g(u_{mem}(x,t)), \qquad (7.2)$$

where g is chosen as the Heaviside step function, $h_{mem_0} < 0$ defines the level to which h_{mem} converges without suprathreshold activity at position x and $\lambda_h > 0$ measures the growth rate when it is present. As the result of the baseline or threshold dynamics a primacy gradient of strengths is established when at different points in time, bumps evolve in response to external input.

The dynamics of the decision field u_{de} and the working memory field u_{wm} are governed by the following equations, respectively:

$$\begin{aligned}
\tau_{u_{de}}\dot{u}_{de}(x,t) &= -u_{de}(x,t) + h_{de}(t) + \int w_{lat}(x-x')f\left(u_{de}(x',t)\right)dx' \\
&\quad - \int w_{osc}(x-x')f\left(u_{wm}(x',t)\right)dx' + u_{mem}(x), \qquad (7.3)\\
\tau_{u_{wm}}\dot{u}_{wm}(x,t) &= -u_{wm}(x,t) + h_{wm} + u_{de}(x,t)f\left(u_{de}(x',t)\right) \\
&\quad + \int w_{osc}(x-x')f\left(u_{wm}(x',t)\right)dx'. \qquad (7.4)
\end{aligned}$$

Since like u_{mem} also u_{wm} has to represent multi-bumps as stable solution we use the same connection function (1.6). The baseline activity $h_{wm} < 0$ is constant. The situation is different for u_{de} where a single localized activity pattern represents a particular event during sequence recall. To ensure the existence of an one-bump solution we use a connection function of lateral inhibition type w_{lat} given by (1.3).

The baseline activity $h_{de}(t)$ evolves continuously in time described by the equa-

tion:

$$\tau_{h_{de}}\dot{h}_{de}(t) = 1, \quad h_{de}(t_0) = h_{u_{de_0}} < 0, \tag{7.5}$$

where $\tau_{h_{de}}$ controls the growth rate of h_{de}.

7.4 Simulation results

For the numerical simulation study, we first discuss the choice of the model parameters that is justified by the mathematical analysis in the previous chapters. As an example, we consider a sequence of five items. In response to the series of five localized inputs, the sequence memory field should trigger a self-localized pattern consisting of five bumps with approximately equal width. Initially, we consider that the resting state is fixed and we choose $h = W(8)$. We suppose that the field is discretized by a 100 units grid and assume that the desired bump width is 8 units.

- Parameters values of w (see Figure 7.3)
  - Since the desired width is 8, we choose $\alpha = \frac{\pi}{8}$. Thus, as $8 = \frac{\pi}{\alpha}$ we have $z_1 < 8 < z_2$ and consequently the condition $w(a) < 0$ is satisfied for all $k > 0$.
  - From the N-bump analysis we conclude that for a sequential formation of a multi-bump solution of approximately equal shape the value of k must be chosen such that the intra-field coupling is relatively weak. We choose $k = 0.25$ and $A = 2$.

- Parameters values of S

  Each input is given by the bell-shaped function (3.5). From Theorem 3, it is possible to generate a stable one-bump solution with input if the conditions $S(0) > W(8)$, $S\left(\frac{z_1}{2}\right) > 0$ and $S\left(\frac{z_2}{2}\right) < 0$ are satisfied.
  - Choosing $S_s = 8$ and $S_i = 0.01$ we have $S(0) = 7.99 > W(8) \approx 3.6904$.
  - Choosing $\sigma = 1.5$ we have $S\left(\frac{z_1}{2}\right) \approx 2.0194 > 0$ and $S\left(\frac{z_2}{2}\right) \approx -0.0093 < 0$.

The three conditions on the input shape are then satisfied.

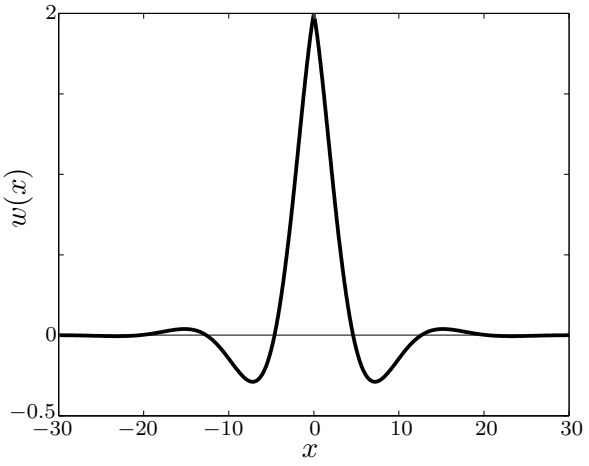

Figure 7.3: The coupling function, $w(x)$, defined in (1.6) for $A = 2$, $\alpha = \frac{\pi}{8}$ and $k = 0.25$.

To avoid the fusion of a newly evolving pattern with an already existing bump, the relative distance between the inputs has to be taken into account. Since $k^2 < \alpha$, we know from Theorem 5 that there exists a two-bump solution with width 8 and distance between bumps equal to $-\frac{\arctan\left(\frac{\alpha k + k}{k^2 - \alpha}\right)}{\alpha} + \frac{\pi}{\alpha} \approx 10.0675$. Thus for convenience we choose $x_c \in \{8, 26, 44, 62, 80\}$ as centres for the inputs. Figure 7.4 shows the response to five inputs of the desired shape for a fixed value of h. The amplitude of the bumps are approximately equal.

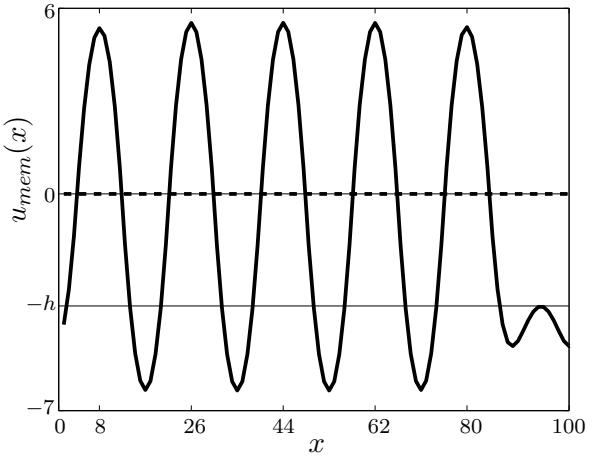

Figure 7.4: Example of 5-bump solution in response to a sequence of five transient inputs defined by $S(x - x_c) = 8e^{\left(-\frac{(x-x_c)^2}{2\times 1.5^2}\right)} - 0.01$ with $x_c \in \{8, 26, 44, 62, 80\}$. The coupling function shown in Figure 7.3 was used.

Figure 7.5 shows a snapshot of a simulation of a one-dimensional version of the sequence model. Due to the threshold accommodation dynamics (dashed line) the bump amplitudes reflect the temporal order of events (Figure 7.5, left). Figure 7.5 (right) shows the activation patterns in the decision field (solid line) and the working memory field (dashed line) at a time when all representations in u_{de} are below threshold because the activation bump at $x = 44$ in u_{wm} has just suppressed the representation of the first event and the representation of the second event at $x = 26$ is just about to reach the threshold.

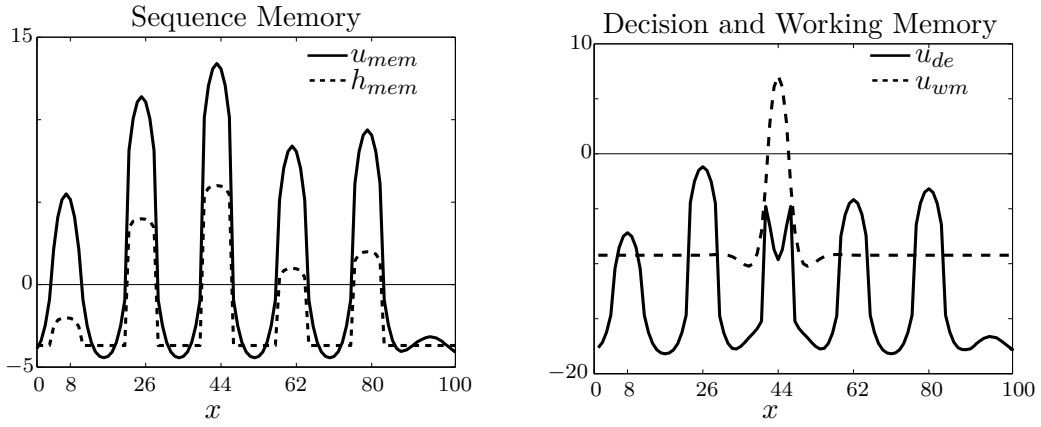

Figure 7.5: A snapshot of a simulation of a one-dimensional version of the sequence model is shown. The connection function parameters k and α were equal for all fields, $k = 0.25$, $\alpha = \frac{\pi}{8}$, and $A = 2$ for u_{mem} and $A = 5$ for the others fields. Choice of the others parameters for 1) u_{mem}: $\tau_{u_{mem}} = 20$, $h_{mem_0} = -W(8)$, $\lambda_h = \frac{1}{100}$; 2) u_{de}: $\tau_{u_{de}} = 20$, $w_{exc} = 16$, $\sigma_{exc} = 4$ and $w_{inh} = 0.01$, $\tau_{h_{de}} = 100$, $h_{de_0} = -15$; 3) u_{wm}: $h_{wm} = -W(8)$ and $\tau_{u_{wm}} = 40$.

To directly compare the timing of events during encoding and recall, Figure 7.6 compares the time courses of the population activity in the sequence memory field (top) and the decision field (bottom) for two different choices of the time scale for the baseline dynamics in u_{de}. Time $t = 0$ indicates the start of the sequence and the first event (i.e., first object reached) is perceived at about $t = 200$. Note that the events are irregularly spaced in time. As can be seen in the bottom figures, all subpopulations in the recall field appear to be from the beginning on pre-activated with a strength reflecting the rank order of execution. This model behaviour reflects nicely the main findings about parallel processing of serial order in the neurophysiological study of Averbeck et al. (2002, 2003). If the time scale of the baseline dynamics is chosen

as inversely related to the parameter λ_h controlling the growth rate of the threshold accommodation dynamics, $\tau_{h_{de}} = 1/\lambda_h$, the recall dynamics nearly perfectly reproduces the timing of events (bottom left). If the time scale for the baseline dynamics is chosen to be faster, $\tau_{h_{de}} < 1/\lambda_h$, proactive timing of events can be observed (bottom right). The total execution time decreases but the proportion of total time for each event of the sequence remains essentially invariant. It is worth noting that this model behaviour is in line with key principles of interval timing in humans and other animals (Machado et al., 2009). When people are asked to speed up or slow down the execution of a movement sequence they do so with near constancy in the relative timing. Moreover, assuming that noise may affect the growth rate $\tau_{h_{de}}$ of the baseline shift from trial to trial, the model predicts that the variability of time estimation grows proportionally with interval duration (Weber's law for timing). Table 7.1 and Figure 7.7 show the results of model simulations in which the variability of the time of decision, defined as the time when population activity in u_{de} reaches threshold, is tested for different interval duration between successive events. The so-called Weber fraction calculated as the standard deviation (σ) divided by the the mean estimation (μ) remain approximately constant over tested durations.

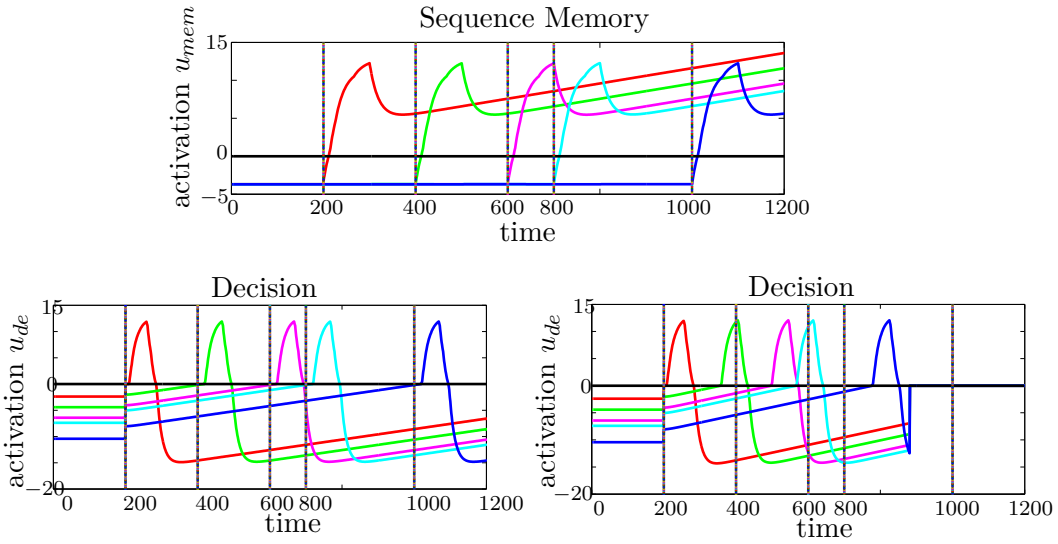

Figure 7.6: The time course of the maximal activation of each subpopulation in Figure 7.5 (*left*) is shown during sequence encoding (top) and during sequence recall (bottom) for two different execution speeds. For the recall $\tau_{h_{de}} = 100$ (left) and $\tau_{h_{de}} = 70$ (right) was chosen.

Time interval (Δt)	Mean (μ)	Standard deviation (σ)
100	100,325	5,9829
120	120,025	7,1861
140	139,595	8,2240
160	159,240	9,6334
180	180,785	10,8296
200	199,950	11,7364
220	220,280	12,9516
240	239,850	14,4927
260	259,470	15,2844
280	280,430	16,8005
300	300,260	17,7276

Table 7.1: Mean estimates and standard deviations are shown for interval duration in the range of 100 to 300 time steps. For each interval, the value represent the average of 200 simulation runs with $\tau_{h_{de}}$ randomly taken from a uniform distribution on the interval $[90, 110]$. The coefficient of variation, σ/μ, is approximately $0,06$ in all cases.

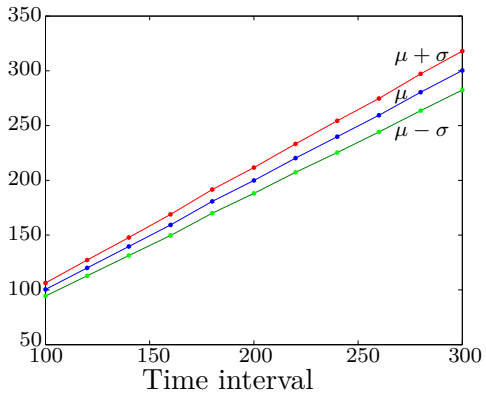

Figure 7.7: Plot of the mean(μ) and standard deviation (σ) as function of interval duration.

7.5 Discussion

We have presented a dynamic neural field model of sequential events that implements the idea of closely related neural systems for controlling the interval and ordinal dimensions. Serial order is stored in short term memory by assuming that memory strength for each event decreases as a function of elapsed time between sequence onset and the event. During recall, the ordinal and temporal structure is recovered from the memory list by applying a simple dynamics for the baseline activity of the decision field. An interesting feature of the model is that a speeding up of the baseline dynamics leads to a proactive timing of events. For a cognitive agent such a mechanism may be important for instance to timely prepare the next action or to allocate attention. The field model shares key features like parallel response activation and activation gradient

with “Competitive Queuing” models (Grossberg, 1978; Houghton, 1990) that have been applied to a wide variety of serial order problems (mostly concerning the ordinal dimension). Compared to connectionist implementations, the dynamic field approach offers advantages because it allows us to rigorously understand the existence and stability of activation patterns and their dependence on external inputs (Amari, 1977; Laing et al., 2002; Coombes and Owen, 2007). This understanding may guide the development of more complex cognitive models. An example is the DNF model of sequence learning presented in the next chapter.

Chapter 8

DNF model for fast learning of sequential task

The DNF model presented in the previous chapter shows that an activation based memory of order and timing may be used to robustly reproduce sequential events. Since our ultimate interest is to apply this sequence model in the domain of human-robot interactions, the question is how a robot may efficiently acquire this knowledge through the interaction with its environment including humans. Obviously, the DNF model has to be extended by at least two components to achieve this goal. First, the robot should be able to perceive the events defining the sequence through its sensors, and generate internal representations of the stimuli. In the extended model, a perceptual field contains neural populations that represent in their self-sustained activation patterns the sensory information. Second, the robot should be endowed with the capacity to iteratively acquire the order and timing of sequential events through repeated exposure to correct sequential behaviour. As an elementary form of learning, we exploit here the notion of the build-up of memory traces in the perceptual field generated by subthreshold input from a "past" field representing the sequence memory of preceding experimental trials.

Although the proposed sequence learning model may be applied to a wide variety of tasks, we use as an example study the learning of a musical sequence since the timing of musical events is essential to meaning. People with varying musical experience are able to reproduce from memory a precisely timed series of pitches at fast production rates with very few errors . Moreover, despite their serial and temporal complexity, new

melodies can be remembered with little practice. The DNF model aims at providing insights about the neuro-cognitive mechanisms that support such a fast and efficient learning in successive demonstration-execution cycles.

8.1 Preshaping of neuronal population by past experience

The idea that input representing prior task knowledge may pre-activate neuronal populations in a field below the threshold necessary to trigger a self-sustained activation pattern has been first introduced in the context of modelling the planning of reaching movements to spatial targets (Erlhagen and Schöner, 2002; Thelen et al., 2001; Erlhagen et al., 1999). Imagine for instance the situation in which several potential targets may be available but only one is selected by a specific visual cue in each experimental trial. The activation field that represents the decision to which target to reach is spanned over the dimension movement direction. When the visual cue indicating the target direction is presented, the evolution of suprathreshold activity of a subpopulation tuned to that direction does not start from scratch but from a prestructured state representing movement history. The probability of choice in previous trials is reflected by varying levels of preshaping of different subpopulations representing all potential movement directions. This neural preshaping mechanism implemented in DNF models of motor preparation has been directly observed in reaching paradigms with monkeys. In the experiments, a pre-cue explicitly instructed the monkey about the spatial range of potential targets before the specific input was presented. Neuronal populations tuned to movement direction in the premotor cortex, which is believed to be crucially involved in motor planning, showed a pre-activation pattern consistent with the spatial information given by the pre-cue (Bastian et al., 2003; Erlhagen et al., 1999).

In the cognitive psychology literature, this activation based learning in form of memory traces is known as priming, because the main behavioural manifestation is a speed-up in reaction time, or an increased probability of making a particular behavioural response (Erlhagen and Schöner, 2002). Experimental signatures of response biases that are consistent with the preshaping hypothesis have been observed for in-

stance in developmental studies with infants. The DNF model of preservative reaching proposed by Thelen and colleagues 2001 explains the classical "A-not-B" error by memory traces laid by the reaching history. In the A-not-B paradigm, an attractive toy is first shown to the infant and then hidden in a box at one of two reachable locations, A or B. After a few seconds, the infant is encouraged to make a motor decision either toward the A or the B location. Young infants at an age of 11-12 months typically make the A-not-B error of reaching toward the A location even though they saw the adult hiding the toy at location B. This error occurs after the researcher repeatedly hides the toy in position A and the infant correctly searches for it at that position. In the reaching decision, movement history seemingly overrides the visual information about the actual toy location. Older infants, however, who are better able to pay attention to the visual input (or/and to memorize the visual input) make the correct decision (Thelen et al., 2001).

For the present context of sequence learning, the impact of the preshaping mechanism on the time course of neural population activity and its biasing effect in decision processes are both important.

8.2 Model overview

Figure 8.1 presents an overview of the model architecture with several interconnected, one-dimensional fields representing the single cue (e.g., colour, position, pitch) that guides sequence learning. The three fields on top of the figure implement the memory of perceived events, whereas the two bottom fields become active during sequence recall.

A bump in the perceptual field u_{per} representing a specific value of the sensory cue drives through excitatory connections (solid line) the evolution of localized activity pattern at the corresponding site in the sequence memory field u_{mem}. Inhibitory feedback (dotted line) from u_{mem} to u_{per} in turn destabilizes the existing bump in the perceptual field. This feedback inhibition ensures that newly arriving input to u_{per} will automatically create a bump at a different (albeit neighbouring) field location even if the specific cue value is repeated during the course of the sequence. This is quite important for the representation of musical sequences since musical pitches often repeat in different orders. The stable multi-bump pattern in u_{mem} stores all demonstrated

sequence elements with a strength of activation decreasing from element to element as a function of elapsed time since sequence onset. This activation gradient is achieved by combining the field dynamics with a threshold accommodation dynamics for the firing rate function as introduced in the previous chapter. The decision field u_{de} receives the stable multi-bump pattern in u_{mem} as subthreshold input. Immediate sequence recall starts with a continuous increase of the baseline activity of the preshaped decision field. The dynamics retrieves the order and relative timing of sequence elements by subsequently triggering a suprathreshold response of the population with the currently highest pre-activation. The moment in time of reaching the threshold is assumed to initiate the corresponding overt behaviour (e.g., a pressing a key of a musical keyboard). The excitatory-inhibitory interactions between the decision field u_{de} and the working memory field u_{wm} guarantee that the latest decision in u_{de} is first stored and subsequently suppressed so that the representation of the succeeding sequence element can become suprathreshold.

A key role in the ability of the system to improve its performance in successive demonstration-execution cycles plays the past sequence memory field u_{pa}. It gets excitatory input from corresponding sub-populations in u_{mem} and has excitatory connections with the perceptual field u_{per}. During successive sequence demonstrations, a fading memory trace of the multi-bump in u_{pa} builds up. The important functional role of this memory trace is a preshaping of corresponding neural populations in the perceptual field u_{per}. Functionally, this priming by past experience can be interpreted as creating an expectation about subsequent perceptual events.

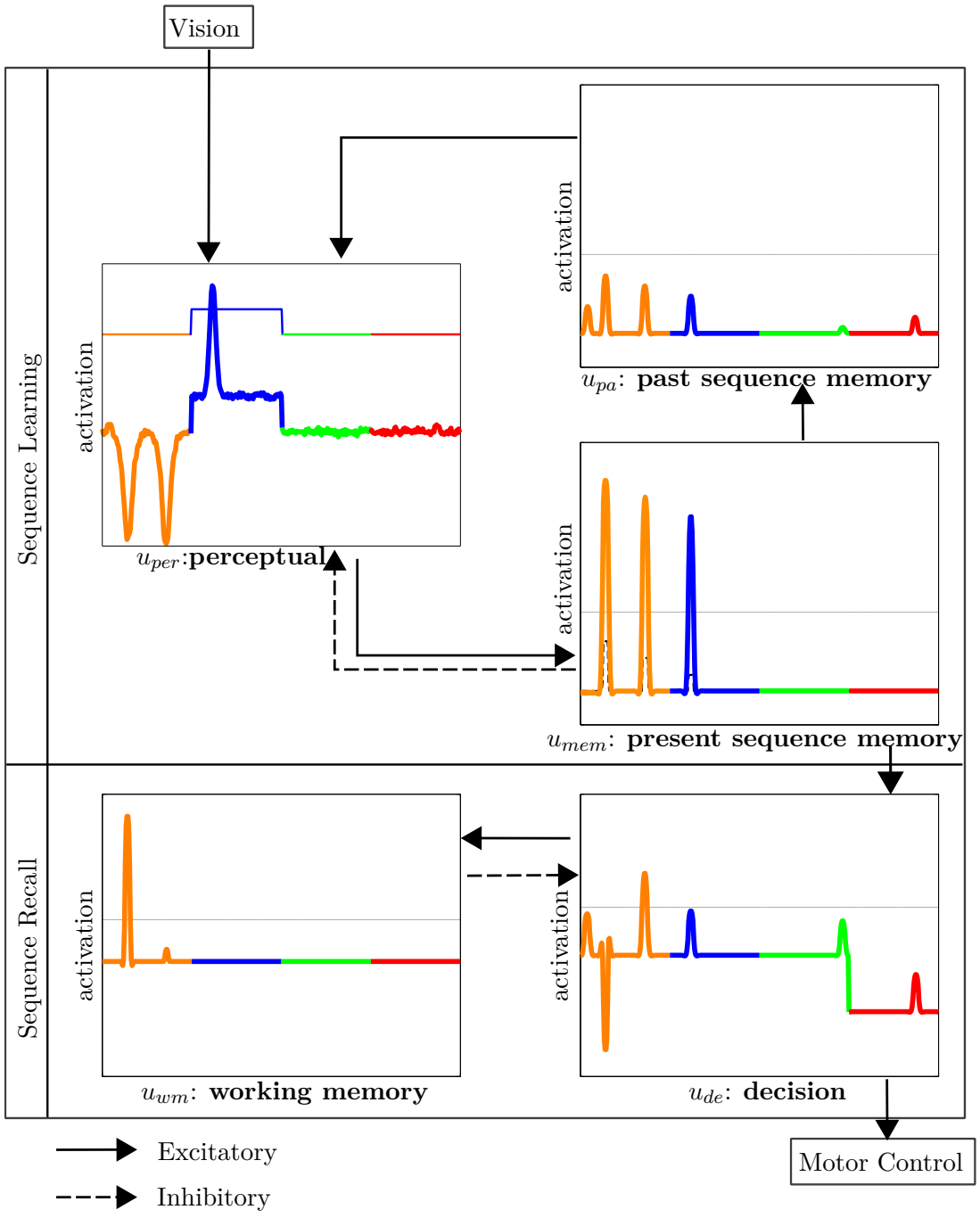

Figure 8.1: Sketch of the distributed architecture of the field model. Dashed lines indicate inhibitory connections, solid lines excitatory connections. For details see the text.

8.3 Model equations

The dynamics of the perceptual field u_{per}, the present sequence memory field u_{mem} and the past sequence memory field u_{pa} are governed by the following field equations:

$$\begin{aligned}
\tau_{per}\dot{u}_{per}(x,t) &= -u_{per}(x,t) + u_{pa}(x,t) + I(x,t) + \int w_{lat}(x-x')f\left(u_{per}(x',t)\right)dx' \\
&\quad - \int w_{osc}(x-x')f\left(u_{pr}(x',t)\right)dx' + \xi(x,t), \qquad (8.1)\\
\tau_{mem}\dot{u}_{mem}(x,t) &= -u_{mem}(x,t) + h_{mem}(t) + u_{per}(x,t)f(u_{per}(x,t)) \\
&\quad + \int w_{osc}(x-x')f\left(u_{mem}(x',t)\right)dx', \qquad (8.2)\\
\tau_{pa}\dot{u}_{pa}(x,t) &= -u_{pa}(x,t) + h_p + \lambda_{pa}u_{mem}(x,t)f(u_{mem}(x,t)). \qquad (8.3)
\end{aligned}$$

Here, $u_{per}(x,t)$, $u_{mem}(x,t)$ and $u_{pa}(x,t)$ represents the activity at time t of a neuron encoding dimension x. The positive constants τ_{per}, τ_{mem} and τ_{pa} define the time scale of each field. The firing rate function f is taken as the Heaviside step function with threshold 0 for all fields. The perceptual field u_{per} receives a localized visual input $I(x,t)$ which we chose for simplicity as being of rectangular shape with constant amplitude. The width of this input is assumed to be much larger than the width of an individual bump. Each position in this field is affected by additive Gaussian white noise $\xi(x,t)$ that represents spontaneous activity and defines the position at which a new bump evolves in response to the external stimulus. The connection functions w_{lat} and w_{osc} determines the coupling between neurons within the field. For the perceptual field and the decision field in which only one bump at a time should evolve, we use a kernel of lateral inhibition type given by (1.3). To enable multi-bump solutions in the memory fields, we use a kernel with oscillatory rather than monotonic decay given by (1.6).

The constant $h_p < 0$ is the global resting level for the past memory field u_{pa}. The parameter λ_{pa} represents the rate at which the subthreshold pattern of the past sequence memory is built. To ensure that the building is stronger than the forgetting, in successive sequence presentations, the rate λ_{pa} must be larger than 1.

The dynamics of the working memory field u_{wm}, the decision field u_{de} and its baseline dynamics are given by the equations (7.4), (7.3) and (7.5) respectively. The threshold accommodation of the u_{mem} is governed by equation (7.2).

8.4 Modelling results

8.4.1 Repeated items

Music provides an excellent example for complex sequences containing repetitions. Musical pitches repeat often within a melody, yet people do not confuse their sequential ordering and timing. How do they achieve this? Different classes of sequence models have proposed in the past distinct solutions for this problem (Henson, 1998). Simple chaining models in which each item becomes cue for the next item cannot deal with repetitions since a repeated item will become associated with more than one successor. This ambiguity can be reduced by assuming that the current item is determined by the history of past events rather than just the last one. Recurrent neural networks (RNN) have been successfully applied to learn these long-term dependencies for a context-sensitive chaining (e.g., Elman, 1990). However, the supervised learning algorithms of RNN models typically require a large number of sequence demonstrations which precludes their use for fast and unsupervised sequence learning.

The problem of repeated items is also well known for non-associative models that store order by an activation gradient (Page and Norris, 1998). Since in these models, a specific item (e.g., defined by a colour cue) is typically represented by a single node, a second instance of that item will further increase its activation, and as a consequence, the gradient will not correctly represent the two instances. Some ad-hoc solutions to solve this problem have been proposed like for instance a pre-processing of the input sequence in "chunks of items" that do not contain repeats, or the use of a tokenizer that attributes different nodes to repeated items (e.g., Bradski et al., 1994). In a similar vein, competitive cueing models in which the competitive item selection is followed by item suppression, face the obvious problem of representing immediate (or temporally close) repetitions. In principle, this problem can be overcome by hypothesizing a specific "repetition mode" that temporally disables the usual inhibitory feedback (Houghton, 1990). However, this ad-hoc solution requires at least to learn the repetition pattern (e.g., two or more repeats) and the point at which during sequence recall the "repetition mode" must be entered (for a modelling account see Shieh and Elman, 2006).

The field dynamics resolves the problem of item repetition without the need to

refer to additional processing or learning mechanisms. Figure 8.2 shows a snapshot of a model simulation in which the same sensory input is applied twice to the perceptual field u_{per}. The inhibitory feedback from the memorized first event in u_{mem} guarantees that the second bump evolves at a different position within the range of the external stimulation. With respect to the build-up of the sequence memory in u_{mem} there is no difference whether the currently processed item is a repeated item or not. What determines the ordinal position of the item is the time at which population activity reaches the threshold and not where in the field the localized pattern evolves.

Note that since the model is essentially one-dimensional we have used for simplicity a scalar field with a localized input that is much larger than the width of individual bumps. This ensures that the same input pattern may generate bumps at different field sites. A more general solution would be to use a two-dimensional field of lateral inhibition type with an input in form of a ridge (Erlhagen and Schöner, 2002; Faubel and Schöner, 2008). Two-dimensional bumps that evolve along this ridge in response to the presentation of the stimulus at different points in time would represent repeated items.

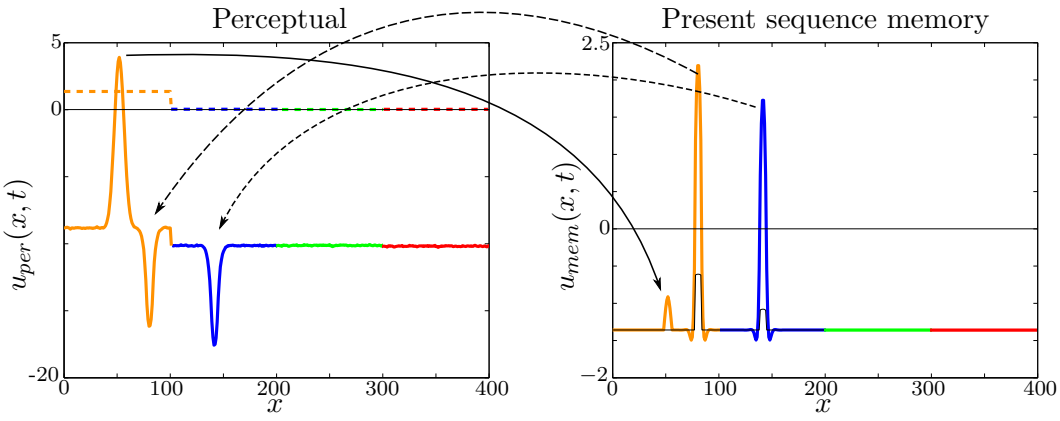

Figure 8.2: Snapshots of the activation of the perceptual field, u_{per} (left, solid line) in the presence of external input (dashed line), and the activation of the present sequence memory field, u_{mem} (right) are shown. The dashed arrows indicate inhibitory connections and the solid arrow excitatory connections between the two fields.

8.4.2 Importance of preshaping

Figure 8.3 presents a model simulation in which a sequence of 6 colour coded stimulus events with repletion of items is presented in 3 successive experimental trials. It is assumed that after each trial remaining suprathreshold activity (e.g. in the working memory field) is reset to resting level except in the past sequence memory field in which a memory trace builds up. The pre-structured state of the perceptual field at the beginning of the second and third trial (left panel) reflects the growing experience with the task. This has dramatic consequences for the processing of sensory information and consequently also for the encoding of events in memory. In the right panel, the time course of population activities in u_{mem} is compared relative to the onset of the individual stimuli (vertical lines). In the first trial, the second stimulus, which is a repetition of the first, is not represented. This is due to the relatively short inter-stimulus interval. At the moment when the second input is applied to the perceptual field, the population representation of the first stimulus is still suprathreshold (not shown), resulting in a strong inhibition of neighbouring neurons. As a result, the second stimulus is not able to trigger a suprathreshold response. The situation is different in the second trial in which the processing of inputs in u_{per} already starts from an activation level closer to the threshold. The time course of transient population activity is now fast enough to represent also the second stimulus. The activation gradient established at the end of the trial reflects the correct serial order of all 6 items. However, the variability in the time delay between stimulus onset and the moment of reaching the threshold is relatively large, indicating that the relative timing of events is still not well represented in memory. As can be seen in the evolution of the population activities in the third trial, a larger pre-activation of populations significantly reduces this variability, resulting in a nearly identical delay for all item memories.

8.4.3 Sequence errors

Traditionally, specific sequence recall errors that are frequently observed in experiments with humans have been used to discuss the advantages and limitation of different theories and models of sequence learning and memory (Henson, 1998; Rhodes et al., 2004). Rather than trying to fit detailed error patterns that may depend on the exact nature

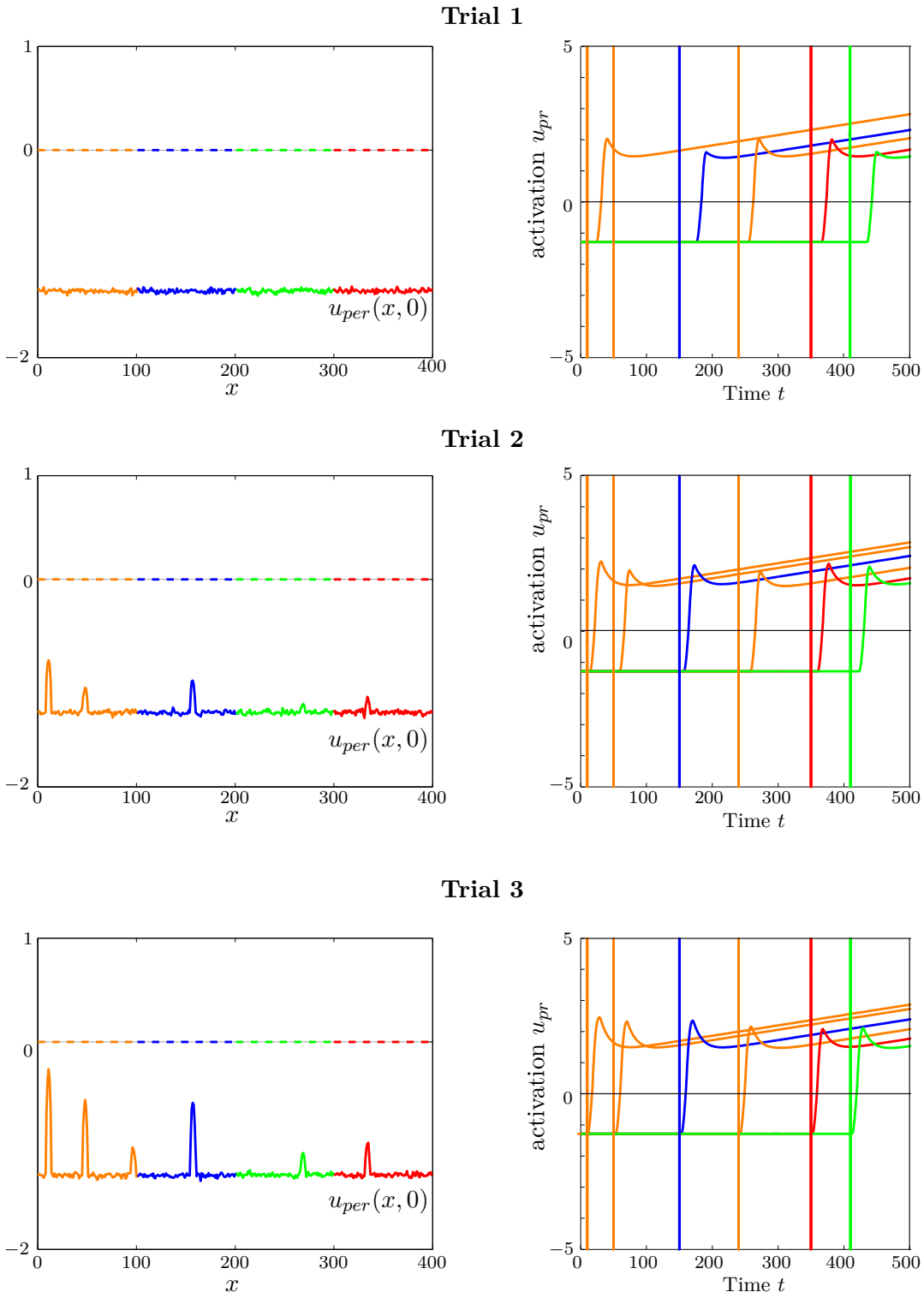

Figure 8.3: Snapshots of the initial state of the perceptual field (left) and the time course of the maximal activation of each subpopulation representing the different sequence elements are shown for the present sequence memory field (right) in each of the three trials. Parameters value used here: $\tau_{u_{per}} = 10$, $w_{exc_1} = 4$, $\sigma_{exc} = 4$ and $w_{inh} = 2.5$, $A = 2$, $k = 0.4$ and $\alpha = \pi/20$, for u_{per}, and $\tau_{u_{mem}} = 15$, $\tau_{h_{mem}} = 300$, $h_{mem_0} = h_p$, $A = 1$, $k = 0.6$ and $\alpha = \pi/5$, for u_{mem}, $\tau_{u_{pa}} = 10000$, $\lambda_{pa} = 5$, $h_p = W(5)$, for u_{pa}.

and design of sequential tasks, we show in model simulations how the occurrence of certain types of errors may be explained by the dynamic field concepts.

Erroneous sequence recall performance may have different origins. It may be result of a mistake in stimulus encoding like in the example of Figure 8.3 (top), or reflects a conflict on the output or sequence production level. Many errors involve the production of a sequence element in a serial position other than the intended one. Like in other gradient based models of serial performance, production errors can be generated in the DNF model by adding random fluctuations to the decision field. However, since order and timing errors after learning and practice are relatively rare events, the noise level should be carefully chosen not to completely override the information encoded in the activation strengths of the sequence memory.

Figure 8.4 shows a simulation example for a sequence with 4 memorized events (top). The Gaussian noise added to each site of the decision field does not prevent the field dynamics from recalling the sequence in the correct order, as shown by the transient population activation profiles (bottom left). Moreover, the interval between successive decisions, measured at the time of reaching the threshold, matches well the inter-stimulus intervals of the sequence (bottom right). With the given noise level, the variation is below 2.5% of the duration for all three inter-stimulus intervals.

Many errors involve the production of a sequence element in a different serial position from that intended by the performer, which supports the notion of a parallel activation of several items during sequence planning and execution. Moreover, there is a tendency that people confuse more often elements close together in a sequence than far apart, which is consistent with the idea of an activation gradient. These "contextual errors" can either be anticipatory (items intended for future positions) or preservative (intended for past positions) in nature. Figure 8.5 depicts model simulations with the noise level used in Figure 8.4 for both error types. In the right panel, the noise in the decision process causes a change in the order of recall of the two last items. The left panel shows an erroneous recall of the first item in position 3. The latter error cannot be explained by noise alone since a strong feedback inhibition from the memory of already performed items in u_{wm} usually prevents repetition errors. In the simulation, the choice of a weaker feedback inhibition due for instance to a failure in the memory

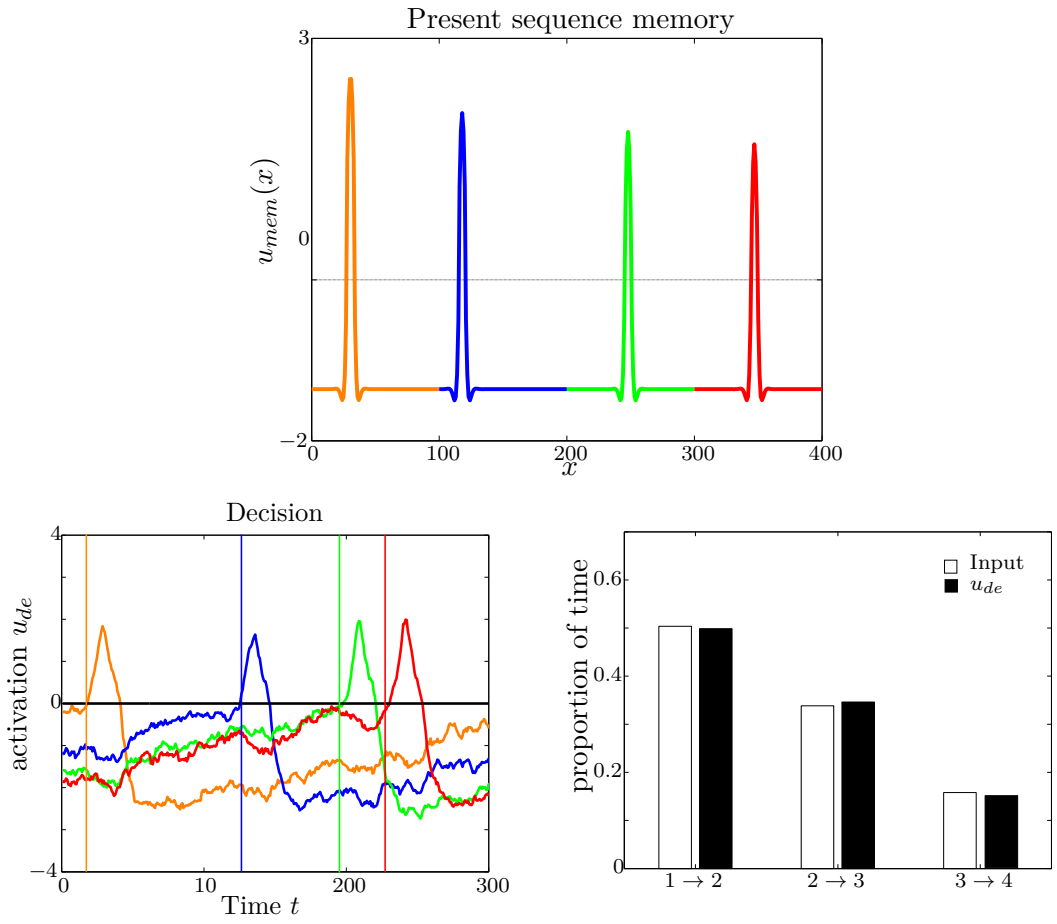

Figure 8.4: Activation pattern corresponding to the correct memory of a sequence with four different elements (top). The time course of population activity in u_{de} representing the different sequence elements is shown (bottom left). The vertical lines indicate the time of cue presentation. The exact inter-stimulus intervals (white) and compared with the predicted intervals from suprathreshold population activity in u_{de} (black, bottom right).

process (e.g., no self-sustained bump evolves) explains this error.

Anticipatory behaviour is commonly believed to be correlated with the level of practice and to reflect the advanced preparation of future sensorimotor events. The error rate of sequence recall decreases in general with practice but the proportion of anticipatory errors increase in many domains (speech, sport, music performance, for discussion see Palmer and Pfordresher, 2003). Interestingly, there exists also a relation between the sequence production rate and the number of anticipation errors. This specific speed-accuracy trad-off has been described for instance for expert piano players (Pfordresher et al., 2007). The prediction of DNF model are in line with these

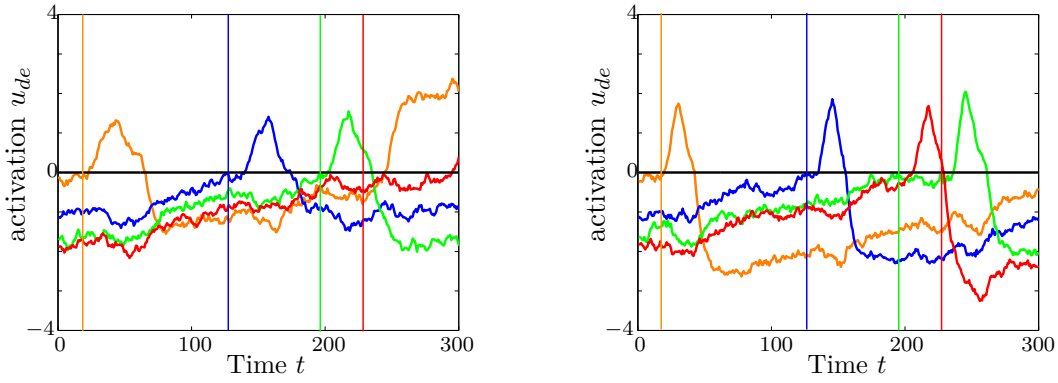

Figure 8.5: Example of a repetition error (left) and an anticipatory error (right) are shown.

experimental findings. Figure 8.6 shows that the rate of anticipatory errors (number of anticipatory errors/ number of trials) increase approximately linearly with execution speed ($r = 0.938867, P < 0.01$). In the simulations, the execution speed has been changed by adapting the growth rate of the of the h-dynamics in the decision field accordingly (compare).

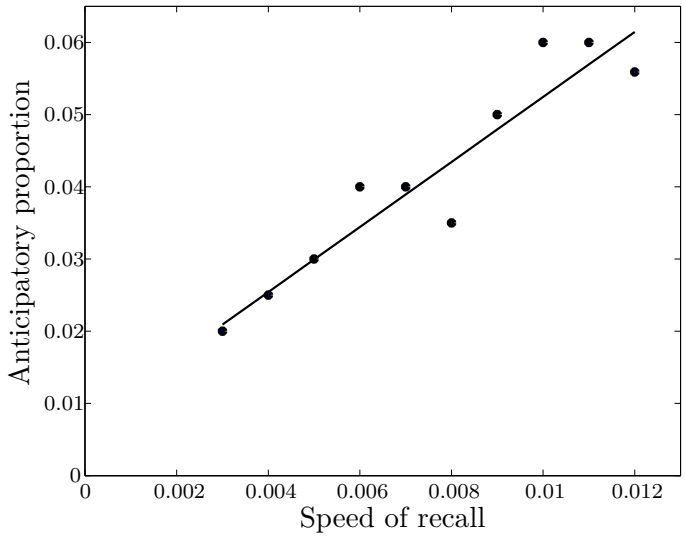

Figure 8.6: Correlation between the number of anticipatory errors and the speed of serial recall.

8.5 Discussion

The main purpose of the model extensions introduced in this chapter was to explain how the ordinal and timing properties encoded in the neuronal activation patterns may be acquired during exposure to correct sequence demonstrations. The simulation results highlight the importance of the time course of population activity for the memory process. The preshaping of neural population by past experience speeds up the processing of sensory information. This ensures not only that all sensory events become stored in memory in the correct order but also that the temporal relationship between events can be quickly acquired. Moreover, the dynamics of the perceptual field which is shaped by the excitatory and inhibitory inputs from the memory fields automatically generates population representation for each new sensory event. The field dynamics thus autonomously solves the problem of repeated items without the need to refer to additional processing or learning mechanisms.

During sequence recall, the decision time for each event is determined by the amount of preshaping by the excitatory input from u_{mem} and the resting dynamics which provides a linearly growing, additional input to the decision field. Since the difference in pre-activation between successive events is linearly related to elapsed time, the relative timing of events is automatically preserved during recall. Two observation are worth mentioning in this context. Firstly, the assumed linear increase of activation is in line with neural data showing an approximately linear build up of activity until a fixed activation threshold associated with a predicted event is reached (Durstewitz, 2004). It is important to notice however that the linear growth is by no means a necessary model assumption. More complex dynamics for the threshold accommodation and the resting state like for instance an exponential growth could have been used as well. This is important to keep in mind when thinking about possible neural implementation of the simple resting dynamics used in the model simulations. Secondly, the time course of suprathreshold activation in the different model layers unavoidably causes processing delays in the internal representation of external events (compare for instance the time courses of activation in Figure 8.3). The system has to compensate these delays if a task requires to synchronize the behaviour with external events (e. g., caused by others' action in a shared tasks). The anticipation of external events can be achieved

in the model by choosing an adequate value for a "default" resting state from which the linear h-dynamics starts (e.g., compare the simulations of Figure 8.4 where the activation reaches threshold at the exact time of the external event). Interestingly, the idea of a task-dependent proactive inhibition of motor behaviour to control premature responses (Wardak et al., 2012) is in line with a context-dependent adaptation of the global baseline level of the field dynamics defined by the parameter $h < 0$. Lowering or increasing the global inhibition in the decision field will result in shorter or longer reaction times, respectively. How can the system learn to predict the timing of future events by choosing an adequate resting level? One possibility is to postulate an event monitoring system (Bicho et al., 2011) that compares the time course of suprathreshold activity in the perceptual and the decision field during the recall of a sequence from memory. If the monitoring system detects a delay between the onset of suprathreshold activity in both layers (that is, a mismatch between the expected and the real timing of an event), the h-value of the decision field will be adapted until synchrony is achieved.

Chapter 9

A real-world robotics experiment

In this chapter, we present results of a real-world robotics experiments which was designed to directly test the assumptions and predictions of the sequence learning model discussed in the previous chapter. First the humanoid robot ARoS has to memorize and subsequently, execute a short musical sequence that a human teacher demonstrates on a keyboard. Specifically, we were interested to evaluate the real-time constraints of the perceptually-cued learning task on the processing of order and timing information in the layered dynamic field model.

9.1 Physical and Virtual Frameworks

9.1.1 The robot ARoS

ARoS (**A**nthropomorphic **Ro**botic **S**ystem) is an anthropomorphic robot which has been developed at the Anthropomorphic and Mobile Robots Laboratory at the University of Minho (Figure 9.2).

The body of ARoS consists of a metallic support structure on which a seven degrees of freedom anthropomorphic robotic arm and a stereo camera system with a pan-tilt unit are attached (Figure 9.1, (b)). A three-fingered hand mounted on the arm allows the robot to grasp and manipulate objects that are detected by the vision system in a flexible, that is, task dependent manner (Figure 9.1, (a), for details see Silva, 2008). In the past, ARoS has been successfully tested in several cooperative human-robot interaction (HRI) tasks. Its cognitive control architecture based on the

dynamic neural field framework is inspired by neuro-cognitive mechanisms supporting human joint action (Bicho et al., 2012).

The present experiments advance the robotics research in two main directions. Firstly, while in our previous HRI studies the information about the sequential task execution was hand-coded, the robot now efficiently learns the sequential order in just a few demonstration trials. Secondly, aspects of action timing were addressed in our previous work mainly in the sense of an anticipation of action outcomes ahead of their realization to guarantee smooth and fluent human-robot interactions. For executing a musical sequence in a recognizable manner, anticipated planning of future events is necessary but not sufficient. Playing a melody requires precisely timed motor responses at intervals of varying durations.

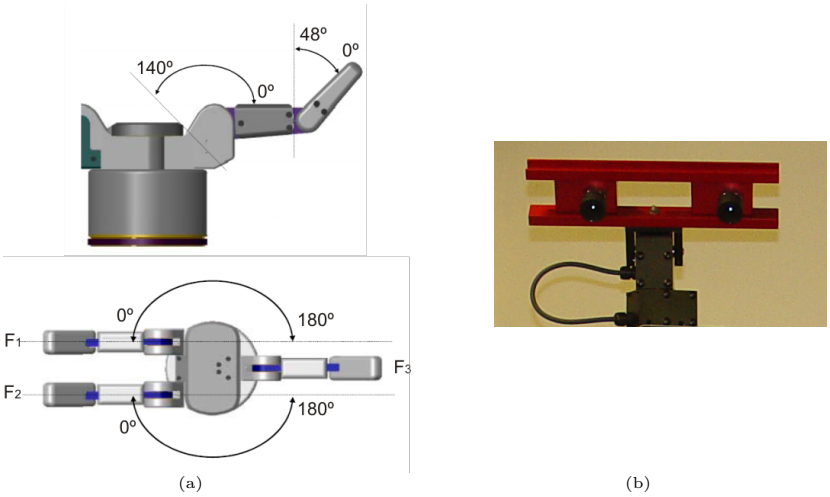

Figure 9.1: The ARoS hand (a) and stereo vision system (b).

9.2 Learning a musical sequence by observation

The ultimate goal of the experiment was that after learning the robot should be able to play a simple melody on a toy keyboard with four keys. We adopted a learning by observation paradigm since evidence from serial response tasks (SRT) suggests that knowledge of serial order can be acquired perceptually even in the absence of a motor response (e.g., Howard et al., 1992, Robertson and Pascual-Leone, 2001, but see Willingham et al., 1989). There is still a debate in the literature under which conditions

and to which extent (implicit) learning can occur in the absence of motor sequencing. Conditions that seemingly favour perceptual learning of sequential information are simple mappings between a perceptual cue and the corresponding motor response. Such simple mappings allow the subject to pay attention to the perceptual events. Inspired by learning experiments with elementary music students Rogers (1991), we used a display with colour coded piano keys as sensory modality and not the auditory channel (which would be in principle also possible). A key press by the human demonstrator produced not only a sound but also activated a coloured square on a computer screen that was easy to detect for the robot (orange for C, blue for D, green for E and red for F, see Figure 9.2). Moreover, the visual cues on the display matched the colour and relative position of the keys. During sequence recall, the fingers where positioned directly above the keys to execute a pre-defined tapping movement whenever the associated population activity in decision field reached a threshold value. Learning the arbitrary mapping between the visual cue and the required response was thus not part of the sequence learning process.

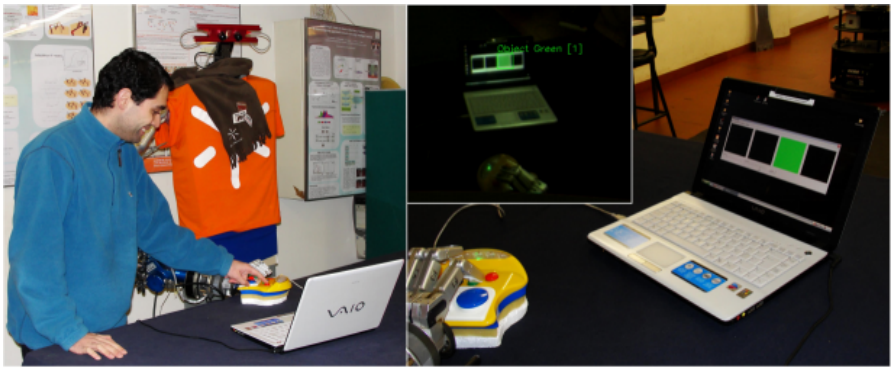

Figure 9.2: Human and robot playing a melody on a keyboard.

Since the robot has only three fingers and the hand does not move, the human partner has to execute one note of the musical sequence. A joint execution of the learned melody can be achieved by applying at the start of sequence recall an additional inhibitory input to the respective pitch representation in the decision field. As a consequence, the neural populations representing this pitch do not reach the threshold for overt motor behaviour. Such a proactive inhibitory control of a motor response has been proposed as a general processing mechanisms to adjust neuronal decisions as a

function of the prior knowledge that subjects have about their environment (Wardak et al., 2012).

9.2.1 Experimental results

As an example of an easily recognizable melody, we selected the first part of the “Happy Birthday" melody for the learning experiments. The musical sequence is composed of six elements with three repetitions of the note C (C-C-D-C-F-E). The human demonstrates the melody until the robot is able to play all keys in the correct order and with the correct timing. To quantitatively validate the model in terms of its ability to produce sounds with the correct temporal pattern, we compared the interval between successive tones (in percentage of sequence duration) in the demonstrations with the model predictions. In the majority of the experiments, the robot was able to reproduce the melody after only three demonstrations (a video with an example of the experiments can be found at `http://marl.dei.uminho.pt/public/videos/Learn_a_musical_sequence.html`).

The top panel of Figure 9.3 shows for three successive demonstrations the activation pattern in the present sequence memory field, u_{mem}. Due to the threshold accommodation dynamics, the bump amplitudes reflect the temporal order of the demonstrated musical sequence. The middle panel compares the exact point in time in which each note was played by the teacher (vertical lines) with the time course of the maximal activation of the corresponding population representation in u_{mem}. The bottom panel compares the relative timing of the played melody (white bar) and the model prediction when the fixed read-out threshold is applied to the evolving population activity in u_{mem} (black bar).

After the first demonstration, the robot memorized only five of the six notes as shown by the five bumps in the top panel of Trial 1. The fourth note was lost, due to the time delay in encoding the first three notes (compare the time course in the middle panel of Trial 1). When the fourth note is played, the population representation of the third note has just reached threshold and due the strong competition mediated by lateral inhibition no suprathreshold activity representing the forth note evolves (panel 2, Trial 1). The processing delay in u_{mem} is due to a relatively slow formation of bumps

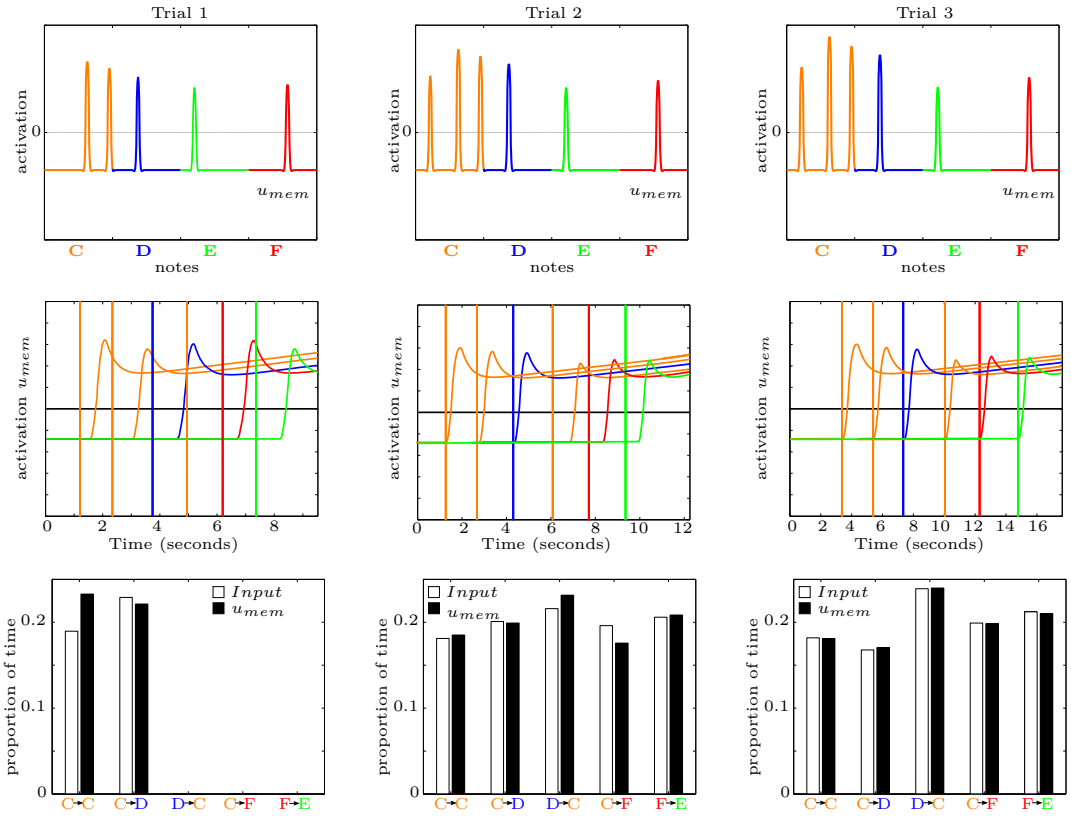

Figure 9.3: Comparison of population activity in u_{mem} in 3 successive demonstration trials. *top panel*: Self-stabilized activation pattern. *middle panel*: Time course of population activity representing the different sequence elements, and timing of notes during demonstration (vertical lines). *bottom panel*: Relative time intervals between successive tones (white) and predicted intervals from suprathreshold population activity in u_{mem} (black).

in the perceptual layer which does not follow the presentation rate of the demonstration.

During the second demonstration, the preshaping from the past sequence memory field lead to a much faster processing of the colour information in u_{per}, and consequently also to a speeded processing in u_{mem} (middle panel, Trial 2). The robot is able to memorize all notes of the melody (top panel, Trial 2). The errors in the relative timing, however, are still considerable (bottom panel, Trial 2). When playing the musical sequence with the encoded temporal pattern, the difference to the demonstrated pattern is easy to detect for a human listener. In the third experimental trial, the processing of the preshaped input and sensory input in u_{mem} results in a time course of suprathreshold activity of the different populations that robustly matches the relative timing of all notes in the demonstrated sequence.

9.2.2 Different execution speeds

The top panel of Figure 9.4 compares the time course of population activity in the decision field when the robot jointly executes with the human partner the melody from memory with two different speeds. As can be nicely seen, the population representations of all notes that the robot has to play appear to be pre-activated at the time of sequence onset with a relative strength reflecting the temporal order. For the joint execution of the learned melody, the F-key has been assigned to the human partner and therefore its population representation receives additional inhibitory input. Consequentially, the input from the memory field u_{mem} is not sufficient to drive the population representing F (red line Figure 9.3) beyond threshold.

Different execution speeds are achieved by adapting the time constant of the baseline dynamics in the decision field, τ_{de}. If τ_{de} is chosen equal to the parameter τ_{mem} controlling the growth rate of the threshold accommodation dynamics, the recall dynamics nearly perfectly reproduces the stored timing of notes of the sequence demonstrations (vertical lines). If the time scale for the baseline dynamics is chosen smaller, the execution of the sequence appears to be accelerated.

In line with a key principle of interval timing in humans and other animals (Machado et al., 2009), the characteristic temporal pattern of the melody appears to be preserved in the speeded execution. A comparison of the two bottom panels of Figure 9.4 shows that the pattern of interval timing between successive events in the two execution trials is nearly identical and matches the relative timing information encoded in the memory gradient in u_{mem}.

In this context it is worth noting that the variability in decision timing introduced by additive noise in u_{de} violates Weber's law, another hallmark of interval timing. As shown in Figure 7.7, the model predicts a nearly constant variability σ independent of the interval to time T. This means that the Weber fraction defined as the coefficient of variation ($CV = \frac{\sigma}{T}$) decreases with interval length and thus does not reproduce the scalar property of interval timing (compare Figure 7.7). Interestingly, a recent study in which participants reproduced different target intervals with finger tapping found that for some duration ranges training led to a reduction of variability to a value that remained constant over interval length (Grondin and Killeen, 2009). Moreover, the

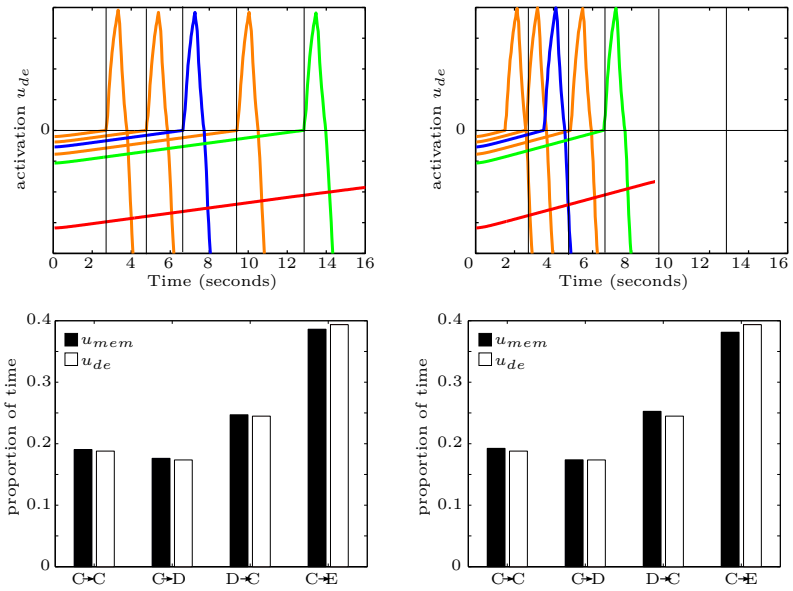

Figure 9.4: Time course of the maximal activation of each element in the decision field (top). Relative timing of successive tones in u_{mem} and in u_{de} (bottom).

authors report a significant difference between musicians and non-musicians in task performance. Only participants which lacked an intensive musical training showed an invariant CV. Seemingly, skilled musicians have learned to minimize variability over trials since the correct timing of intervals with different lengths is fundamental to give meaning to a musical sequence. In the model simulation of the Weber law, the subthreshold population activity in the decision layer rises linearly to the threshold for response initiation at a rate that varies from trial to trail with a Gaussian distribution (compare Figure 7.7). Assuming that this source of variability can be reduced to nearly zero by training would explain the decrease of the CVs of musicians with interval length since only the noise-induced variability in the timing of the decision process would contribute.

9.3 Discussion

Learning to play a piece of music is an excellent example for studying the intimate coupling between ordinal and timing properties of complex sequence behaviour. At first glance, the fact that in music performance the duration of the sequence and therefore

also the timing of the single movements can be changed without affecting the sequential order speaks for a (at least partly) separated representation of both aspects of sequential behaviour. The observation in many motor sequence learning studies that serial order is typically leaned much quicker than the temporal properties has been interpreted as further evidence for a separated view (e.g., Kornysheva et al., 2013). The robotics experiments show that a fully integrated representation in form of an adaptive activation gradient is sufficient to achieve both precise interval timing and proper order. To adapt the speed of performance, the only additional assumption to make is that a growing signal related to elapsed time is integrated with the learned sequential information to control the time of motor decision. In the model, the urgency of motor preparation can be "voluntarily" changed by simply adapting the time constant of the baseline dynamics (for a discussion of a possible neural substrate see Lewis and Miall, 2006). The experiments also show that an integrated memory of order and timing is not in disagreement with a two-stage learning process since the activation gradient representing order is established first followed by a fine tuning of the activation strengths representing the timing information.

The present work complements previous experimental and modelling studies with the serial reaction time task that also advocates the integrated view (Dominey, 1998; Shin and Ivry, 2002; O'Reilly et al., 2008; Gobel et al., 2011).

In the field of human-robot interactions, robot learning by observation is considered highly attractive since it allows in principle a normal user to teach a robot new tasks in an intuitive and simple manner (Dautenhahn and Nehaniv, 2002). Importantly, since users will not likely invest time in many repeated demonstrations, the learning should be efficient and fast. In the activation based dynamic field model, correctly representing the musical sequence takes just a few demonstrations. This contrasts with the performance of typical recurrent neural network models of serial behaviour that usually need a large number of training trials to successfully store sequential information in connection weights (e.g., Cleeremans and McClelland, 1991; Dominey, 1998).

The present learning experiments were simplified in two important ways. The visuomotor associations, or mapping between the visual cues and the required responses were pre-defined. In principle the arbitrary mapping could be also learned using stan-

dard associative (Hebbian) learning rules between the neuronal representations of the cue (colour or pitch) and the respective position on the keyboard or the specific effector. More challenging is the learning of anticipatory finger motion towards upcoming key presses when the hand has to move during the execution of more complex musical sequences.

In the context of robotics applications it is important to stress that due to the self-stabilized properties of the field dynamics the model runs autonomously without feedback from the environment. This can be used by the robot for instance to "mentally" simulate the order and timing of sequential events. Such an internal simulation offers new perspectives for learning generalized sequence knowledge in task that are for instance not defined by a unique order (Bicho et al., 2011). A fast activation based learning system like the one presented here could be used to train a slow learning system based on the synaptic weight adaptation to extract from different examples generalized task knowledge (e.g., different orders of task execution, Sousa et al., 2014).

Part IV

General discussion and future work

Chapter 10

General discussion and Future Work

10.1 Discussion

The work presented in this thesis was guided by two closely related objectives. Firstly, the formation of multi-bump solution of a scalar neural field in the presence of localized external input was studied. Secondly, the new mathematical insights allowed us to develop and apply an innovative sequence learning model that stores the order and the timing of events in stable multi-bump patterns of neuronal activity.

For modeling the recurrent interactions in neuronal populations, we applied a coupling function with oscillatory rather than monotonic decay first suggested by Laing et al. (2002), and used a step function to approximate the nonlinear firing rate or activity of neurons. The proofs of the existence and stability of patterns followed the ideas introduced by Amari in his seminal 1977 paper for the case of lateral inhibition type connections (for follow up studies see Pinto and Ermentrout, 2001; Guo and Chow, 2005a,b).

The main mathematical results of Part II of the thesis are summarized as follows. We achieved:

1. the derivation of sufficient and necessary conditions for the existence of one-bump solutions (with a range of possible widths) (Theorem 1);

2. the derivation of a sufficient condition that guarantees the existence and stability of a one-bump solution with a minimum width (Theorem 2);

3. the derivation of a sufficient criterion that guarantees the existence of a value of a^* that satisfies the necessary condition for the existence of one-bump solutions in a presence of localized external input (Theorem 3);

4. the derivation of sufficient conditions that guarantee the existence of equal width two-bump solutions for a specific value of h (Theorem 4);

5. the derivation of a sufficient condition that guarantees the existence and stability of equal width two-bump solutions with a minimum width and minimum distance between bumps for a particular value of h (Theorem 5);

6. the derivation of a sufficient criterion that guarantees the existence of the two values of a^* and of b^* that satisfy the two necessary conditions for the existence of equal width two-bump solutions in a presence of external input (Theorem 6).

The rigorous mathematical results obtained for the cases of one and two bumps allowed us to systematically test analytical and in numerical studies pattern formation for the case $N > 2$. The specific focus of the numerical integration of the field dynamics was on the impact of the spatio-temporal characteristics of the external input applied to the field. The results provide important constraints for the applications in which the spatial shape and the relative distance of inputs to the field are important.

The theoretical results of Part II were the backbone for the DNF models of sequence learning and memory developed and tested in Part III. To generate a stable multi-bump solution with an activation gradient, a threshold accommodation dynamics was applied. Neurons with suprathershold activity adapt according to a simple linear dynamics their threshold for triggering the recurrent interactions within the local population. It is important to notice that this accommodation dynamics increases the stability of the patterns since excited neurons with higher threshold appear to be less sensitive to spatial perturbations of the activity profile. In neurophysiological terms, the gradient of activation of different subpopulations in the field not only represents specific values of a stimulus dimension (e.g. colour in the robotics example,

for discussion see Erlhagen et al., 1999), but also encodes in addition elapsed time as a second dimension in the relative activation strengths. In general, the model builds on the assumption that self-sustained activity in neuronal populations constitutes a fundamental processing principle supporting several high-level cognitive functions like working memory, timing and decision making (Miller, 2000).

Coupled with an h-adaptation dynamics in the decision field, the sequence learning model allows not only to recall the order of events but also the relative timing of events. The model makes a new contribution to the hotly debated question in cognitive neuroscience (e.g., Kornysheva et al., 2013) whether the timing of events is stored independently of the order of events. While results of the serial response time (SRT) paradigm are in general interpreted as evidence for an integrated representation of these dimensions (Shin and Ivry, 2002), evidence from learning studies and studies imposing constraints on sequence duration seemingly favour the existence of separate representations. For instance, learning a musical sequence typically occurs in two phases. The order of notes is memorized first which is followed by an adjustment of their exact timing. After the sequence has been learned, it can be executed with different speeds thereby preserving the relative timing of notes (Janata and Grafton, 2003). Both findings show that significant changes in the temporal structure of the sequence can be observed without affecting the ordinal dimension. The DNF model demonstrates that the development of memory representations that are sensitive both to the sequential structure and the timing of events is not in contradiction with experimental findings showing a relative independence of the two dimensions.

The implementations of the model as part of the DNF architecture for human-robot interactions on the humanoid robot ARoS (Bicho et al., 2010, 2011) allowed us to test hidden model assumptions. For instance, the time course of the field dynamics has to be adapted so that the evolution and decay of self-stabilized population activity may follow the real-time presentation of the musical sequence. Indeed, even if the visual system of the robot is fast enough to detect the colour code of each note and the robot knows the mapping onto the respective key press, existing suprathreshold activity from a previous event may prevent a newly presented signal to be encoded due to the competitive field dynamics. This happens to occur in the perceptual layer

in the first demonstration trials and caused an omission error. The mechanism of preshaping of populations due to prior experience is not only responsible for speeding up the processing in general, but also for the correct timing of the key presses on the keyboard. The memory of the previous sequence demonstration in the past memory field generates an expectation of each sensory event in the perceptual field and primes the corresponding motor preparation in the decision field. The learning experiments show that the robot is able to correct in a series of demonstration-execution cycles initial order and timing errors.

Although the sequence model presented in Chapter 8 has been developed with the goal to apply it for the learning of short musical sequence, it can be easily adapted for many others situations in which ordinal and timing information are tightly coupled (e.g. typing, speech, social interactions). For instance, a fluent and pleasant human-robot cooperation in routine service tasks such as preparing the dinner table or handing over (or receiving) a set of objects to an elderly, a judgement about the ordinal sequence structure but also a metrical judgement that involves the analysis of elapsed time between routine events is essential. Moreover, the robot should be able to synchronize its actions and decisions with different users, making the capacity to adjust its timing of actions a central one. With an integrated representation of ordinal and timing properties of sequential tasks the robot is able not only to anticipate what the user needs next (Bicho et al., 2010), but may also predict the moment in time when it should for instance start a handing over sequence.

10.2 Future Work

10.2.1 Mathematical analysis

10.2.1.1 Existence and stability of multi-bump solution

In this thesis, we have analysed the existence and stability of N-bump solution for $N > 2$ for specific cases only. A more rigorous mathematical analysis in the sense of Chapters 3 and 4 that also includes external inputs remains an open question for future research.

10.2.1.2 Extension to two space dimensions

For the two-dimensional case, the dynamic field equation (1.1) can be generalized to

$$\tau \frac{\partial u(x,y,t)}{\partial t} = -u(x,y,t) + \int\int_{\Omega} w\left(x-q, y-s\right) f\left(u(q,s,t)\right) dqds + h + S(x,y,t), \tag{10.1}$$

where Ω is an open connected subset of $\mathbb{R}^2$, $f(u)$ is the Heaviside function, and w represents a two-dimensional connectivity function given by

$$w(r) = w(x,y) = Ae^{-k\sqrt{x^2+y^2}} \left(k \sin\left(\alpha\sqrt{x^2+y^2}\right) + \cos\left(\alpha\sqrt{x^2+y^2}\right)\right). \tag{10.2}$$

Laing et al. (2002) show numerical results supporting the notion that also in two-dimensional fields multiple localized excitations may co-exist simultaneously when the class of connectivity functions used for the scalar case is generalized to two dimensions. A rigorous existence and stability analysis remain an open problem.

10.2.2 Sequence model

10.2.2.1 Generalization to two dimensions

In robotics applications there are many situations in which the position of a bump in two-dimensional domain would be of interest. For instance, the bump may not only encode the colour but also the position of a specific object in space. Figure 10.1 shows an example of self-stabilized bump in a two-dimensional sequence memory field with a gradient of activation encoding the order and elapsed time of 5 sequence elements.

It is straightforward generalize the model equations presented in Sections 7.3 and in 8.3 to two dimensions. However, new mathematical insights about the conditions for pattern formation in the presence of time-varying input from connected fields would be highly desirable to constrain the model parameters for the numerical studies.

10.2.2.2 Chunking mechanisms

The melody used for the learning experiments was very short. Typical musical sequences that can be readily memorized and recalled consist of hundreds of tones. The idea of a single activation gradient cannot be applied to robustly represent such large numbers of elements. The solution could be to exploit structural and relational aspects

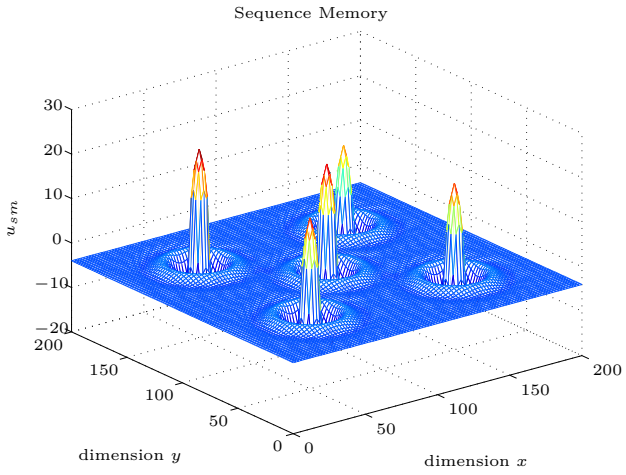

Figure 10.1: Example of multiple self-stabilized bumps a two-dimensional in sequence memory field.

of individual elements to group them together to larger units (Janata and Grafton, 2003). We are currently exploring in simulation studies how "chunking" mechanisms may be integrated in dynamic neural field models of serial behaviour to cope with this challenge (Sousa et al., 2014).

10.2.3 Robotics applications

10.2.3.1 Coding of note duration

The model presented in Chapter 8 and tested in represents Chapter 9 the serial order of notes and their relative onsets. This information is sufficient to reproduce in a recognizable manner a simple melody. However, for more complex melodies also the tone duration (time length) of each note has to be taken in consideration. Figure 10.2 sketches an extended version of the model described in Section 8.2 in which also the tone duration is memorized. The basis idea is that during demonstration not only the onset but also the offset of the sensory signal (visual or auditory) is registered. There is therefore an "on" memory field like in the previous version and in addition an "off" memory field. The "off" field receives input from the perceptual field and the multi-bump pattern from the "on" field as preshaping input. As a further modification, the working memory field for already executed movements is replaced by an "off" decision field. Evolving suprathreshold activities in the "on" or the "off" decision fields are associated with pressing or lifting finger movements, respectively. Moreover, inhibitory

feedback connections form the “off” decision field to corresponding positions in the “on” decision field guarantee that an already executed note of the melody is not accidentally repeated.

The implementation of this extended model on ARoS and its validation in learning by demonstration tasks is part of future work.

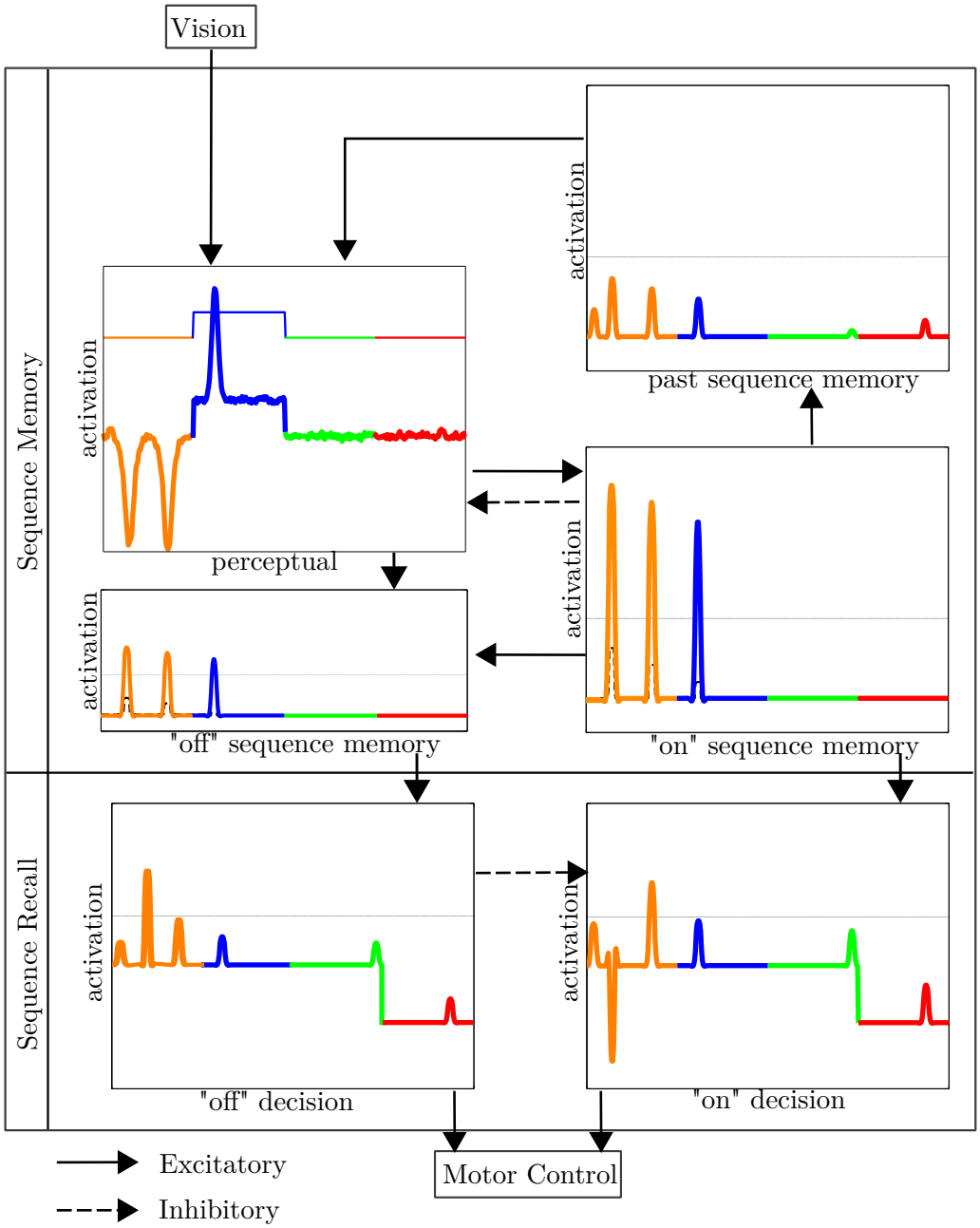

Figure 10.2: Sketch of the distributed architecture of the musical sequence model with the codification of note duration. Dashed arrows indicate inhibitory connections, solid arrows excitatory connections.

10.2.3.2 Playing with two hands

In the experiment presented in Chapter 9, the robot used its three-fingered hand to play on a keyboard with four keys. Since the robot is not moving its hand, it needs the cooperation of a human partner to play simple pieces with 4 notes (as in the example shown in Subsection 9.2.1). Although playing more notes does not present a new challenge for the neural mechanisms implemented in the model, it is obviously more impressive. One of the next steps of the robotics experiments is therefore to implement the sequence leaning model on the robot ARoS with two arms and two three-fingered hands. We have already bought a new keyboard for this purpose which can be easily controlled by a computer and is sufficiently large to place the two robot hands (see Figure 10.3). A nice side effect of this more sophisticated keyboard is that it allows us to demonstrate a human-robot team playing a real duet in which each partner plays a significant part of a melody. Such demonstration would ideally complements previous work on human-robot interactions with ARoS in sequential tasks by focusing on the timing aspects of joint action.

Figure 10.3: The new keyboard.

Part V

Appendix

Appendix A

Proofs

We start by summarising all conditions on the connection functions and the external input that have been used for the existence and stability proofs presented in Part II of the thesis.

(H_1) $w(x)$ is symmetric, i.e., $w(-x) = w(x)$ for all $x \in \mathbb{R}$;

(H_2) w is both continuous and integrable on $\mathbb{R}$;

(H_3) $w(x) > 0$ on an interval $(-\overline{x}, \overline{x})$, and $w(-\overline{x}) = w(\overline{x}) = 0$;

(H_4) $w(x) < 0$ on $(-\infty, -\overline{x}) \cup (\overline{x}, \infty)$;

(H_5) $w(x)$ is decreasing on $(0, \infty)$;

(H_6) $w(x)$ is an oscillatory function that tends to zero as $x \to \pm\infty$;

(H_7) $w(0) > 0$, and $w(x)$ changes sign infinitely often on $(0, \infty)$;

(H_8) w has infinite positive zeros at values $z_n = -\frac{\arctan\left(\frac{1}{k}\right)}{\alpha} + \frac{n\pi}{\alpha}$ for all $n \in \mathbb{N}$;

(H_9) $W(z_2) > 0$;

(H_{10}) $W(z_2) > \frac{p_1 p_2}{\left(1+e^{\frac{2k\pi}{\alpha}}\right)}$, with $p_1 = \frac{A}{k^2+\alpha^2}$, $p_2 = \alpha k + k$;

(SH_1) $S(x)$ is continuous on $\mathbb{R}$ and symmetric, i.e., $S(-x) = S(x)$ for all $x \in \mathbb{R}$;

(SH_2) $S(x) > 0$ on an interval $(-\overline{x}, \overline{x})$, $S(x) < 0$ on $(-\infty, -\overline{x}) \cup (\overline{x}, \infty)$, and $S(-\overline{x}) = S(\overline{x}) = 0$;

(SH_3) $S(x)$ is increasing on $(-\infty, 0]$ and is decreasing on $[0, \infty)$;

(SH_4) $S(x) > 0$ on $(-\overline{x_2}, -\overline{x_1}) \cup (\overline{x_1}, \overline{x_2})$, $S(-\overline{x_2}) = S(-\overline{x_1}) = S(\overline{x_1}) = S(\overline{x_2}) = 0$, and $S(x) < 0$ on $(-\infty, -\overline{x_2}) \cup (-\overline{x_1}, \overline{x_1}) \cup (\overline{x_2}, \infty)$;

(SH_5) $S(x)$ is increasing on $\left(-\infty, -\frac{\overline{x_2}-\overline{x_1}}{2}\right)$ and on $\left(0, \frac{\overline{x_2}-\overline{x_1}}{2}\right)$, and is decreasing on $\left(-\frac{\overline{x_2}-\overline{x_1}}{2}, 0\right)$ and on $\left(\frac{\overline{x_2}-\overline{x_1}}{2}, \infty\right)$.

A.1 Proof of Theorem 1 :

Theorem 1 *Suppose that hypotheses (H_1) and (H_2) hold. The equation $u(x) = W(x) - W(x-a) - h$ defines an one-bump solution with $R[u] = (0, a)$ if and only if the following three conditions are satisfied*

(i) $W(x) - W(x-a) - h = 0$, *if* $x = a$,

(ii) $W(x) - W(x-a) - h > 0$, *if* $x \in \left(\frac{a}{2}, a\right)$,

(iii) $W(x) - W(x-a) - h < 0$, *if* $x > a$.

Proof:

If $u(x) = W(x) - W(x-a) - h$ is an one-bump solution with $R[u] = (0, a)$, we have $u(0) = u(a) = 0$, $u(x) > 0$ on $(0, a)$ and $u(x) < 0$ otherwise. Thus, $u(a) = 0$, $u(x) > 0$ if $x \in \left(\frac{a}{2}, a\right)$ and $u(x) < 0$ if $x > a$. These relations can be transformed into *(i)*, *(ii)* and *(iii)*.

On the contrary, we assume that *(i)-(iii)* hold. Hypotheses (H_1) and (H_2) imply that W is continuous and odd. Using the oddness of W we have that $u(x)$ is symmetric with respect to $x = \frac{a}{2}$, that is, $u\left(x - \frac{a}{2}\right) = u\left(x + \frac{a}{2}\right)$. Then, $u(0) = u\left(\frac{a}{2} - \frac{a}{2}\right) = u\left(\frac{a}{2} + \frac{a}{2}\right) = u(a) = 0$, $u(x) > 0$ if $x \in \left(0, \frac{a}{2}\right)$ and $u(x) < 0$ if $x < 0$. Therefore, $u(0) = u(a) = 0$, $u(x) > 0$ on $(0, a)$ and $u(x) < 0$ otherwise, that is, $u(x)$ is an one-bump solution with $R[u] = (0, a)$.

A.2 Proof of Theorem 2 :

Theorem 2 *Assume that hypotheses* (H_1), (H_2), $(H_6)-(H_9)$ *hold. Let* $a \in (z_1, z_2)$ *be a solution of* $W(a) = h$. *If* $h > W(z_3)$ *then*

$$u(x) = W(x) + W(x-a) - h$$

defines a stable one-bump solution.

Before proving Theorem 2, we consider the following result:

Lemma 3 *If* $w(x)$ *is given by (1.6) and* $a \in (z_1, z_2)$, *then* $F(x) = W(x) - W(x-a)$ *is increasing on* $\left[0, \frac{a}{2}\right]$ *and decreasing on* $\left[\frac{a}{2}, a\right]$.

Proof of Lemma 3: The function $w(x)$ is positive and decreasing on $[0, z_1)$. Thus, as $\left[0, \frac{a}{2}\right] \subset [0, z_1)$ and $\left[\frac{a}{2}, z_1\right) \subset [0, z_1)$ it follows

$$w(x) \geq w\left(\frac{a}{2}\right), \text{ when } 0 \leq x \leq \frac{a}{2}, \tag{A.1}$$

and

$$w(x) \leq w\left(\frac{a}{2}\right), \text{ when } \frac{a}{2} \leq x < z_1. \tag{A.2}$$

The function $w(x)$ is negative on (z_1, z_2). Thus, as $a \in (z_1, z_2)$ we have $(z_1, a] \subset (z_1, z_2)$ and then

$$w(x) < 0, \text{ when } z_1 < x \leq a. \tag{A.3}$$

From (A.2) and (A.3), and as $w(z_1) = 0$ we have

$$w(x) < w\left(\frac{a}{2}\right), \text{ when } \frac{a}{2} \leq x \leq a, \tag{A.4}$$

and consequently

$$-w(a-x) > -w\left(\frac{a}{2}\right), \text{ when } 0 \leq x \leq \frac{a}{2}. \tag{A.5}$$

From (A.1) and (A.5) we obtain

$$w(x) - w(a-x) > w\left(\frac{a}{2}\right) - w\left(\frac{a}{2}\right) = 0, \text{ when } 0 \leq x \leq \frac{a}{2}. \tag{A.6}$$

Therefore $F(x)$ is increasing on $\left[0, \frac{a}{2}\right]$.

From (A.1) we obtain

$$-w(a-x) < -w\left(\frac{a}{2}\right), \text{ when } \frac{a}{2} \leq x \leq a. \tag{A.7}$$

Then from (A.4) and (A.7) we have

$$w(x) - w(a-x) < w\left(\frac{a}{2}\right) - w\left(\frac{a}{2}\right) = 0, \text{ when } \frac{a}{2} \leq x \leq a. \tag{A.8}$$

Therefore $F(x)$ is decreasing on $\left[\frac{a}{2}, a\right]$ and the proof of Lemma 3 is complete.

Proof of Theorem 2 :

Let $W(x)$ be the integral of $w(x)$ satisfying (H_1), (H_2) and $(H_6) - (H_8)$. The value of $W(z_2)$ is the first relative minimum of W when $x > 0$. From (H_9) and the fact that W is odd, continuous and its oscillations decay with distance, we can conclude that $W(x) \geq 0$ for all $x \geq 0$ and $W(x) < 0$ for all $x < 0$.

Let $a \in (z_1, z_2)$ be a solution of $W(a) = h$, the value of $W(z_3)$ is the first relative maximum of W when $x > a$. Thus, if $h > W(z_3)$ then

$$W(x) < W(a), \text{ for all } x > a. \tag{A.9}$$

From (A.9) and the fact that W is odd it follows that

$$W(x-a) > W(-a), \text{ for all } x < 0. \tag{A.10}$$

Then, if $x < 0$

$$u(x) < 0 - W(-a) - h = W(a) - h = 0, \text{ for all } x < 0. \tag{A.11}$$

By Lemma 3, $u(x)$ is increasing on $\left(0, \frac{a}{2}\right)$ and it follows that

$$u(x) > W(0) - W(-a) - h = 0, \text{ when } 0 < x < \frac{a}{2}. \tag{A.12}$$

As $u(x)$ is symmetric with respect to $x = \frac{a}{2}$ $\left(u\left(\frac{a}{2} - x\right) = u\left(\frac{a}{2} + x\right)\right)$, $u(x) > 0$ when $\frac{a}{2} < x < a$ and $u(x) < 0$ when $x > a$. Therefore, $u(x)$ is an one-bump solution with $R[u] = (0, a)$.

Because $a \in (z_1, z_2)$, we have $w(a) < 0$, and therefore the solution is stable.

A.3 Proof of Lemma 1

Lemma 1 *Let n be a natural number, x be any non-negative real number, and W is defined by (3.1). Then*

$$W\left(x+\frac{n\pi}{\alpha}\right)=\begin{cases}-e^{-\frac{kn\pi}{\alpha}}W(x)+p_1p_2\left(1+e^{-\frac{kn\pi}{\alpha}}\right), \textit{if } n \textit{ is odd}\\ e^{-\frac{kn\pi}{\alpha}}W(x)+p_1p_2\left(1-e^{-\frac{kn\pi}{\alpha}}\right), \textit{if } n \textit{ is even}\end{cases},$$

and

$$W\left(x-\frac{n\pi}{\alpha}\right)=\begin{cases}-e^{\frac{kn\pi}{\alpha}}W(x)+p_1p_2\left(1+e^{\frac{kn\pi}{\alpha}}\right), \textit{if } n \textit{ is odd}\\ e^{\frac{kn\pi}{\alpha}}W(x)+p_1p_2\left(1-e^{\frac{kn\pi}{\alpha}}\right), \textit{if } n \textit{ is even}\end{cases},$$

hold, if $x-\frac{n\pi}{\alpha}>0$.

Proof:

From (3.1) it follows that $W\left(x+\frac{n\pi}{\alpha}\right)$, for all $n\in\mathbb{N}$, can be written as

$$W\left(x+\tfrac{n\pi}{\alpha}\right)=-p_1\left(e^{-k\left(x+\frac{n\pi}{\alpha}\right)}\left(p_3\sin\left(\alpha x+n\pi\right)+p_2\cos(\alpha x+n\pi)\right)-p_2\right).$$

If n is odd we have

$$\begin{aligned}&W\left(x+\tfrac{n\pi}{\alpha}\right)=-p_1e^{-kx}e^{-\frac{kn\pi}{\alpha}}\left(-p_3\sin\left(\alpha x\right)-p_2\cos(\alpha x)\right)+p_1p_2\\&=-e^{-\frac{kn\pi}{\alpha}}\left(-p_1e^{-kx}\left(p_3\sin\left(\alpha x\right)+p_2\cos(\alpha x)\right)+p_1p_2\right)+e^{-\frac{kn\pi}{\alpha}}p_1p_2+p_1p_2\\&=-e^{-\frac{kn\pi}{\alpha}}W(x)+p_1p_2\left(1+e^{-\frac{kn\pi}{\alpha}}\right).\end{aligned}$$

On the other hand, if n is even we have

$$\begin{aligned}&W\left(x+\tfrac{n\pi}{\alpha}\right)=-p_1e^{-kx}e^{-\frac{kn\pi}{\alpha}}\left(p_3\sin\left(\alpha x\right)+p_2\cos(\alpha x)\right)+p_1p_2\\&=e^{-\frac{kn\pi}{\alpha}}\left(-p_1e^{-kx}\left(p_3\sin\left(\alpha x\right)+p_2\cos(\alpha x)\right)+p_1p_2\right)-e^{-\frac{kn\pi}{\alpha}}p_1p_2+p_1p_2\\&=e^{-\frac{kn\pi}{\alpha}}W(x)+p_1p_2\left(1-e^{-\frac{kn\pi}{\alpha}}\right).\end{aligned}$$

This proves the first equality, second equality can be proven similarly.

A.4 Proof of Lemma 2:

Lemma 2 *Assume that W is defined by (3.1) and that (H_1) holds. Then $W\left(\frac{\pi}{\alpha}\right)>W(z_3)$.*

Proof:

By Lemma 1 we obtain

$$W\left(\frac{\pi}{\alpha}\right) = W\left(0+\frac{\pi}{\alpha}\right) = -e^{-\frac{k\pi}{\alpha}}W(0) + p_1p_2\left(1+e^{-\frac{k\pi}{\alpha}}\right);$$

and

$$W\left(z_3\right) = W\left(z_2+\frac{\pi}{\alpha}\right) = -e^{-\frac{k\pi}{\alpha}}W\left(z_2\right) + p_1p_2\left(1+e^{-\frac{k\pi}{\alpha}}\right).$$

As $W(0)=0$,

$$W\left(\frac{\pi}{\alpha}\right) = p_1p_2\left(1+e^{-\frac{k\pi}{\alpha}}\right).$$

Suppose that $W\left(z_2\right)>0$, then $-e^{-\frac{k\pi}{\alpha}}W\left(z_2\right)<0$ and

$$p_1p_2\left(1+e^{-\frac{k\pi}{\alpha}}\right) > -e^{-\frac{k\pi}{\alpha}}W\left(z_2\right) + p_1p_2\left(1+e^{-\frac{k\pi}{\alpha}}\right)$$

i.e.,

$$W\left(\frac{\pi}{\alpha}\right) > W\left(z_3\right).$$

A.5 Proof of Theorem 3:

Theorem 3 *Assume that hypotheses* (H_1), $H_2)$, $(H_6)-(H_9)$, *and* $(SH_1)-(SH_3)$ *hold. If* $S(0) > W\left(\frac{\pi}{\alpha}\right)$, $S\left(\frac{z_1}{2}\right)>0$ *and* $S\left(\frac{z_2}{2}\right)<0$ *then the equation*

$$W\left(\frac{\pi}{\alpha}\right) - S\left(\frac{x}{2}\right) = W(x)$$

has an unique positive solution a^* *that belongs to* (z_1,z_2).

Proof:

From (H_2) and (SH_1) the function defined by $G(x) = W(x) + S\left(\frac{x}{2}\right) - W\left(\frac{\pi}{\alpha}\right)$ is continuous for all $x \geq 0$. Because $\frac{\pi}{\alpha} \in (z_1,z_2)$ and W is decreasing on (z_1,z_2) we conclude that

$$W(z_1) > W\left(\frac{\pi}{\alpha}\right), \tag{A.13}$$

and

$$W\left(\frac{\pi}{\alpha}\right) > W(z_2). \tag{A.14}$$

Assuming that $S\left(\frac{z_1}{2}\right)>0$ and from (A.13) we obtain

$$W(z_1) + S\left(\frac{z_1}{2}\right) - W\left(\frac{\pi}{\alpha}\right) > 0. \tag{A.15}$$

On the other hand, assuming that $S\left(\frac{z_2}{2}\right) < 0$ and from (A.14) we obtain

$$W(z_2) + S\left(\frac{z_2}{2}\right) - W\left(\frac{\pi}{\alpha}\right) < 0. \tag{A.16}$$

Thus, by the Intermediate Value Theorem, there exists $a^* \in (z_1, z_2)$ such that $G(a^*) = 0$. As $G(x)$ is monotonically decreasing on $[z_1, z_2]$ there exists a unique $a^* \in (z_1, z_2)$ that satisfy the equation $G(x) = 0$. In additional, when $x \in (0, z_1]$ we have $W\left(\frac{\pi}{\alpha}\right) - S\left(\frac{x}{2}\right) - W(x) < 0$ because $W\left(\frac{\pi}{\alpha}\right) - S\left(\frac{x}{2}\right) - W(x)$ is decreasing and $S(0) > W\left(\frac{\pi}{\alpha}\right)$. When $x \geq z_2$ we have $W\left(\frac{\pi}{\alpha}\right) - S\left(\frac{x}{2}\right) - W(x) > 0$ because $W\left(\frac{\pi}{\alpha}\right) > W(x)$, $S\left(\frac{x}{2}\right)$ is decreasing and $S\left(\frac{z_2}{2}\right) < 0$. Therefore the equation

$$W\left(\frac{\pi}{\alpha}\right) - S\left(\frac{x}{2}\right) = W(x) \tag{A.17}$$

has an unique positive solution a^* that belongs to (z_1, z_2).

A.6 Proof of Theorem 4

Theorem 4 *Assume that the coupling function w is given by (1.6). If $h = W\left(\frac{\pi}{\alpha}\right)$ and τ a triple of the form $(a, b, a+b)$, then there exists an a-quasi-solution u_τ of (1.1).*

Proof:

If $h = W\left(\frac{\pi}{\alpha}\right)$ $\left(W\left(\frac{\pi}{\alpha}\right) = p_1 p_2\left(1 + e^{-\frac{k\pi}{\alpha}}\right) > 0\right)$ and τ is a triple of the form $(a, b, a+b)$, then u_τ is a a-quasi-solution if and only if $u_\tau(0) = u_\tau(a+b) = 0$ and $u_\tau(a) = u_\tau(b) = 0$. Next, we find a non-trivial solution to the system of the follows two equations

$$W(a+b) - W(b) = 0, \tag{A.18}$$

and

$$W(b) - W(b-a) = 0. \tag{A.19}$$

Let $a = \frac{\pi}{\alpha}$, it follows that

$$W\left(\frac{\pi}{\alpha} + b\right) - W(b) = 0, \tag{A.20}$$

and

$$W(b) - W\left(b - \frac{\pi}{\alpha}\right) = 0. \tag{A.21}$$

Using (3.1) and by Lemma 1 we obtain

$$-e^{-\frac{k\pi}{\alpha}}W(b)+p_1p_2\left(1+e^{-\frac{k\pi}{\alpha}}\right)-W(b)=0, \tag{A.22}$$

and

$$W(b)+e^{\frac{k\pi}{\alpha}}W(b)-p_1p_2\left(1+e^{\frac{k\pi}{\alpha}}\right)=0, \tag{A.23}$$

It follows

$$W(b)=p_1p_2. \tag{A.24}$$

Since $b>a$ and $W(b)=p_1p_2$ we obtain

$$b=\frac{\pi}{2\alpha}+\frac{n\pi}{\alpha} \text{ for some } \ n\in\mathbb{N}, \text{if } p_3=0, \tag{A.25}$$

or

$$b=-\frac{\arctan\left(\frac{p_2}{p_3}\right)}{\alpha}+\frac{n\pi}{\alpha} \text{ for some } \ n\in\mathbb{N}, \text{if } p_3<0, \tag{A.26}$$

or

$$b=-\frac{\arctan\left(\frac{p_2}{p_3}\right)}{\alpha}+\frac{n\pi}{\alpha} \text{ for some } \ n\in\mathbb{N}\setminus\{1\}, \text{if } p_3>0. \tag{A.27}$$

Thus, for $a=\frac{\pi}{\alpha}$ there exists a value for b such that the conditions (A.18) and (A.19) are satisfied. This complete the proof of the theorem.

A.7 Proof of Theorem 5:

Theorem 5 *Assume that the coupling function w is given by (1.6), and that hypothesis (H_{10}) holds. If $a=\frac{\pi}{\alpha}$ and $b\in(z_2,z_3)$ such that $W(b)=p_1p_2$, then*

$$u(x)=W(x)-W(x-a)+W(x-b)-W(x-a-b)-W\left(\frac{\pi}{\alpha}\right)$$

defines a stable two-bump solution.

Proof:

If $a=\frac{\pi}{\alpha}$ and $b\in(z_2,z_3)$ such that $W(b)=p_1p_2$ by Theorem 4 we have that $u(0)=u\left(\frac{\pi}{\alpha}\right)=u(b)=u\left(b+\frac{\pi}{\alpha}\right)=0$. As $b\in(z_2,z_3)$ and $W(b)=W(b+\frac{(n-3)\pi}{\alpha})=p_1p_2$ for all $n\in\mathbb{N}$ we have for all $x\in\left[b+\frac{(n-3)\pi}{\alpha},b+\frac{(n-2)\pi}{\alpha}\right]$

$$W(x)\geq p_1p_2, \text{ if } n \text{ is odd}, \tag{A.28}$$

and

$$W(x) \leq p_1 p_2, \text{ if } n \text{ is even.} \tag{A.29}$$

When $b + \frac{\pi}{\alpha} < x \leq b + \frac{2\pi}{\alpha}$, from (A.28) and (A.29) we have $W(x) \leq p_1 p_2$, $W\left(x - \frac{\pi}{\alpha}\right) \geq p_1 p_2$, $W(x-b) < \frac{\pi}{\alpha}$, and $W\left(x - b - \frac{\pi}{\alpha}\right) > 0$. Thus, we obtain

$$u(x) < p_1 p_2 - p_1 p_2 + W\left(\frac{\pi}{\alpha}\right) - 0 - W\left(\frac{\pi}{\alpha}\right) = 0, \text{ when } b + \frac{\pi}{\alpha} < x \leq b + \frac{2\pi}{\alpha}. \tag{A.30}$$

When $x > b + \frac{2\pi}{\alpha}$, we have $W(x) < W(z_5)$, $W\left(x - \frac{\pi}{\alpha}\right) > W(z_4)$, $W(x-b) < W(z_3)$, and $W\left(x - b - \frac{\pi}{\alpha}\right) > W(z_2)$, consequently we obtain

$$u(x) < W(z_5) - W(z_4) + W(z_3) - W(z_2) - W\left(\frac{\pi}{\alpha}\right). \tag{A.31}$$

By Lemma 1 it follows that

$$u(x) < -\left(e^{-\frac{3k\pi}{\alpha}} + e^{-\frac{2k\pi}{\alpha}}\right)\left(1 + e^{\frac{2k\pi}{\alpha}}\right) W(z_2) + p_1 p_2 \left(e^{-\frac{3k\pi}{\alpha}} + e^{-\frac{2k\pi}{\alpha}}\right). \tag{A.32}$$

From (H_5) we obtain

$$u(x) < -\left(e^{-\frac{3k\pi}{\alpha}} + e^{-\frac{2k\pi}{\alpha}}\right) p_1 p_2 + p_1 p_2 \left(e^{-\frac{3k\pi}{\alpha}} + e^{-\frac{2k\pi}{\alpha}}\right) = 0 \text{ when } x > b + \frac{2\pi}{\alpha}. \tag{A.33}$$

Therefore, from (A.30) and (A.33) $u(x) < 0$, for all $x > b + \frac{\pi}{\alpha}$.

By Lemma 3, $W(x) - W\left(x - \frac{\pi}{\alpha}\right) \geq W(0) - W\left(0 - \frac{\pi}{\alpha}\right)$ if $x \in \left[0, \frac{\pi}{2\alpha}\right]$ and $W(x) - W\left(x - \frac{\pi}{\alpha}\right) \geq W\left(\frac{\pi}{\alpha}\right) - W\left(\frac{\pi}{\alpha} - \frac{\pi}{\alpha}\right)$ if $x \in \left[\frac{\pi}{2\alpha}, \frac{\pi}{\alpha}\right]$. Thus

$$W(x) - W\left(x - \frac{\pi}{\alpha}\right) \geq W\left(\frac{\pi}{\alpha}\right), \text{ when } 0 < x < \frac{\pi}{\alpha}. \tag{A.34}$$

Since W is odd, $W(x-b) - \left(x - b - \frac{\pi}{\alpha}\right) = -W(b-x) + \left(b + \frac{\pi}{\alpha} - x\right)$, from (A.28) and (A.29) it follows that

$$W(x-b) - \left(x - b - \frac{\pi}{\alpha}\right) > -p_1 p_2 + p_1 p_2 = 0, \text{ when } 0 < x < \frac{\pi}{\alpha}. \tag{A.35}$$

Then, from (A.34) and (A.35) we obtain

$$u(x) > W\left(\frac{\pi}{\alpha}\right) + 0 - W\left(\frac{\pi}{\alpha}\right) = 0, \text{ when } 0 < x < \frac{\pi}{\alpha}. \tag{A.36}$$

Therefore, $u(x) > 0$, when $0 < x < \frac{\pi}{\alpha}$.

If $\frac{\pi}{\alpha} < x \leq \frac{b}{2} + \frac{\pi}{2\alpha}$ we have $W(x) < W\left(\frac{\pi}{\alpha}\right)$, $W\left(x - \frac{\pi}{\alpha}\right) > 0$, as $\frac{b}{2} - \frac{\pi}{2\alpha} \geq b - \frac{2\pi}{\alpha}$ from (A.28) follows $W(x-b) = -W(b-x) \leq -p_1p_2$ and as $\frac{b}{2} + \frac{\pi}{2\alpha} \leq b - \frac{\pi}{\alpha}$ from (A.29) follows $-W\left(x - b - \frac{\pi}{\alpha}\right) = W\left(b + \frac{\pi}{\alpha} - x\right) \leq p_1p_2$. Then

$$u(x) < W\left(\frac{\pi}{\alpha}\right) - 0 - p_1p_2 + p_1p_2 - W\left(\frac{\pi}{\alpha}\right) = 0, \text{ when } \frac{\pi}{\alpha} < x \leq \frac{b}{2} + \frac{\pi}{2\alpha}. \quad \text{(A.37)}$$

Therefore, $u(x) < 0$, when $\frac{\pi}{\alpha} < x \leq \frac{b}{2} + \frac{\pi}{2\alpha}$.

As $u(x)$ is symmetric with respect to $x = \frac{\pi}{2\alpha} + \frac{b}{2}$, that is, $u\left(\frac{\pi}{2\alpha} + \frac{b}{2} - x\right) = u\left(\frac{\pi}{2\alpha} + \frac{b}{2} + x\right)$, $u(x) < 0$ if $x < 0$ and if $\frac{b}{2} + \frac{\pi}{2\alpha} < x < b$, and $u(x) > 0$ if $b < x < b + \frac{\pi}{\alpha}$.

Therefore we have $u(x)$ is a two-bump solution with $R[u] = \left(0, \frac{\pi}{\alpha}\right) \cup \left(b, b + \frac{\pi}{\alpha}\right)$.

We recall from the stability analysis in Subsection 4.1.1 that the solution corresponding to $(a, b) = \left(\frac{\pi}{\alpha}, b\right)$ is stable if $b \in (z_{2n}, z_{2n+1})$ for some $n \in \mathbb{N}$. Since $b \in (z_2, z_3)$ we conclude that the solution is stable with respect to perturbations that do not break the equal-width condition. This complete the proof of the theorem.

A.8 Proof of Theorem 6:

Theorem 6 *Assume that the coupling function w given by (1.6), and that hypotheses (H_{10}), (SH_1), (SH_4) and (SH_5) hold. If $S\left(\frac{\overline{x_2} - \overline{x_1}}{2}\right) > W\left(\frac{\pi}{\alpha}\right)$, $S\left(\frac{z_1}{2}\right) < 0$, $S\left(\frac{z_2}{2}\right) > 0$, $S\left(\frac{z_3}{2}\right) > 0$ and $S\left(\frac{z_4}{2}\right) < 0$, then there exists a point (a^*, b^*) belonging to the region $\Omega \subset \mathbb{R}^2$ (4.26) such that*

$$W(a^*) + W(b^*) - W(b^* - a^*) - W\left(\frac{\pi}{\alpha}\right) + S\left(\frac{b^* - a^*}{2}\right) = 0,$$

and

$$W(a^*) - W(b^*) + W(a^* + b^*) - W\left(\frac{\pi}{\alpha}\right) + S\left(\frac{b^* + a^*}{2}\right) = 0.$$

Recall that the region Ω is defined by

$$\Omega = \left\{(x, y) \in \mathbb{R}^2 | x > z_1 \wedge x + z_1 < y < x + z_2 \wedge -x + z_3 < y < -x + z_4\right\}$$

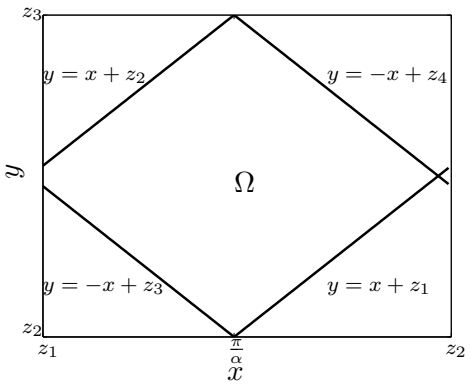

Figure A.1: Region $\Omega \subset \mathbb{R}^2$.

Proof:

We define

$$F_1(x,y) = W(x) + W(y) - W(y-x) - W\left(\frac{\pi}{\alpha}\right) + S\left(\frac{y-x}{2}\right) \tag{A.38}$$

and

$$F_2(x,y) = W(x) - W(y) + W(x+y) - W\left(\frac{\pi}{\alpha}\right) + S\left(\frac{x+y}{2}\right). \tag{A.39}$$

First consider the line $y = x + z_1$ for $\frac{\pi}{\alpha} \leq x < z_2$ and the line $y = x + z_2$ for $z_1 < x \leq \frac{\pi}{\alpha}$. Substituting y by $x + z_1$ and $x + z_2$ in (A.38) we obtain

$$F_1(x, x+z_1) = W(x) + W(x+z_1) - W(z_1) - W\left(\frac{\pi}{\alpha}\right) + S\left(\frac{z_1}{2}\right), \tag{A.40}$$

and

$$F_1(x, x+z_2) = W(x) + W(x+z_2) - W(z_2) - W\left(\frac{\pi}{\alpha}\right) + S\left(\frac{z_2}{2}\right). \tag{A.41}$$

Since $S\left(\frac{z_1}{2}\right) < 0$ by hypothesis, $W(x) < W\left(\frac{\pi}{\alpha}\right)$ and $W(x+z_1) < W(z_1)$ for all $x \in \left[\frac{\pi}{\alpha}, z_2\right)$, we conclude that

$$F_1(x, x+z_1) < 0 \text{ for all } x \in \left[\frac{\pi}{\alpha}, z_2\right). \tag{A.42}$$

On the other hand, since $S\left(\frac{z_2}{2}\right) > 0$ by hypothesis, $W(x) > W\left(\frac{\pi}{\alpha}\right)$ and $W(x+z_2) > W(z_2)$ for all $x \in \left(z_1, \frac{\pi}{\alpha}\right]$, we conclude that

$$F_1(x, x+z_2) > 0 \text{ for all } x \in \left(z_1, \frac{\pi}{\alpha}\right]. \tag{A.43}$$

Thus, in the line that joins the two points $P_1 = (x_1, x_1 + z_1)$ and $P_2 = (x_2, x_2 + z_2)$ with $x_1 \in \left[\frac{\pi}{\alpha}, z_2\right)$ and $x_2 \in \left(z_1, \frac{\pi}{\alpha}\right]$, there exists a point (x^*, y^*) such that $F_1(x^*, y^*) = 0$. In addition $\frac{\partial F_1}{\partial y}(x, y)$, the partial derivative of $F_1(x, y)$ with respect to y, is positive in the region

$$\Omega_1 = \left\{(x, y) \in \mathbb{R}^2 | x + z_1 < y < x + z_2 \wedge r_1 < y < r_2\right\}, \tag{A.44}$$

where r_1, r_2 are the lines defined by the points P_1 and P_2 with $x_1 = \frac{\pi}{\alpha}$, $x_2 = z_1$, and $x_1 = z_2$, $x_2 = \frac{\pi}{\alpha}$, respectively. Therefore, by the implicit function theorem, the equation $F_1(x, y) = 0$ defines y implicitly as a increasing function of x in the region Ω_1.

Now, consider the line $y = -x + z_3$ for $z_1 < x \leq \frac{\pi}{\alpha}$ and the line $y = -x + z_4$ for $\frac{\pi}{\alpha} \leq x < z_2$. Substituting y by $-x + z_3$ and $-x + z_4$ in (A.39) we conclude that

$$F_2(x, -x + z_3) = W(x) - W(-x + z_3) + W(z_3) - W\left(\frac{\pi}{\alpha}\right) + S\left(\frac{z_3}{2}\right), \tag{A.45}$$

and

$$F_2(x, -x + z_4) = W(x) - W(-x + z_4) + W(z_4) - W\left(\frac{\pi}{\alpha}\right) + S\left(\frac{z_4}{2}\right). \tag{A.46}$$

Because $S\left(\frac{z_3}{2}\right) > 0$ by hypothesis, $W(x) > W\left(\frac{\pi}{\alpha}\right)$ and $W(z_3) > W(-x + z_3)$ for all $x \in \left(z_1, \frac{\pi}{\alpha}\right]$, we conclude that

$$F_2(x, -x + z_3) > 0 \text{ for all } x \in \left(z_1, \frac{\pi}{\alpha}\right]. \tag{A.47}$$

On the other hand, $S\left(\frac{z_4}{2}\right) < 0$ by hypothesis, $W(x) < W\left(\frac{\pi}{\alpha}\right)$ and $W(z_4) < W(-x + z_4)$ for all $x \in \left[\frac{\pi}{\alpha}, z_2\right)$, we have

$$F_2(x, -x + z_4) < 0 \text{ for all } x \in \left[\frac{\pi}{\alpha}, z_2\right). \tag{A.48}$$

Thus, in the line that joins the two points $P_3 = (x_3, -x_3 + z_3)$ and $P_4 = (x_4, -x_4 + z_4)$ with $x_3 \in \left(z_1, \frac{\pi}{\alpha}\right]$ and $x_4 \in \left[\frac{\pi}{\alpha}, z_2\right)$, there exists a point (x^*, y^*) such that $F_2(x^*, y^*) = 0$. In addition $\frac{\partial F_2}{\partial y}(x, y)$, the partial derivative of $F_2(x, y)$ with respect to y is negative. Thus, the equation $F_2(x, y) = 0$ defines y implicitly as a increasing function of x, in the region

$$\Omega_2 = \left\{(x, y) \in \mathbb{R}^2 | -x + z_3 < y < -x + z_4 \wedge r_3 < y < r_4\right\}, \tag{A.49}$$

where r_3, r_4 are the lines defined by points P_3 and P_4 with $x_3 = \frac{\pi}{\alpha}, x_4 = z_1$ and $x_3 = z_2, x_4 = \frac{\pi}{\alpha}$, respectively.

Therefore, we can conclude that there exists a unique point $(a^*, b^*) \in \Omega_1 \cap \Omega_2 \subset \Omega$ that satisfies the system of equations $F_1(a^*, b^*) = 0$ and $F_2(a^*, b^*) = 0$.

A.9 Proof of Proposition 1:

Proposition 1 *Suppose that hypotheses* (H_1), (H_2), (H_6) *and* (H_7) *hold. If* u *is symmetric with respect to the point* $\frac{a_0+a_{2N-1}}{2}$, *the system of equations*

$$\begin{cases} u(a_0) = 0 \\ u(a_1) = 0 \\ \quad ... \\ u(a_{2N-1}) = 0 \end{cases}$$

can be reduced to

$$\begin{cases} u\left(a_0\right) = 0 \\ ... \\ u\left(a_{N-1}\right) = 0 \end{cases}.$$

Proof:

From (5.2) we can write

$$u\left(a_{N+m}\right) = \sum_{i=0}^{N-1} \left(W\left(a_{N+m} - a_{2i}\right) - W\left(a_{N+m} - a_{2i+1}\right)\right) - h, \quad m \in \{1, ..., N-1\}. \tag{A.50}$$

As u is symmetric with respect to the point $\frac{a_0+a_{2N-1}}{2}$, we have $a_{N+m} = a_N + a_{N-1} - a_{N-(1+m)}, m \in \{1, ..., N-1\}$ and then

$$u\left(a_{N+m}\right) = \sum_{i=0}^{N-1} \left(W\left(a_N + a_{N-1} - a_{N-(1+m)} - a_{2i}\right) - W\left(a_N + a_{N-1} - a_{N-(1+m)} - a_{2i+1}\right)\right) - h. \tag{A.51}$$

As $a_{N+m} = a_N + a_{N-1} - a_{N-(1+m)}$, for $m = N-1-2i$ and $m = N-2-2i$ we have

$$a_N + a_{N-1} - a_{2i} = a_{2(N-i)-1} \tag{A.52}$$

and

$$a_N + a_{N-1} - a_{2i+1} = a_{2(N-i-1)}, \tag{A.53}$$

respectively. Thus, we obtain

$$u\left(a_{N+m}\right) = \sum_{i=0}^{N-1} \left(W\left(a_{2(N-i)-1} - a_{N-(1+m)}\right) - W\left(a_{2(N-i-1)} - a_{N-(1+m)}\right)\right) - h. \tag{A.54}$$

Using the oddness of W it follows that

$$u\left(a_{N+m}\right) = \sum_{i=0}^{N-1} \left(-W\left(a_{N-(1+m)} - a_{2i+1}\right) + W\left(a_{N-(1+m)} - a_{2i}\right)\right) - h,\ m \in \{1, ..., N-1\}. \tag{A.55}$$

Therefore,

$$u\left(a_{N+m}\right) = u\left(a_{N-(1+m)}\right) \tag{A.56}$$

and the system (5.3) can be reduced to

$$\begin{cases} u(a_0) = 0 \\ u(a_1) = 0 \\ \quad ... \\ u(a_{N-1}) = 0. \end{cases} \tag{A.57}$$

Appendix B

Numerical methods

For the numerical integration of the computational models, specific code written in MATLAB has been developed.

B.1 Forward Euler method

We used a simple forward Euler scheme (Kincaid and Cheney, 2002; Elvin and Laing, 2005) to find approximate solutions of the neural field equation

$$\tau \frac{\partial u(x,t)}{\partial t} = -u(x,t) + \int_{-\infty}^{\infty} w(x-y) f\left(u(y,t)\right) dy + g(x,t), \tag{B.1}$$

where $g(x,t)$ denotes a function that depends on the resting level h and the external $S(x,t)$ to the field.

We assume a finite domain Ω with length L and discretise over space by dividing the domain Ω into n equal intervals of size Δ_x such that $\Delta_x = \frac{L}{n}$. The spatial discretisation defines the position of neurons labelled as $x_i = i\Delta_x$ for $i = 0, 1, ..., n$. To find $u(x,T)$ where $T > 0$, we discretise time T into m equal steps of size Δ_t and write $t_j = j\Delta_t$ for $j = 0, 1, ..., m$. The derivative in (B.1) is replaced by the forward difference approximation

$$u_t = \frac{v_{i,j+1} - v_{i,j}}{\Delta_t} + O(\Delta_t), \tag{B.2}$$

where $v_{i,j}$ denotes the approximation of $u(x_i, t_j) = u(i\Delta_x, j\Delta_t)$. Ignoring the integral term, we have the scheme

$$v_{i,j+i} = (1 - \frac{\Delta_t}{\tau})v_{i,j} \frac{\Delta_t}{\tau} g(x_i, t_j). \tag{B.3}$$

This method is stable if the coefficient of $v_{i,j}$ is non-negative, i.e., if $1 - \frac{\Delta_t}{\tau} \geq 0$. Therefore the condition for stability is

$$\tau \geq \Delta_t \tag{B.4}$$

with truncation error of $O(\Delta_t)$. The time step Δ_t must not be greater than τ to maintain stability.

To solve equation (B.1) numerically, the nonlinear term that correspond to the convolution integral is evaluated at step j (the previous time step) using the function *conv* of MATLAB with circular boundary conditions. Then the forward Euler scheme is given by

$$v_{i,j+i} = (1 - \frac{\Delta_t}{\tau})v_{i,j} + \frac{\Delta_t}{\tau} \left(g(x_i, t_j) + W_j \right), \tag{B.5}$$

where W_j denotes the evaluation of the nonlinear integral term at time step j.

B.2 Newton's iteration method for solution of nonlinear equations

We use Newton's method to solve systems of n non-linear equations given by

$$\begin{cases} f_1(x_1, x_2, \ldots, x_n) = 0 \\ f_2(x_1, x_2, \ldots, x_n) = 0 \\ \vdots \\ f_n(x_1, x_2, \ldots, x_n) = 0 \end{cases} . \tag{B.6}$$

The system can be written in a single expression using vectors, i.e.,

$$f(x) = 0, \tag{B.7}$$

where $x = (x_1, x_2, \ldots, x_n) \in \mathbb{R}^n$ and $f = (f_1, f_2, \ldots, f_n)$, $f : \mathbb{R}^n \to \mathbb{R}^n$. Newton's method is started with an initial guess x_0. Using a linear approximation of f at x_0

$$f(x) \approx f(x_0) + J(x_0)(x - x_0), \tag{B.8}$$

where $J(x_0)$ is Jacobian matrix

$$J(x_0) = \begin{pmatrix} \frac{\partial f_1}{\partial x_1}(x_0) & \frac{\partial f_1}{\partial x_2}(x_0) & \frac{\partial f_1}{\partial x_3}(x_0) & \cdots & \frac{\partial f_1}{\partial x_n}(x_0) \\ \frac{\partial f_2}{\partial x_1}(x_0) & \frac{\partial f_2}{\partial x_2}(x_0) & \frac{\partial f_2}{\partial x_3}(x_0) & \cdots & \frac{\partial f_2}{\partial x_n}(x_0) \\ \vdots & \vdots & \vdots & \ddots & \vdots \\ \frac{\partial f_n}{\partial x_1}(x_0) & \frac{\partial f_n}{\partial x_2}(x_0) & \frac{\partial f_n}{\partial x_3}(x_0) & \cdots & \frac{\partial f_n}{\partial x_n}(x_0) \end{pmatrix}. \tag{B.9}$$

To approximate teh zero of the nonlinear function $f(x)$ the iteration

$$x_{n+1} = x_n - (J(x_n))^{-1} f(x_n), n = 0, 1, \ldots \tag{B.10}$$

is applied where J^{-1} denotes the inverse matrix of the Jacobian.

As convergence criterion for the solution of the system, we use the difference between consecutive values

$$|x_{n+1} - x_n| < \epsilon. \tag{B.11}$$

where the tolerance is given by $\epsilon = e^{-10}$.

Bibliography

Amari, S. (1977). Dynamics of pattern formation in lateral-inhibition type neural fields. *Biological Cybernetics*, 27(2):77–87.

Amari, S. (1980). Topographic organization of nerve fields. *Bulletin of Mathematical Biology*, 42(3):339–364.

Amari, S. (1982). Competitive and cooperative aspects in dynamics of neural excitation and self-organization. In Amari, S.-i. and Arbib, M. A., editors, *Competition and Cooperation in Neural Nets*, volume 45, chapter I, pages 1–28. Springer Berlin Heidelberg.

Andry, P. (2004). Learning Invariant Sensorimotor Behaviors: A Developmental Approach to Imitation Mechanisms. *Adaptive Behavior*, 12(2):117–140.

Averbeck, B. B., Chafee, M. V., Crowe, D. A., and Georgopoulos, A. P. (2002). Parallel processing of serial movements in prefrontal cortex. *Proceedings of the National Academy of Sciences of the United States of America*, 99(20):13172–13177.

Averbeck, B. B., Crowe, D. A., Chafee, M. V., and Georgopoulos, A. P. (2003). Neural activity in prefrontal cortex during copying geometrical shapes. II. Decoding shape segments from neural ensembles. *Experimental brain research*, 150(2):142–153.

Baddeley, A. (1992). Working memory. *Science*, 255(5044):556–559.

Bastian, A., Schoner, G., and Riehle, A. (2003). Preshaping and continuous evolution of motor cortical representations during movement preparation. *European Journal of Neuroscience*, 18(7):2047–2058.

Bicho, E. (2000). *Dynamic approach to behavior-based robotics : design, specification, analysis, simulation and implementation*. Shaker Verlag, Aachen.

Bicho, E., Erlhagen, W., Louro, L., and e Silva, E. C. (2011). Neuro-cognitive mechanisms of decision making in joint action: a human-robot interaction study. *Human Movement Science*, 30(5):846–868.

Bicho, E., Erlhagen, W., Sousa, E., Louro, L., Hipolito, N., Silva, E. C., Silva, R., Ferreira, F., Machado, T., Hulstijn, M., Maas, Y., de Bruijn, E., Cuijpers, R. H., Newman-Norlund, R., van Schie, H., Meulenbroek, R., and Bekkering, H. (2012). The power of prediction: Robots that read intentions. In *2012 IEEE/RSJ International Conference on Intelligent Robots and Systems (IROS 2012)*, pages 5458–5459, Vilamoura, Portugal.

Bicho, E., Louro, L., and Erlhagen, W. (2010). Integrating verbal and nonverbal communication in a dynamic neural field architecture for human-robot interaction. *Frontiers in neurorobotics*, 4, doi:10.3389/fnbot.2010.00005.

Bicho, E., Louro, L., Hipólito, N., and Erlhagen, W. (2008). A dynamic neural Field architecture for Flexible and Fluent human-robot interaction. In *Proceedings of the 2008 International Conference on Cognitive Systems*, pages 179–185, Karlsruhe, Germany. University of Karlsruhe.

Bicho, E., Louro, L., Hipólito, N., and Erlhagen, W. (2009). A dynamic field approach to goal inference and error monitoring for human-robot interaction. In Dautenhanhn, E., editor, *AISB Convention 2009 on Adaptive & Emergent Behaviour & Complex Systems : proceedings of the International Symposium on New Frontiers in Human-Robot Interaction*, pages 31–37, Edinburgh, Scotland.

Bicho, E. and Schöner, G. (1997). The dynamic approach to autonomous robotics demonstrated on a low-level vehicle platform. *Robotics and Autonomous Systems*, 21(1):23–35.

Botvinick, M. and Plaut, D. C. (2004). Doing without schema hierarchies: a recurrent connectionist approach to normal and impaired routine sequential action. *Psychological Review*, 111(2):395–429.

Botvinick, M. M. and Plaut, D. C. (2006). Short-term memory for serial order: a recurrent neural network model. *Psychological Review*, 113(2):201–233.

Botvinick, M. M., Wang, J., Cowan, E., Roy, S., Bastianen, C., Patrick Mayo, J., and Houk, J. C. (2009). An analysis of immediate serial recall performance in a macaque. *Animal Cognition*, 12(5):671–678.

Bradski, G., Carpenter, G. A., and Grossberg, S. (1994). STORE working memory networks for storage and recall of arbitrary temporal sequences. *Biological Cybernetics*, 71:469–480.

Brown, G. D. A., Preece, T., and Hulme, C. (2000). Oscillator-based memory for serial order. *Psychological Review*, 107(1):127–181.

Burgess, N. and Hitch, G. J. (1999). Memory for serial order: A network model of the phonological loop and its timing. *Psychological Review*, 106(3):551–581.

Cleeremans, A. (1993). *Mechanisms of implicit learning: Connectionist models of sequence processing*. MA: MIT Press, Cambridge.

Cleeremans, A. and McClelland, J. L. (1991). Learning the structure of event sequences. *Journal of Experimental Psychology: General*, 120(3):235–253.

Conrad, R. (1965). Order error in immediate recall of sequences. *Journal of Verbal Learning and Verbal Behavior*, 4(3):161–169.

Coombes, S. (2005). Waves, bumps, and patterns in neural field theories. *Biological Cybernetics*, 93(2):91–108.

Coombes, S. and Owen, M. (2007). Exotic dynamics in a firing rate model of neural tissue with threshold accommodation. *AMS Contemporary Mathematics*, 440:123–144.

Cowan, N. (2008). What are the differences between long-term, short-term, and working memory? *Progress in Brain Research*, 169:323–338.

Dautenhahn, K. and Nehaniv, C. L. (2002). *Imitation in animals and artifacts*. MIT Press.

Dominey, P. F. (1998). A shared system for learning serial and temporal structure of sensori-motor sequences? Evidence from simulation and human experiments. *Cognitive Brain Research*, 6(3):163–172.

Durstewitz, D. (2004). Neural representation of interval time. *NeuroReport*, 15:745–749.

Elman, J. (1990). Finding structure in time. *Cognitive Science*, 14(2):179–211.

Elvin, A. and Laing, C. (2005). Evaluation of numerical integration schemes for a partial integro-differential equation. *Research Letters in the Information and Mathematical Sciences*, (7):171–186.

Erlhagen, W., Bastian, A., Jancke, D., Riehle, A., and Schöner, G. (1999). The distribution of neuronal population activation (DPA) as a tool to study interaction and integration in cortical representations. *Journal of Neuroscience Methods*, 94(1):53–66.

Erlhagen, W. and Bicho, E. A dynamic neural field approach to natural and efficient human-robot collaboration. In *Progress in Dynamic Field Theory*. Springer, in press.

Erlhagen, W. and Bicho, E. (2006). The dynamic neural field approach to cognitive robotics. *Journal of Neural Engineering*, 3(3):R36–54.

Erlhagen, W., Mukovskiy, A., Bicho, E., Panin, G., Kiss, C., Knoll, A., van Schie, H., and Bekkering, H. (2006). Goal-directed imitation for robots: A bio-inspired approach to action understanding and skill learning. *Robotics and Autonomous Systems*, 54(5):353–360.

Erlhagen, W. and Schöner, G. (2002). Dynamic field theory of movement preparation. *Psychological Review*, 109(3):545–572.

Faubel, C. and Schöner, G. (2008). Learning to recognize objects on the fly: a neurally based dynamic field approach. *Neural Networks*, 21(4):562–576.

Ferreira, F., Erlhagen, W., and Bicho, E. (2011). A dynamic field model of ordinal and timing properties of sequential events. In Honkela, T., Duch, W., Girolami, M., and Kaski, S., editors, *Artificial Neural Networks and Machine Learning -ICANN 2011*, volume 6792 of *LNCS*, pages 325–332. Springer Berlin Heidelberg.

Genovesio, A., Brasted, P. J., and Wise, S. P. (2006a). Representation of future and previous spatial goals by separate neural populations in prefrontal cortex. *The Journal of Neuroscience*, 26(27):7305–7316.

Genovesio, A., Tsujimoto, S., and Wise, S. P. (2006b). Neuronal activity related to elapsed time in prefrontal cortex. *Journal of Neurophysiology*, 95(5):3281–3285.

Gobel, E. W., Sanchez, D. J., and Reber, P. J. (2011). Integration of temporal and ordinal information during serial interception sequence learning. *Journal of Experimental Psychology. Learning, Memory, and Cognition*, 37(4):994–1000.

Grondin, S. and Killeen, P. R. (2009). Tracking time with song and count: different Weber functions for musicians and nonmusicians. *Attention, Perception & Psychophysics*, 71(7):1649–1654.

Grossberg, S. (1978). Behavioral contrast in short term memory: Serial binary memory models or parallel continuous memory models? *Journal of Mathematical Psychology*, 17(3):199–219.

Grossberg, S. (1982). A theory of human memory: Self-organization and performance of sensory-motor codes, maps, and plans. In *Studies of Mind and Brain*, volume 70, pages 498–639. Springer Netherlands.

Guo, Y. and Chow, C. C. (2005a). Existence and Stability of Standing Pulses in Neural Networks: I. Existence. *SIAM Journal on Applied Dynamical Systems*, 4(2):217–248.

Guo, Y. and Chow, C. C. (2005b). Existence and Stability of Standing Pulses in Neural Networks: II. Stability. *SIAM Journal on Applied Dynamical Systems*, 4(2):249–281.

Gutkin, B. S., Bard Ermentrout, G., and O'Sullivan, J. (2000). Layer 3 patchy recurrent excitatory connections may determine the spatial organization of sustained activity in the primate prefrontal cortex. *Neurocomputing*, 32-33:391–400.

Henson, R. N. (1998). Short-term memory for serial order: the Start-End Model. *Cognitive Psychology*, 36(2):73–137.

Houghton, G. (1990). The problem of serial order: A neural network model of sequence learning and recall. In Dale, R., Mellish, C., and Zock, M., editors, *Current research in natural language generation*, pages 287–319. Academic Press, London.

Howard, J. H., Mutter, S. A., and Howard, D. V. (1992). Serial pattern learning by event observation. *Journal of Experimental Psychology: Learning, Memory, and Cognition*, 18(5):1029–1039.

Janata, P. and Grafton, S. T. (2003). Swinging in the brain: shared neural substrates for behaviors related to sequencing and music. *Nature Neuroscience*, 6(7):682–687.

Jancke, D., Erlhagen, W., Dinse, H. R., Akhavan, a. C., Giese, M., Steinhage, A., and Schöner, G. (1999). Parametric population representation of retinal location: neuronal interaction dynamics in cat primary visual cortex. *The Journal of Neuroscience*, 19(20):9016–9028.

Janssen, P. and Shadlen, M. N. (2005). A representation of the hazard rate of elapsed time in macaque area LIP. *Nature Neuroscience*, 8(2):234–241.

Johnson, J. S., Spencer, J. P., and Schöner, G. (2008). Moving to higher ground: The dynamic field theory and the dynamics of visual cognition. *New Ideas in Psychology*, 26(2):227–251.

Kincaid, D. and Cheney, W. (2002). *Numerical Analysis: Mathematics of Scientific computing*. American Mathematical Society, 3 rd edition.

Kishimoto, K. and Amari, S. (1979). Existence and stability of local excitations in homogeneous neural fields. *Journal of Mathematical Biology*, 7(4):303–318.

Kornysheva, K., Sierk, A., and Diedrichsen, J. (2013). Interaction of temporal and ordinal representations in movement sequences. *Journal of Neurophysiology*, 109(5):1416–1424.

Kubota, S., Hamaguchi, K., and Aihara, K. (2009). Local excitation solutions in one-dimensional neural fields by external input stimuli. *Neural Computing and Applications*, 18(6):591–602.

Laing, C. R. and Troy, W. C. (2003). Two-bump solutions of Amari-type models of neuronal pattern formation. *Physica D: Nonlinear Phenomena*, 178(3-4):190–218.

Laing, C. R., Troy, W. C., Gutkin, B., and Ermentrout, G. B. (2002). Multiple Bumps in a Neuronal Model of Working Memory. *SIAM Journal on Applied Mathematics*, 63(1):62–97.

Lashley, K. S. (1951). *The problem of serial order in behavior*. Number 7. Jonh Wiley & Sons, New York.

Levesque, H. and Lakemeyer, G. (2008). Cognitive Robotics. In van Harmelen, F., Lifschitz, V., and Porter, B., editors, *Handbook of Knowledge Representation*, pages 869–886. Elsevier B.V.

Lewis, P. a. and Miall, R. C. (2006). Remembering the time: a continuous clock. *Trends in Cognitive Sciences*, 10(9):401–406.

Machado, A., Malheiro, M. T., and Erlhagen, W. (2009). Learning to Time: a perspective. *Journal of the Experimental Analysis of Behavior*, 92(3):423–458.

Miller, E. K. (2000). The prefrontal cortex and cognitive control. *Nature Reviews Neuroscience*, 1(1):59–65.

Murdock, A. J., Botelho, F., and Jamison, J. E. (2006). Persistence of spatial patterns produced by neural field equations. *Physica D: Nonlinear Phenomena*, 215(2):106–116.

Murdock, B. B. (1995). Developing TODAM: Three models for serial-order information. *Memory & Cognition*, 23(5):631–645.

Nissen, M. J. and Bullemer, P. (1987). Attentional requirements of learning: Evidence from performance measures. *Cognitive Psychology*, 19(1):1–32.

O'Reilly, J. X., McCarthy, K. J., Capizzi, M., and Nobre, A. C. (2008). Acquisition of the temporal and ordinal structure of movement sequences in incidental learning. *Journal of Neurophysiology*, 99(5):2731–2735.

Page, M. P. A. and Norris, D. (1998). The primacy model: A new model of immediate serial recall. *Psychological Review*, 105(4):761–781.

Palmer, C. and Pfordresher, P. Q. (2003). Incremental planning in sequence production. *Psychological Review*, 110(4):683–712.

Perko, L. (1996). *Differential Equations and Dynamical Systems*, volume 7 of *Texts in Applied Mathematics*. Springer US, New York, NY.

Pfordresher, P. Q., Palmer, C., and Jungers, M. K. (2007). Speed, accuracy, and serial order in sequence production. *Cognitive Science*, 31(1):63–98.

Pinto, D. J. P. and Ermentrout, B. G. (2001). Spatially Structured Activity In Synaptically Coupled Neuronal Networks: I. Traveling Fronts And Pulses. *SIAM Journal on Applied Mathematics*, 62:206–225.

Rhodes, B. J., Bullock, D., Verwey, W. B., Averbeck, B. B., and Page, M. P. a. (2004). Learning and production of movement sequences: behavioral, neurophysiological, and modeling perspectives. *Human Movement Science*, 23(5):699–746.

Robertson, E. and Pascual-Leone, a. (2001). Aspects of sensory guidance in sequence learning. *Experimental Brain Research*, 137(3-4):336–345.

Rogers, G. L. (1991). Effect of Color-Coded Notation on Music Achievement of Elementary Instrumental Students. *Journal of Research in Music Education*, 39(1):64–73.

Schaal, S. (1999). Is imitation learning the route to humanoid robots? *Trends in Cognitive Sciences*, 3(6):233–242.

Schöner, G. (2008). Dynamical systems approaches to cognition. In Sun, R., editor, *The Cambridge Handbook of Computational Psychology*, pages 101–126. Cambridge University Press, Cambridge.

Schöner, G. (2009). Development as Change of System Dynamics: Stability, Instability, and Emergence. In McClelland, J., Spencer, J., and Thomas, M., editors, *Toward a unified theory of development. Connectionism and dynamic systems theory re-considered.*, pages 25–47. Oxford University Press, New York.

Schöner, G., Dose, M., and Engels, C. (1995). Dynamics of behavior: Theory and applications for autonomous robot architectures. *Robotics and Autonomous Systems*, 16(2-4):213–245.

Shieh, D. X. and Elman, J. L. (2006). The Divergent-Reconvergent Model of Serial Order Encoding and Retrieval. In *Proceedings of the 29th Annual Meeting of the Cognitive Science Society*, pages 786–791.

Shin, J. C. and Ivry, R. B. (2002). Concurrent learning of temporal and spatial sequences. *Journal of Experimental Psychology: Learning, Memory, and Cognition*, 28(3):445–457.

Silva, R. (2008). *Design e construção de um robot antropomórfico*. Master thesis, University of Minho.

Smyth, M. M. and Scholey, K. A. (1996). Serial order in spatial immediate memory. *The Quarterly Journal of Experimental Psychology. A, Human Experimental Psychology*, 49(1):159–177.

Sousa, E., Erlhagen, W., and Bicho, E. (2014). On observational learning of hierarchies in sequential tasks: A dynamic neural field model. In *Computational Models of Cognitive Processes*, pages 196–210. World Scientifc.

Tanji, J., Shima, K., and Mushiake, H. (2007). Concept-based behavioral planning and the lateral prefrontal cortex. *Trends in Cognitive Sciences*, 11(12):528–534.

Thelen, E., Schöner, G., Scheier, C., and Smith, L. B. (2001). The dynamics of embodiment: A field theory of infant perseverative reaching. *Behavioral and Brain Sciences*, 24(1):1–34.

Wardak, C., Ramanoël, S., Guipponi, O., Boulinguez, P., and Ben Hamed, S. (2012). Proactive inhibitory control varies with task context. *The European Journal of Neuroscience*, 36(11):3568–3579.

Willingham, D. B., Nissen, M. J., and Bullemer, P. (1989). On the development of procedural knowledge. *Journal of Experimental Psychology: Learning, Memory, and Cognition*, 15(6):1047–1060.

Wilson, H. R. and Cowan, J. D. (1973). A mathematical theory of the functional dynamics of cortical and thalamic nervous tissue. *Kybernetik*, 13(2):55–80.